ELECTRODEPOSITION OF COPPER ON RUTHENIUM OXIDES AND BIMETALLIC CORROSION OF COPPER/RUTHENIUM IN POLYPHENOLIC ANTIOXIDANTS

Shyam S. Venkataraman, B. Tech.

Thesis Prepared for the Degree of

MASTER OF SCIENCE

UNIVERSITY OF NORTH TEXAS

August 2007

APPROVED:

Oliver M. R. Chyan, Major Professor
Guido F. Verbeck, Committee Member
Michael G. Richmond, Chair of the Department of Chemistry
Sandra L. Terrell, Dean of the Robert B. Toulouse School of Graduate Studies

Venkataraman, Shyam S. Electrodeposition of Copper on Ruthenium Oxides and Bimetallic Corrosion of Copper/Ruthenium in Polyphenolic Antioxidants. Master of Science (Analytical Chemistry), August 2007, 105 pp., 37 figures, references, 97 titles.

Copper (Cu) electrodeposition on ruthenium (Ru) oxides was studied due to important implications in semiconductor industry. Ruthenium, proposed as the copper diffusion barrier/liner material, has higher oxygen affinity to form different oxides. Three different oxides (the native oxide, reversible oxide, and irreversible oxide) were studied. Native oxide can be formed on exposing Ru in atmosphere. The reversible and irreversible oxides can be formed by applying electrochemical potential. Investigation of Cu under potential deposition on these oxides indicates the similarity between native and reversible oxides by its nature of inhibiting Cu deposition. Irreversible oxide formed on Ru surface is rather conductive and interfacial binding between Cu and Ru is greatly enhanced.

After deposition, bimetallic corrosion of Cu/Ru in different polyphenols was studied. Polyphenols are widely used as antioxidants in post chemical mechanical planarization (CMP). For this purpose, different trihydroxyl substituted benzenes were used as antioxidants. Ru, with its noble nature enhances bimetallic corrosion of Cu. Gallic acid (3,4,5 – trihydroxybenzoic acid) was chosen as model compound. A mechanism has been proposed and validity of the mechanism was checked with other antioxidants. Results show that understanding the chemical structure of antioxidants is necessary during its course of reaction with Cu.

ACKNOWLEDGEMENTS

I thank my graduate advisor Dr. Oliver M. R. Chyan for his sincere support and candid critiques of superior objectives. With his teaching and learning philosophy, I am happy to see myself being nurtured from the time I have started to pursue my graduate studies at United States of America. I am sure that his inspirational words will constantly hear in my mind. I will carry his advices to bring fame and success to my mentor and alumni in the future. My special thanks to my colleagues, Dr. Tiruchirapalli Arunagiri and Dr. Praveen Nalla Reddy for their constant motivation to expand my knowledge in the scientific field. I am particularly thankful to Kyle K. Yu for working together with me as a research team. I thank Karthikeyan S. Pillai for his presence by supporting me and I am obligated to share my success of completing master's degree with him. I also thank my other group members Yibin Zhang, Oscar Ojeda, Sarah Flores, and Fan Yang. I would like to extend my acknowledgements to Dr. Teresa Golden, Dr. William Acree, Dr. Michael G. Richmond, and Dr. Guido Verbeck for their support in finishing my Master's work successfully. I express my thanks to all the faculties in the department of chemistry at University of North Texas for their teachings which made me more interested in learning chemistry. My special thanks to Susan Brockington for helping me out for completing necessary requirements for my successful graduation at UNT. I also thank the funding support from Robert Welch Foundation and Semiconductor Research Corporation.

TABLE OF CONTENTS

Page

LIST OF ILLUSTRATIONS

Page

LIST OF MECHANISMS

Page

* Mechanism 3.2 is reprinted with permission from Tulyathan, V.; Boulton, R. B.; and Singleton, V. L. "Oxygen uptake by gallic acid as a model for similar reactions in wines," *J. Agric. Food Chem.*, *37* (4), 1989, 844-849. Copyright 2007 American Chemical Society.

LIST OF ABBREVIATIONS

Materials

Ag/AgCl	Silver/silver chloride
Al	Aluminum
BTA	Benzotriazole
Cu	Copper
Fe	Iron
Ir	Iridium
Os	Osmium
Pd	Palladium
Pt	Platinum
Rh	Rhodium
Ru	Ruthenium
RuO_xH_y	Ruthenium oxide (wet)
Si	Silicon
SiO_2	Silicon dioxide
Ta	Tantalum
TaN	Tantalum nitride

Polyphenols

ElGa	Ellagic acid
GaAc	Gallic acid
MeGa	Methyl gallate
PhGl	Phloroglucinol
PhGlAc	Phloroglucinic acid
PyGa	Pyrogallol
PyGa 4-COOH	Pyrogallol 4- carboxylic acid

Techniques

ASV	Anodic stripping voltammetry
CV	Cyclic voltammetry
DPV	Differential pulse voltammetry
LSV	Linear sweep voltammetry
OCP	Open circuit potential or equilibrium potential

Constants and Symbols

a	Absorptivity coefficient
A	Measured absorbance
b	Path length
c	Concentration of the analyte
c	Velocity of the light = 3 X 10^8 m/s
eV	Electron volts
E_a	Anodic peak potential
E_c	Cathodic peak potential
E_{corr}	Corrosion potential
F	Faraday's constant = 96495 coulombs
h	Planck's constant = 6.626068 X 10^{-34} m^2 kg/s
i_a	Anodic peak current
i_c	Cathodic peak current
i_{corr}	Corrosion current
I_o	Intensity of the incident light
I	Intensity of the light after passing the analyte (or sample)
N_a	Avogadro number (6.0234 x 10^{23})
ν	Frequency of the radiation
Ω	Ohms
R	Universal gas constant = 8.314 J K^{-1} mol^{-1}
Φ	Work function of a metal in eV

Terms

AFM	Atomic force microscope
ALD	Atomic layer deposition
ATR	Attenuated total reflectance
BDE	Bond dissociation energy
CMP	Chemical mechanical planarization
CMOS	Complementary metal oxide semiconductor
CE	Counter electrode
DL	Double layer
ECD	Electro chemical deposition
EM	Electro migration
FTIR	Fourier transform infra red
HER	Hydrogen evolution reaction

IHP	Inner helmholtz plane
IC	Integrated circuit
ILD	Interlayer dielectrics
IHB	Internal hydrogen bonding
IRE	Internal reflection element
ITRS	International technology road map for semiconductors
ML	Monolayer
OHP	Outer helmholtz plane
OPD	Over potential deposition
ORR	Oxygen reduction reaction
PVD	Physical vapor deposition
RE	Reference electrode
RC	Resistive capacitance
STM	Scanning tunneling microscope
SoC	System on chip
TOF	Time of flight
THBA	Trihydroxyl benzoic acid
ULSI	Ultra Large scale integration
UV Vis	Ultra violet visible
UPD	Under potential deposition
WE	Working electrode
XANES	X-ray absorption near edge structure
XPS	X-ray photoelectron spectroscopy

CHAPTER 1

INTRODUCTION

Science has always motivated me to find something new from my research experiments. This dissertation is the compilation of my findings which I have done in the Interfacial Electrochemistry and Materials Research Lab (IEMR) at the University of North Texas under the guidance of Dr. Oliver M. R. Chyan. In the first part of my research (chapter 2), electrodeposition of copper (Cu) on ruthenium (Ru) and the affinity of Ru to form different oxides on its surface will be discussed in detail. Furthermore, the influence of the thin layer of oxide on Ru in Cu electrodeposition will be focused. Second part of my research (chapter 3) is dedicated in the investigation of bimetallic corrosion of Cu and different barrier layer substrates like Ru, tantalum (Ta), tantalum nitride (TaN) in different trihydroxyl substituted benzene antioxidants. Understanding the interaction between the antioxidants and Cu with Ru or Ta as underlying substrates is complex and various factors involved in this system were investigated in detail. Finally, chapter 4 summarizes and gives an outlook of the research from chapters 2 and 3.

1.1 Copper Interconnects

On 22 September 1997, IBM announced its full scale manufacture of chips that use Cu rather than Aluminium (Al).[1] Copper interconnects were first implemented in IBM's seventh generation CMOS (complementary metal oxide semiconductor) technology. The electrical resistance of copper interconnects is less than two thirds of Al

interconnects. Also Cu has higher electro migration (EM) resistance compared to Al which made its position strong for the interconnect replacement.[2,3]

1.2 Dual Damascene Process

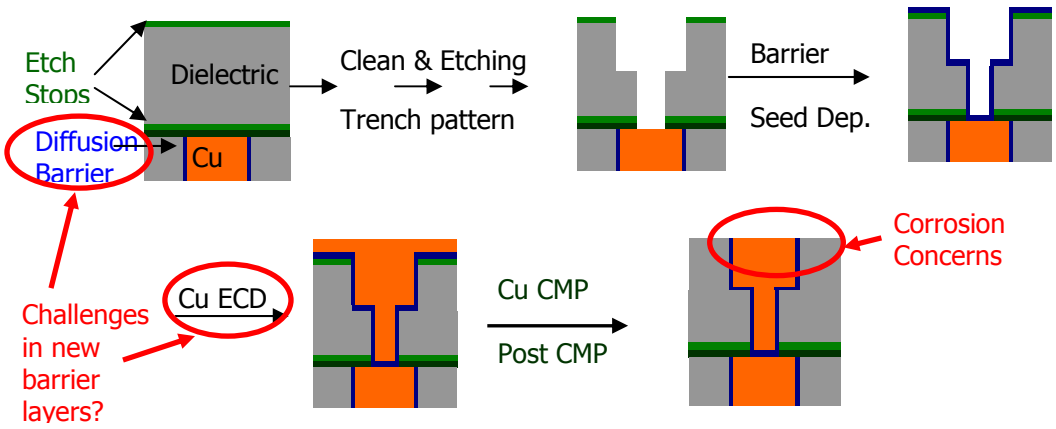

Figure 1.1 Simplified dual damascene process used in IC fabrication to build multilevel metal (copper) interconnections.

Integrated circuits (ICs) find wide applications in computers, TV, cell phones, and other electronic devices. Without integrated circuits, modern computing including the internet, communications, manufacturing systems, all will be extinct. Digital revolution bought by the integrated circuits is a history in mankind. However fabricating ICs is not simple. The method of building ICs is the dual damascene fabrication process which can be broadly classified into front end and back end processes.[5,6] Dual damascene is used to make multilevel, high density metal interconnections, needed for sophisticated and high performance ICs. Front end involves the construction of silicon (Si) based

interlayer dielectrics (ILDs) components by different techniques like lithography, etching, baking, doping etc. Back end process primarily involves the deposition of different metal layers like Ta/TaN followed by Cu and planarization of the top over-bump Cu surface. Figure 1 show the brief procedure involved in the dual damascene process.

1.2.1 Challenges in Copper Diffusion Barriers

Earlier Cu was directly deposited on silicon dioxide (SiO_2) ILDs. Copper has a higher affinity of forming silicides with Si even at low temperatures 300^oC and eventually leading to the failure of Cu interconnects.[7,8] To prevent Cu diffusing into Si, a bimetallic layer comprising of Ta/TaN was used.[9-12] The need of TaN is to bind Ta to SiO_2 and Cu cannot bind well on nonmetallic TaN. Presently, the trend of miniaturization continues in Cu interconnects technology and the chip dimensions keep shrinking in ultra large scale integration (ULSI). The difficulty in scaling down the thickness of the bimetallic layer is driving the microelectronics industry to find a new barrier layer. Recent results from different research groups have shown that Pt group metals like ruthenium (Ru), osmium (Os), and iridium (Ir) can act as better copper diffusion barrier.[13-19] On 2003, Chyan et al.[13] and Moffat et al.[14] proposed Ru as the novel copper diffusion barrier with the importance of Ru forming a conductive platform for Cu electrodeposition. More recently Arunagiri et al. have shown that 5 nm of Ru can even stop Cu diffusion into Si till 450^oC.[20] However new findings show that Ru with its higher affinity to form oxide on its surface may cause gross failure of the Cu interconnects.[21]

Hence my primary research focused on investigating the interfacial binding between Cu and Ru by electrodeposition of Cu on Ru and its oxides. Detailed discussions are drafted in chapter 2. Two electrochemical techniques namely the open circuit potential and potentiodynamic technique cyclic voltammetry were used in this study.

1.2.2 Issues of Bimetallic Corrosion during Planarization

After the deposition of Cu interconnects on trenches, the next step is planarizing the Cu surface. Two steps are involved in this process. Chemical mechanical planarization (CMP) is the first step to planarize any overfills or bumps of Cu. CMP combines the usage of mechanical force from polishing pads with different chemicals to treat and polish the Cu surface.[22] The chemicals used in CMP are referred to as "slurry" primarily consisting of an oxidant, abrasive particles (Al_2O_3) and a corrosion inhibitor. Hydrogen peroxide is widely used as the oxidant to oxidize Cu surface since oxides of Cu can be easily removed with less mechanical pressure. Abrasive is used to accelerate the removal of Cu. Benzotriazole (BTA) is used as an inhibitor to form a passivation layer on Cu to prevent further corrosion thereby optimizing the removal of Cu layer from the surface. CMP is usually done at low pH (acidic) conditions. Post CMP is the next step which involves cleaning to remove any organic residues adsorbed on the Cu surface during the CMP process. The alkaline cleaning post-CMP solution (pH 9-12) consists of a quaternary ammonium hydroxide, an organic amine, a corrosion inhibitor, an organic acid and water. Organic acids like gallic acid, ascorbic acid, catechol, pyrogallol, and dihydroxybenzoic acids are widely used.[23-25] The primary function of the

organic acids is to serve as antioxidants thereby protecting Cu from oxidation during the post CMP step. Chapter 3 investigates the interaction of different antioxidants with the Cu. Also during CMP and post CMP step, the underlying layer of Cu is the barrier layer which is also exposed to different slurries and bimetallic contacts are made. CMP of Cu on Ta has been well studied. Information on CMP of Cu with underlying new barrier layer like Ru is scarce and hence the purpose of the research in investigating bimetallic corrosion of Cu/Ru comparing Cu/Ta was carried out. In these study different techniques like open circuit potential, cyclic voltammetry, differential pulse voltammetry, tafel plots, ultraviolet visible spectroscopy, and microscopy were used for characterization of different chemicals and their interaction with Cu.

1.3 Techniques Used

Based on the different techniques used in this dissertation, this section is classified into two divisions (1) Electrochemistry and (2) Spectroscopy.

1.3.1 Electrochemistry

1.3.1.1 Birth of Electrochemistry

The 16^{th} - 18^{th} centuries marked the beginning of the understanding of electrical systems from the work done by different scientists like William Gilbert, Otto Von Guericke, Charles Augustin de Coulomb, Luigi Galvani and Alessandro Volta. Galvani discovered that muscle and nerve cells produce electricity by dissecting a frog in a table where he had been conducting static current which was dubbed as galvanism. By the modifications of Galvani's experiments, it was Volta who built the first battery which

became known therefore as voltaic pile. With the first invention of battery, more research was driven in this field of applying current in studying different chemical reactions which eventually became the subject of electrochemistry.

1.3.1.2 Introduction

Hence electrochemistry is a branch of chemistry that studies the reactions between the boundary of an electronic conductor and an ionic conductor. The electronic conductor (or a metal) is technically termed as working electrode and the ionic conductor constitutes the solution (or the electrolyte) which contains different ionic species. Each metal immersed in the same electrolyte takes up different potential which is referred to as electrode potential. In electrochemistry, one cannot measure the absolute potentials, only the difference can be measured in reference to another electrode or the reference electrode. With the modifications of the application of potential lead to the discovery of different voltammetric techniques. Voltammetry is a family of techniques with the general characteristics that the potential of the working electrode is controlled and the current flowing through the electrode is measured. It is usually employed to study the kinetics and mechanisms of electrode reactions when immersed in an electrolyte. Changing different working electrodes with the solution can be done to study the nature of solution species only when the current is passed. Voltammetric techniques like cyclic voltammetry (CV), linear sweep voltammetry (LSV), normal pulse voltammetry, differential pulse voltammetry (DPV), anodic stripping voltammetry (ASV) are widely used in microelectronic applications. For examples, CV

helps us to study metal electrodeposition on foreign metal substrates, LSV helps us to study the tendency of one metal to corrode or passivate in a corrosive environment by measuring the corrosion current and potential, DPV helps to identify the nature of species formed on oxidation or reduction and ASV is widely used for the analysis of trace metals on the surface of an electrode.

1.3.1.3 Metal Solution Interphase

A brief view on the widely accepted model of interphase structure when metal immersed in a solution (aqueous) will be described in this context. Different metal solution interface modes were proposed by Helmholtz, Gouy-Chapman and Stern. In the Helmholtz model the excess charges in the solution were constrained to only one plane closer to the metal surface. Then Gouy and Chapman independently proposed a new model by removing the restriction thereby allowing for the statistical, potential dependent distribution of ions in the solution side of the double layer. Gouy Chapman model didn't fit when concentrated solutions were used. Once again a new theory is called for. Stern model is the combination of Helmholtz and Gouy Chapman theories wherein some ions of excess charges are constrained to single plane close to the metal while others are statistically distributed into the solution. According to Gouy Chapman and Stern theories, all univalent electrolytes should behave in the same way. This is not the case when electrolytes like NaCl, NaBr, KI were used which shows species specific behavior. In order to interpret this specific behavior, Grahame proposed a new model of the metal solution interface – the triple layer model (Figure 2).

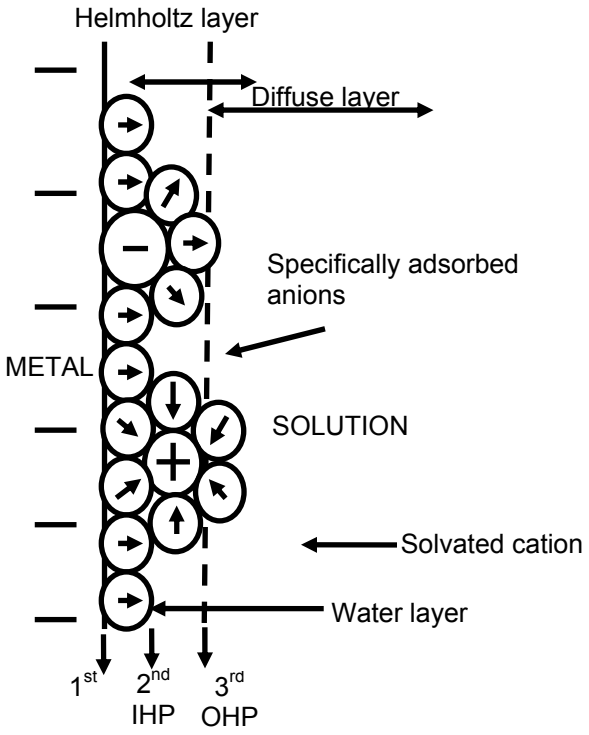

Figure 1.2 Triple layer model proposed by Grahame.

The basic idea in this model is anions gets dehydrated and thus get closer to the electrode. Each anion undergoes different extent of dehydration which eventually leads to the specific behavior of the anions. Ions that are partially or fully dehydrated are closer to the electrode. This contact adsorption of ions allows short range forces between the metal electrode and the ions in addition to the electrostatic coulombic forces. Grahame's model is a modification of Stern's model with the introduction of the inner plane of closest approach or inner Helmholtz plane (IHP). The IHP contains partially or fully hydrated specifically adsorbed ions. The plane of closest approach with only the fully hydrated ions is called outer Helmholtz plane (OHP).

1.3.1.4 Electrochemical Cell

Two electronic conductors (electrodes) in an electrolyte constitute an electrochemical cell. The electrolyte can be either aqueous or non-aqueous depending on the nature of the system to be studied. As an electric current passes, it must change from electronic current to ionic current and back to electronic current. These changes of current modes are always accompanied by oxidation and reduction reactions which are spatially separated. Conventionally the two electronic conductors in an electrochemical cell are referred to as working electrode (W.E) and counter electrode (C.E). To measure the potential of the working electrode, a reference electrode (R.E) is used. The complete configuration of an electrochemical cell is shown below.

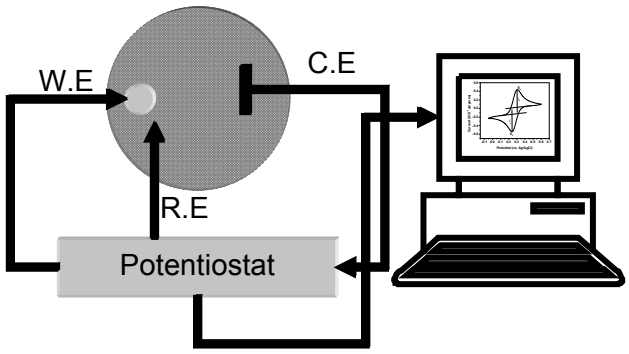

Figure 1.3 Three electrode configuration for electrochemical measurements.

1.3.1.5 Types of Electrodes

Working electrode can either serve as a cathode or anode depending on the nature of the potential applied. When negative potential is applied, the working electrode is said to be cathodic and when positive potential is applied, it is said to be in anodic state. In some contexts (e.g., potentiometry), working electrodes are also

referred as indicator electrodes as they don't take part in chemical reactions. Usually platinum (Pt) and other noble metal electrodes serves this purpose and the potential measured across this electrode can be used for the determination of the concentration of a species in this solution. Counter electrode is used to make an electrical connection to the electrolyte so that a current can be applied to the working electrode. When reduction takes place on the surface of the working electrode, it leads to the oxidation or the dissolution of the counter electrode. To prevent the dissolution of the counter electrode, noble metals (inert in nature) are used. Counter electrodes are also called as auxiliary electrode. An electrode which has a stable equilibrium potential can be used as reference electrode. Reference electrode serves as the reference point to measure the potential of the working electrode. Some common reference electrodes are the silver/silver-chloride electrode, calomel electrode and hydrogen electrode. Usually small changes in the equilibrium potential are always accompanied depending on the electrolyte with more time of usage because of the presence of liquid junction potential. The liquid junction potential can be greatly minimized by using high concentrations of the electrode filling solution. For example in silver/silver-chloride electrode, 3 M KCl is used as the electrode filling solution.

1.3.1.6 Preparation of a Working Electrode

This section describes the step-wise procedure to prepare any metal electrode. Metallic shots from ESPI® (http://www.espi-metals.com/) were used for the electrode preparation. Solder the metal shot using a cut copper wire. Now the metal shot with the

wire is placed in a conical or cylindrical shaped plastic mold. The mold consists of 2 openings on each face. The front face has a wider opening while the back face has a smaller opening. Along the side a small hole is drilled using 5/64 inch drill bit. The smaller hole is for the copper wire connector. For insulating the metal shot, epoxy is poured into the mold and then cured for 24 hours to remove the mold. Epoxy is prepared by mixing resin and hardener in the ratio of 100:14. Removing the mold leaves the metal shot with Cu wire connector. At this stage, the metal shot is ready for the next step namely the "polishing." Polishing is usually done to flatten the surface using abrasive pads (Allied ®, Allied High Tech Products http://www.alliedhightech.com/) of increasing different grit sizes from 600 microns to 1 micron. Care should be taken while polishing to avoid any scratches on the surface and to obtain mirror finish. For abrasive action, poly diamond suspension liquids (Allied High Tech products) are also used along with lubricants. After the mechanical polishing, some electrodes might require electrochemical cleaning. During the electrochemical cleaning, both negative and positive potentials are applied to the indicator electrode and thereby activating the surface.

1.3.1.7 Electrochemical Techniques

The following electrochemical techniques were used for the whole dissertation study.

A. Open circuit potential
B. Cyclic voltammetry

C. Tafel plots

The later 2 techniques are generally referred to as voltammetric techniques. In second chapter, open circuit potential and cyclic voltammetry was used to investigate Cu electrodeposition on Ru and its oxides. In third chapter along with the above electrochemical techniques, spectroscopic techniques were used.

1.3.1.7. A. Open Circuit Potential

Open circuit potential (OCP) or the equilibrium potential is defined as that electrical potential of an electrode measured against a reference electrode when there is no current applied to an electrochemical cell. OCP reflects the stability of a metal when immersed in an electrolyte. Any change in the OCP value indicates the change in the nature of the metal surface.

1.3.1.7. B. Cyclic Voltammetry

Cyclic voltammetry is a type of potentiodynamic electrochemical measurement and the graph obtained from this technique is called cyclic voltammogram (CV). In this technique, the voltage across a metal is varied in a solution and the change in current in measured.

Cyclic voltammetry is used for studying the redox properties of chemicals (organic and inorganic) and interfacial structures. For this measurement, a three electrode cell (see section 1.3.4) is used. The potential is measured between the working electrode and the reference electrode. The current is measured between the

working electrode and the counter electrode. Usually Pt foil is used as the counter electrode. The data obtained is plotted as current (i) vs. potential (V). The combination of the solvent, electrolyte and working electrode material establishes the potential range (or window). A typical CV is shown in the figure. Negative and positive potential regions compared to the equilibrium potential are termed as "cathodic" and "anodic" respectively.

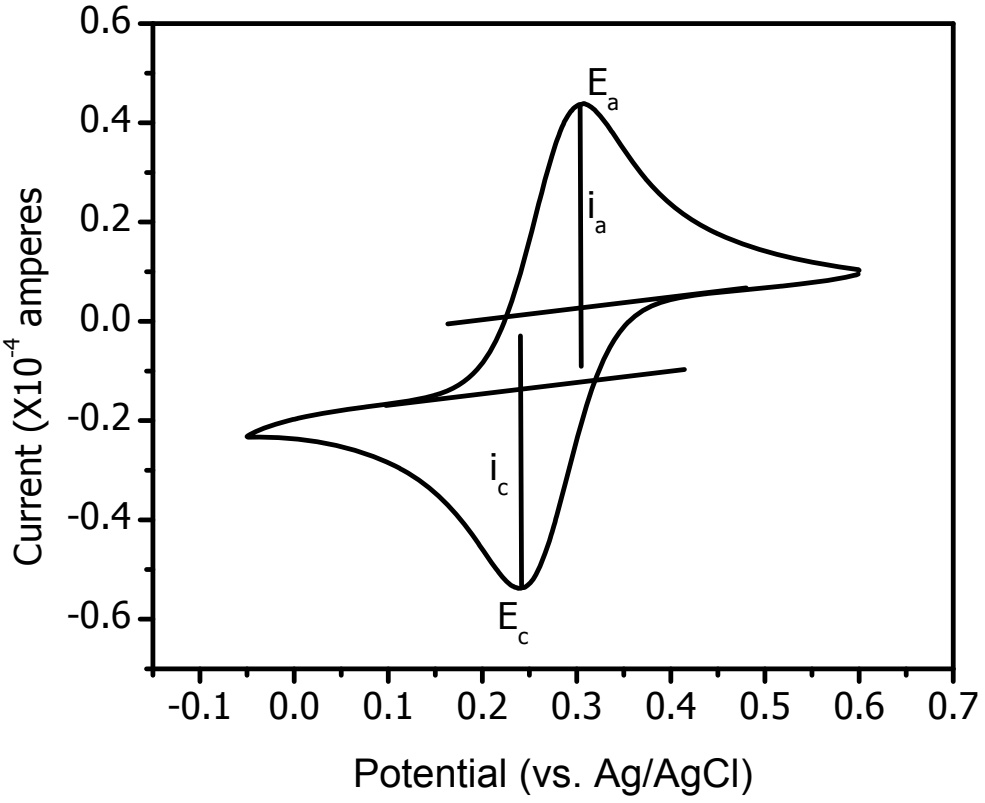

Figure 1.4 Representation of a cyclic voltammogram. E_a – anodic peak potential; E_c – cathodic peak potential; i_a – anodic peak current and i_c – cathodic peak current.

The application of cathodic and anodic potential can be explained by a simple example by immersing a noble metal electrode platinum (Pt) in sulfuric acid. A metal

say Pt is immersed in a solution containing only the supporting electrolyte and then electrochemical potentials were applied to record CV. Applying cathodic potentials make the metal surface to carry negative charge due to the abundant availability of electrons near the surface. The supporting electrolyte contains only hydrogen ions (protons), bisulfate anions and protons with positive charge will move near the negatively charged metal surface. Protons tend to gain electrons from the surface resulting in the evolution of hydrogen which is the main reaction in the cathodic regime. However if anodic potential is applied to the metal, the surface gets oxidized due to the interaction between positively charged platinum with water. However when the electrolyte contains metal ions in the solution apart from the hydrogen evolution and oxidation reactions, metal ions will interact with the surface. Scanning to cathodic potential reduces the metal ions on the Pt surface. The reduction of metal ions to deposit metal is called electrochemical deposition (ECD). Scanning to positive potentials will strip any deposited metal on the Pt surface and this process is called stripping.

Two different electrodeposition phenomena namely the underpotential deposition (UPD) and overpotential deposition (OPD) of metals are well known. Underpotential deposition is a specific type of electrodeposition of a metal on a foreign metal at potentials less negative than the Nernst potential of the deposition reaction. UPD will be favorable only if a strong interaction exists between the two metals. For example, Nernst potential for Cu/Cu^{2+} is around 0.06 V_{SHE} and UPD of Cu on Ru takes place prior to 0.06 V. Deposition followed by UPD or after Nernst potential is termed as OPD resulting in the deposition of metal overlayers. Overpotential deposition as the name

signifies an additional potential or overpotential to force the electrode reaction to proceed at a required rate. Discussion of Cu UPD and OPD on Ru and its oxides will be discussed in Chapter 2.

1.3.1.7. C. Tafel Plots

Tafel plot is an electroanalytical technique from which information relating to the corrosion potential (E_{corr}) and current (i_{corr}) can be obtained.

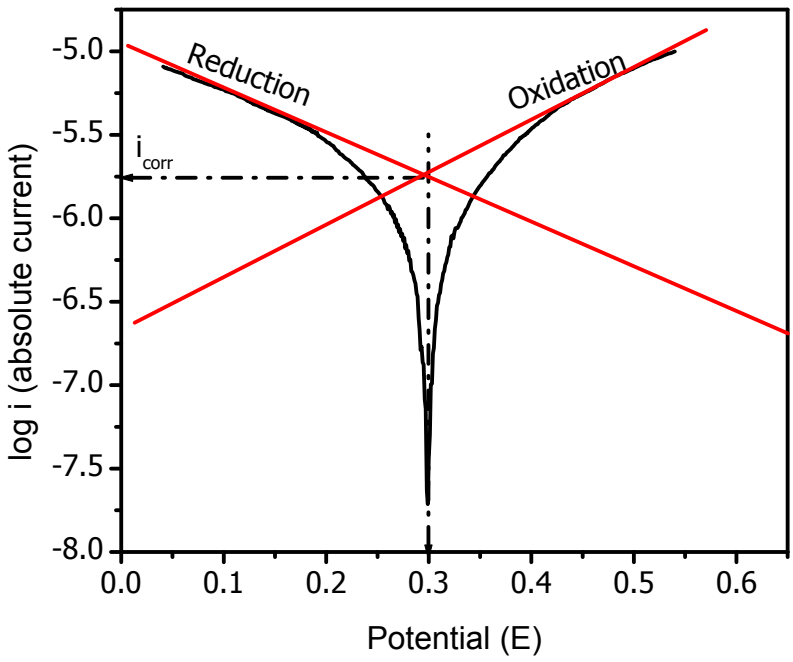

Figure 1.5 Representation and extrapolation of a tafel plot. i_{corr} – corrosion current and E_{corr} – corrosion potential.

From E_{corr} and i_{corr} values, one can determine the corrosion rate, passivity and pitting susceptibility. Using a potentiostat, graph based on Butler Volmer equation can be drawn for logarithmic of current vs. potential. The instrument is set for a series of

different parameters like potential, sensitivity, scan rate etc., The initial potential is set close to the OCP of the metal in the test solution or electrolyte and potential ranges are set to OCP ± 250 mV.

In chapter 3, E_{corr} values of different metals like Cu, Ru and Ta are used to determine the noble or active nature of the electrode in different conditions.

1.3.2 Spectroscopy

Matter consists of atoms, molecules, or ions which is capable of absorbing, emitting or scattering electromagnetic radiation. Electromagnetic radiation is a kind of energy transmitted through space at high velocities. Radiation includes electromagnetic vibrations of ultraviolet, visible, infra red (IR), X-rays and γ (gamma) rays. UV Vis, IR radiations correspond to low frequency region whereas X- and γ- rays correspond to high frequency regions. Spectroscopy is the branch of science dealing with the study of interaction of matter with electromagnetic radiation. Using the above phenomena one investigate qualitatively or quantitatively of the physical process. The interaction of electromagnetic radiation with matter can cause transitions between the electronic energy levels.

1.3.2.1 UV Vis Spectroscopy

Ultraviolet and visible (UV Vis) absorption spectroscopy corresponds to electronic excitations between the energy levels in the molecular orbitals of the system due to the absorption of electromagnetic radiation in the range from 200-800 nm.

When white light passes through a colored substance, portion of different wavelengths are mixed and absorbed. The remaining light will then assume the complementary color to the wavelength's absorbed. The colors of the visible light spectrum and their wavelength interval with the color wheel are:

Violet: 400 – 420 nm; Indigo: 420 – 440 nm; Blue: 440 – 490 nm; Green: 490 – 570 nm; Yellow: 570 – 585 nm; Orange: 585 – 620 nm; and Red: 620 – 780 nm

Figure 1.6 Representation of a color wheel.

Thus absorption at 440-470 nm renders a substance orange whereas absorption at 650-800 nm renders a substance green. Green is unique and sometimes it can have absorption near to 400 nm.

When a molecule absorbs radiation, its energy increases and this increase in energy is given by,

$$E = h\nu = \frac{hc}{\lambda}$$

Where,

h – Planck's constant

ν – Frequency of the radiation

λ – Wavelength of the radiation

c – Velocity of the light

The intensity of the light absorption is expressed in a form referred to as Beer-Lambert law. The law states that the fraction of the incident light absorbed is proportional to the number of molecules in the light path.

$$A = abc = \log \frac{I_0}{I}$$

Where,

A – Measured absorbance

a – Absorptivity coefficient

b – Path length

c – Concentration of the analyte

Io – intensity of the incident light

I – intensity of the light after passing the analyte (or sample)

Beer's law is not ideal and deviates due to different reasons as described below:

1. Environment such as temperature, pressure and solvent
2. Instrumental errors due to stray radiation, stability of the source, slit control, reliability of the optical accessories
3. Chemical deviations such as presence of complexing agents, chemical equilibrium, pH etc.,
4. Change in refractive index of the sample at high concentration

Usually when a molecule is excited, there may be three changes like:

1. Energy change due to transition of an electron from an orbit to another orbit
2. Energy change due to rotation of the molecule as a whole
3. Energy change due to vibration of atoms within in the molecule

Changes from the rotation of the molecule involve small energy and spectra obtained are found in the far infra red region. Vibrations of atoms within in the molecule induce energy change to little higher and can found in the near infra red region. Energy changes due to electronic transitions are found in the UV Vis region due to considerable higher amount of energy involved. Excitation of outer electrons arises due to the absorption of UV or Visible radiation. Usually three types of electronic transition are involved:

1. Transitions involving π, σ and n electrons
2. Transitions involving charge-transfer electrons
3. Transitions involving electrons in d and f orbitals

n → π*, and π → π* transitions are the two lowest energy ones are achieved by the energies available in the 200 to 800 nm spectrum.

UV Vis spectroscopy is highly important to study the transitions involving π orbitals and lone pairs (non-bonding) occurring in conjugated systems which have stronger absorption tendency. The following terms are very often applied to UV Vis spectra:

1. Bathochromic shifts – Shift to longer wavelength
2. Hypsochromic shifts – Shift to shorter wavelength
3. Hyperchromic shift – Shift to greater absorbance
4. Hyprochromic shift – Shift to lower absorbance

Extending conjugation usually results in the bathochromic and hyperchromic shifts due to the influence of π-π* transitions. Conjugation is most common in aromatic

systems. Organic groups undergoing n- π* and π-π* transitions are classified as chromophoric groups or chromophores. Also UV Vis spectra are greatly employed in inorganic chemistry to study complexation between metal ions and ligand species. Complexation is the tendency for metal ions and ligand to bond such that the coordination sphere of the particular ion is filled. Three types of transitions originate due to complexation:

1. Excitation within the ligand
2. Excitation of the metal ions
3. Charge transfer excitation

From the UV Vis spectra, one can find the stoichiometric ratio and formation constant between the metal ions and the ligand. Mole ratio method is employed for the determination of stoichiometric ratio. In this method, the absorbances are measured for a series of solutions containing varying amounts of one constituent with a constant amount of the other. A graph is drawn for absorbance vs. $\frac{M^{2+}}{M^{2+}+L}$. The intersection of the lines gives the stoichiometric ratio of the complex.

1.3.2.2 FTIR ATR Spectroscopy

Chapter 3 use fourier transform infrared spectroscopy (FTIR) with attenuated total reflectance (ATR) to observe the formation of different oxidized species of gallic acid. Infrared spectroscopy is the study of the infrared radiation with matter which typically exists in the range of 4000-400 cm^{-1}. As seen in UV Vis due to electronic transitions, in FTIR spectrum is obtained based on the energy transition due to vibration

within the molecule. A molecule can vibrate in number of ways depending on the number of atoms and thus the number of bonds it contains. The functional groups present in the sample absorb infrared radiation at different regimes depending on its vibrational frequency. FTIR is a measurement technique for collecting infrared spectra by performing mathematical Fourier transform on the interferogram obtained when infrared light is guided through an interferometer. ATR is a sampling technique used in combination with FTIR using the property of internal reflection called the evanescent wave. The meaning of "evanescent" is "tend to vanish" and thus the short lived evanescent wave decays exponentially with distance. Interaction of the evanescent wave with the interface leads to IR absorption and signal enhancement for each internal reflection. FTIR combined with ATR is a powerful technique allowing for discernment of monolayers (ML's) of species absorbed on the Si ATR crystal. To be used as an internal reflection element, the material should possess high refractive index like silicon, germanium, diamond and zinc selenide. For this study a metal (Cu) thin film of 2 nm thickness was deposited on Si crystal by evaporation technique. The bevel edges of the Si crystal were cut and micron polished at 45^{o} as shown below.

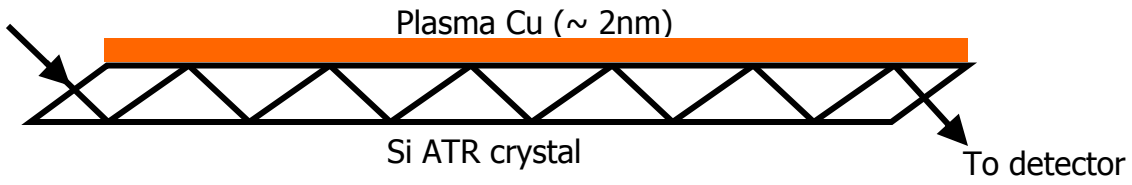

Figure 1.7 Internal reflection element (IRE) used in chapter 3.

1.4 References

1. Edelstein, D.; Heidenreich, J.; Goldblatt, R.; Cote, W.; Uzoh, C.; Lustig, N.; Roper, P.; Mcdevitt, T.; Motsiff, W.; Simon, A.; Dukovic, J.; Wachnik, R.; Rathore, H.; Schulz, R.; Su, L.; Luce, S.; Slattery, *J. IBM Semiconductor Research and Development Center*, Hopewell Junction, NY, USA. Technical Digest - International Electron Devices Meeting, **1997,** 773-776.
2. Hu, C.K; Harper, J. M. E, *Materials Chemistry and Physics*, 52, **1998**, 5-16.
3. Hu, C. K.; Luther, B.; Kaufman, F. B.; Hummel, J.; Uzoh, C.; Pearson, D. J. *Thin Solid Films,* 262, **1995**, 84-92.
4. Lakshminarayanan, S.; Steigerwald, J.; Price, D. T.; Bourgeois, M.; Chow T. P.; Gutmann, R. J.; Murarka, S. P. *IEEE Electron Device Letters*, 15, **1994**, 307-309.
5. Peter Singer, *Semiconductor International*, 20, **1997**, 79-80 and 82.
6. Gross, M. E; Lingk, C; Brown, W. L.; Drese, R; *Solid State Technology,* **1999**, 47-52.
7. Setton, M.; Van der Spiegel, J.; Rothman, B. *Appl. Phys. Lett.,* 57, 1990, 357-359.
8. McBrayer, J. D.; Swanson, R. M., Sigmon, T. W. *J. Electrochem. Soc.*, 6, **1986**, 1242-1246.
9. Olowafe, J. O; Mogab, C. J.; Gregory, R. B.; Kottke M. *J. Appl. Phys.*, 72, **1992**, 4099-4103.
10. Wang, M. T.; Lin, Y. C.; and Chen M. C. *J. Electrochem. Soc.,* 145, **1998.**
11. Holloway, Karen and Fryer, Peter M. *Appl. Phys. Lett.*, 57, **1990**.

12. Ono, H., Nakano, T. and Ohta, T. *Appl. Phys. Lett.*, 64, **1994**.

13. Josell, D.; Wheeler, D.; Witt, C.; and Moffat, T. P.; *Electrochemical and Solid-State Letters*, 6, **2003**, C143-145.

14. Chyan, O.; Arunagiri, T. N.; and Ponnusamy, T. *J. Electrochem. Soc.,* 150, **2003**, C347-C350.

15. Chan, R.; Arunagiri, T. N.; Zhang, Y.; Chyan, O.; Wallace, R. M.; Kim, M. J.; Hurd, T. Q.; *Electrochemical and Solid-State Letters,* 7, **2004**, G154-157.

16. Josell, D.; Bonevich, J. E.; Moffat, T. P.; Aaltonen, T.; Ritala, M.; and Lekela, M.; *Electrochemical and Solid-State Letters,* 9, **2006**, C48-C50.

17. Josell, D.; Witt, C.; and Moffat, T. P. *Electrochemical and Solid-State Letters*, 9, **2006**, C41-C43.

18. Singer, Peter *Semiconductor International*, May **2004**.

19. Goswami, Ishita; and Laxman, Ravi *Semiconductor International*, May **2004**.

20. Arunagiri, T. N.; Zhang, Y.; Chyan, O.; El-Bouanani, M; Kim, M. J.; Chen, K. H.; Wu, T. C., and Chen, L. C. *App. Phys. Letters,* 86, **2005**, 083104.

21. Moffat, T. P.; Walker, M.; Chen, P. J.; Bonevich, J. E.; Egelhoff, W. F.; Richter, L.; Witt, C.; Aaltonen, T.; Ritala, M.; Leskela, M.; and Josell, D. *J. Electrochem. Soc.*, 153, **2006**, C37-C50.

22. Steigerwald, Joseph M.; Murarka, Shyam P.; Gutmann, Ronald J. *Chemical Mechanical Planarization of Microelectronic Materials,* John Wiley & Sons, New York, **1997**.

23. Chandrakant, Tambol; Banerjee, Gautam: *Alkaline post chemical mechanical planarization cleaning compositions*. Eur. Pat. Appl., **2005**, EP 1577934.

24. Naghshineh, Shahriar; Barnes, Jeff; Oldak, Ewa B: *Postchemical mechanical planarization (CMP) cleaning composition*; (ESC, Inc, USA Advanced technology materials, Inc.) US. Pat. Appl. Publ., **2001**.

25. Paunovic, Milan; Schlesinger, Mordechay *Fundamentals of electrochemical deposition,* Electrochemical Society Series, John Wiley & Sons, New York, **1998**

26. Bockris, John O'M; and Khan, Shahed U. M. *Surface electrochemistry: A molecular level approach,* Plenum press, **1993**.

27. Sharma, B. K. , *Instrumental methods of chemical analysis,* Tenth edition, GOEL Publishing house, Meerut, **1990**.

28. Skoog; West; Holler; *Fundamentals of analytical chemistry,* Eighth edition, Saunders College Publishing.

29. Rao, C. N. R. *Ultra-violet and Visible spectroscopy: Chemical applications,* Plenum press, **1967**.

CHAPTER 2

COPPER ELECTRODEPOSITION ON RUTHENIUM OXIDES

2.1 Introduction

Moore's law states that the number of transistors on a chip will double about every two years.[1] In 1965, Moore saw the future. Till May 2004, 130 nm node fabrication processes was used to make Intel® Pentium® M processors which contained 77 million transistors.[2] With the continuing drive to improve communication signal in digital computing, the break through came with the arrival of 90 nm fabrication process which contained 140 million transistors (still 130 nm process is used to make Intel Itanium Server processors). Another major break through came on March 2005 when Texas Instruments delivered first 65 nm digital baseband process and on December 2005 it qualified its 65 nm process.[3] On January 2006, the leading chip manufacturer Intel demonstrated the working of 45 nm chips for the first time and persist its focus on pushing the limits of Moore's law.[4] Followed by Intel, on June 2006 TI disclosed its 45 nm technology to take system on chip (SoC) processors to new levels increasing the performance by 30 % and reducing power consumption by 40 %.[5] Thus these drastic changes within a short period of time indicate the ongoing shrinkage in chip dimensions with increasing high aspect ratio. With this miniaturization, both the back end and front end processes are getting modified with the introduction of new components and techniques. For example, in the front end, more research has been focused on finding new low-k dielectrics which will help to minimize the RC delay.[6,7] In the back end there

is a need for a novel diffusion barrier. At present Cu/Ta/TaN/ILD forms the stack configuration for interconnect structures wherein tantalum/tantalum nitride (Ta/TaN) bimetallic layer acts as diffusion barrier in preventing copper (Cu) interconnects in mixing with the silicon (Si) based ILDs. Till date barrier films are deposited by physical vapor deposition (PVD). Tantalum forms thick tantalum oxide (Ta_2O_5) on its surface making it non-conductive for Cu electrodeposition. Hence Cu seed layer on Ta is necessary for superfilling of Cu to fill trenches and via holes in a bottom up fashion without seams or voids. Cu seed layer is deposited on Ta by PVD technique which is not easy to form a conformal layer in high aspect ratio structures. Also Ta/TaN posses scaling difficulties to cope up with miniaturization. Thus new barrier layers are called for. Platinum (Pt) group metals like ruthenium (Ru), iridium (Ir), osmium (Os), rhodium (Rh) are potential candidates for Cu diffusion barrier.[8-12] Above and beyond looking for an alternative barrier layer, research has also been driven towards atomic layer deposition (ALD) which can be an alternative to PVD in the near future. ALD is a novel technique to improve the conformal layer of barrier films on the high aspect ratio trenches. Recently ALD of Ru thin films have been widely studied.[13,14]

2.1.1 Characteristics of Ruthenium

Of all the above candidates, Ru has been studied widely due to its important characteristics like:

- Low resistivity or higher electrical conductivity
    - Ru = 7.1 μΩ cm

- Ta = 13 μΩ cm

- High melting point – 2250^{o}C
- Phase diagram shows negligible solubility with Cu till 900^{o}C[15]

2.1.2 Ruthenium as a Potential Diffusion Barrier

From all the above results it is clear that Ru possess all significant characteristics to be introduced into the integrated circuit (IC) fabrication process. Chyan et al.[8] and Moffat et al.[9] have proposed Ru as an alternative Cu diffusion barrier with the importance of the conductive nature of Ru for viable direct electrodeposition and Cu seed layer is not required. Yibin Zhang et al.[16] indicated the strong interfacial binding between Cu and Ru by demonstrating favorable underpotential deposition of Cu on Ru. Arunagiri et al.[17] have shown that 5 nm Ru film can stop Cu diffusion into Si till 450^{o}C. Recently it has been shown that ultra thin barrier metal like ruthenium and rhodium combined with nanoclustering silica resulted in 86 % less RC delay than the value listed in international technology road map for semiconductors (ITRS).[18]

2.1.3 Oxygen Affinity of Ruthenium

However Ru too has its demerits. Of all the Pt group elements, Ru has higher tendency for oxidation.[19] On exposure to atmosphere, Ru forms thin layer of oxide ~ 0.18 nm which is termed as native oxide or air exposed oxide.[20] Presence of native oxide on Ru can have detrimental effects during Cu superfilling in trenches and eventually leading to the gross failure of interconnects.[21] Electrochemistry of Ru reveals

the higher affinity for oxygen thus forming two different oxides namely the reversible and the irreversible oxides on its surface depending on the potential applied to Ru.[22] Zhang et al. showed that Ru forms a conductive oxide at + 1.3 V vs. Ag/AgCl and forms a better platform for Cu underpotential deposition (UPD) thereby improving the interfacial binding strength.[16]

2.1.4 Ruthenium Oxide

Ruthenium oxide or Ruthenium dioxide (RuO_2) has metal like electronic conductivity[23] (35 μΩ cm) originating from the partial filling of the 4d shells in its tetragonal rutile structure. Ruthenium oxide is widely used as electrodes in chlor-alkali industry. Due to its higher double layer (DL) capacitance charging current, ruthenium oxide is used as ultra capacitor to store charge.[24] Since ruthenium oxide is robust in nature, it is used as catalyst for CO oxidation in fuel cells.[25] It also has attracted wide interest in IC device applications as diffusion barrier for Al interconnects and conductive wirings.[26]

2.1.5 Broader Impacts

This chapter discusses the control growth rate of native oxide on Ru surface thereby providing the exact information to control the desired surface nature of Ru to improve its barrier performance. Besides the air exposed oxide, this study demonstrates two different electrochemical oxides on the Ru surface. For this study, both

underpotential and overpotential deposition of Cu on oxide covered Ru was used to explain the interfacial binding between Cu and Ru.

2.2 Experimental Methods

Three electrode cell setup as described in section 1.3.1.4 was used for all electroanalytical investigations. Ruthenium was used as the working electrode. Preparation of electrode is described in section 1.3.1.6. A thin Pt sheet with double the area of the working electrode constitutes the counter electrode. Ag/AgCl was used as the reference electrode and all potentials are referred against this reference electrode in this study. High purity copper sulfate pentahydrate ($CuSO_4$. $5H_2O$, 99.99 %) (Sigma-Aldrich Co., Milwaukee, WI, http://www.sigma-aldrich.com) and sulfuric acid (H_2SO_4, Mallinckrodt Inc., Hazelwood, MO, http://www.mallinckrodt.com) were used as received to prepare electrolytes. All solutions were diluted using Milli-Q® Elix 5® Ultrapure water (Millipore Corp., Bedford, MA, http://www.millipore.com). Millipore® 0.22 µm sterile microfilters (Millipore Corp., Bedford, MA, http://www.millipore.com) were used to remove organic and suspended particles from the solution. For ambient control experiments, nitrogen (N_2) and hydrogen (H_2) were prepurged into the solution for 15 minutes and during the course of the experiments, corresponding gas blanket was maintained around the cell for constant diffusion of the gas molecules into the solution. Electroanalytical measurements were performed by CHI 760 B (CH instruments, http://www.chinstruments.com/) potentiostat. Cyclic voltammograms (CV's) were performed in 0.5 M H_2SO_4 and 2 mM $CuSO_4$ + 0.5 M H_2SO_4 solutions to study the

nature of the working electrode prior to any experiment and Cu electrodeposition respectively. Charge values from CV were automatically calculated by the software for the operation of CHI 760 B.

2.3 Results and Discussions

2.3.1 Activation of the Ru Surface

Freshly polished Ru electrode immersed in N_2 purged 0.5 M H_2SO4 yields an open circuit potential (OCP) of 0.45 V. Cyclic voltammogram (CV) was obtained by sweeping the potentials from OCP to more cathodic till -0.4 V and back to anodic regime till 0.47 V. Scanning to negative potentials indicates the evolution of hydrogen gas and at positive potentials oxide will be formed on the Ru surface. Another consecutive cycle was obtained at the same potential limits after the completion of the first scan. Figure 2.1 shows the successive 1^{st} and 2^{nd} scan CV's recorded at a scan rate of 50 mV/s. A reduction wave ca. -0.15 V can be seen in the 1^{st} scan which is completely absent during the 2^{nd} scan. The disappearance of the reduction wave on scanning to more negative potentials indicates the removal of oxide layer present on the freshly polished Ru surface. This process of making the surface free of oxide by the application of negative potentials is termed as "activation" and the surface is said to be "activated."

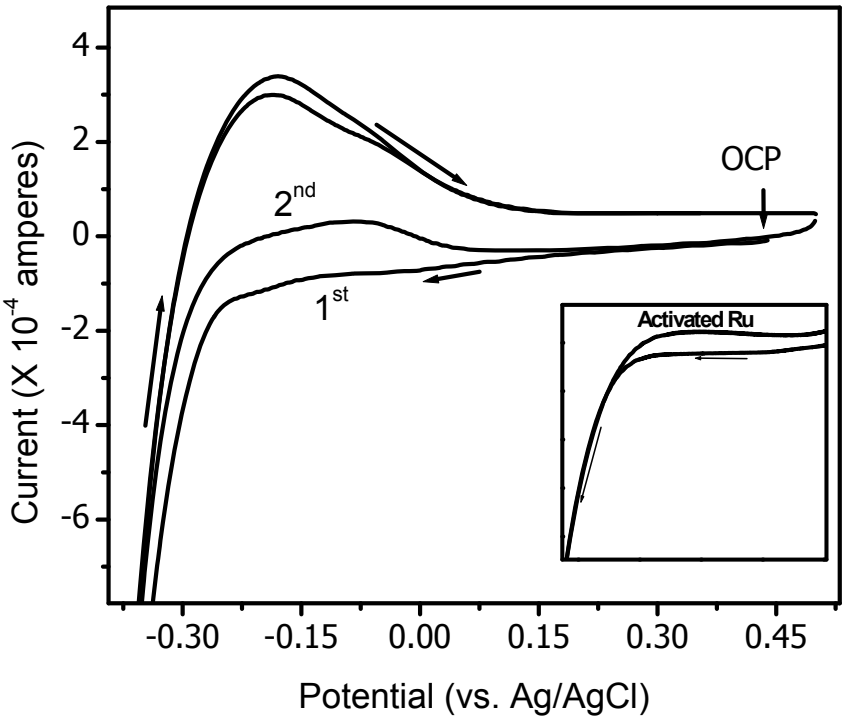

Figure 2.1 CV of freshly polished Ru in N_2 purged 0.5 M H_2SO_4 solution. The scan rate is 50 mV/s. *Insert:* CV of activated Ru in N_2 purged 0.5 M H_2SO_4.

Of course, after polishing the Ru surface is exposed to atmosphere but only for a short period of time (less than a minute). Also the amount of oxygen present in the solution is greatly minimized by purging N_2 into the solution. Insert in figure 2.1 is the CV of activated Ru in N_2 purged 0.5 M H_2SO_4 solution. Activation of Ru was done by holding the electrode at negative potential -0.2 V for 2 minutes. CV shows the decreased charging capacitance current background due to the absence of oxide on the activated Ru surface. Therefore the rapid formation of oxide layer on Ru surface is attributed to the air exposed effect and it is clear that the thin layer of oxide is always present on a freshly polished Ru surface. The air formed oxide on Ru will be termed as

"native oxide" in this chapter. Other experiment by iodine adsorption was done to confirm the presence of oxide layer on Ru surface. Freshly polished Ru on immersion in 1 mM KI didn't favor chemisorption of iodine due to the oxide layer present on the surface and activated Ru can chemisorb iodine.[27]

2.3.2 Growth of Native Oxide

Similar electroanalytical experiments as described above were done on 24 hr (1 day) exposed Ru electrode. The cathodic current (or charge) of the native oxide reduction wave was higher indicating the presence of thicker oxide on Ru which had formed due to prolonged exposure in air. To determine the approximate time period of complete coverage of oxide layer on Ru surface, CV's were recorded for different time exposures and charge was calculated. Since polycrystalline Ru electrode was used, polishing each time prior to air exposure will result in non-homogenous surface. As a result the surface homogeneity was achieved by polishing Ru electrode only once and activation was done each time prior to exposure in air at different time intervals. Again activation was done by holding Ru electrode at -0.2 V in N_2 purged 0.5 M H_2SO_4 for 2 minutes.

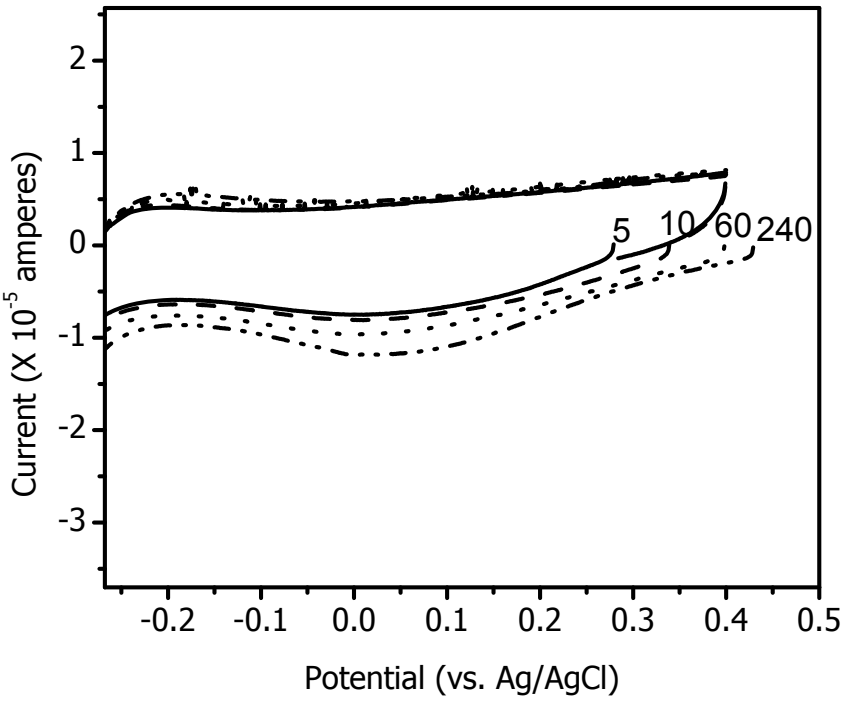

Figure 2.2 CV of activated Ru exposed in air at different time intervals 5, 10, 60 and 240 minutes.

Figure 2.2 shows the CV of activated Ru exposed to different time intervals from 5 minutes to 4 hrs. However the final time of exposure was recorded at 24 hrs (not shown). It can be clearly seen that the cathodic current increases for increasing time of exposure. Figure 2.3 is the combined plot of OCP and charge of native oxide reduction recorded at different times of exposure.

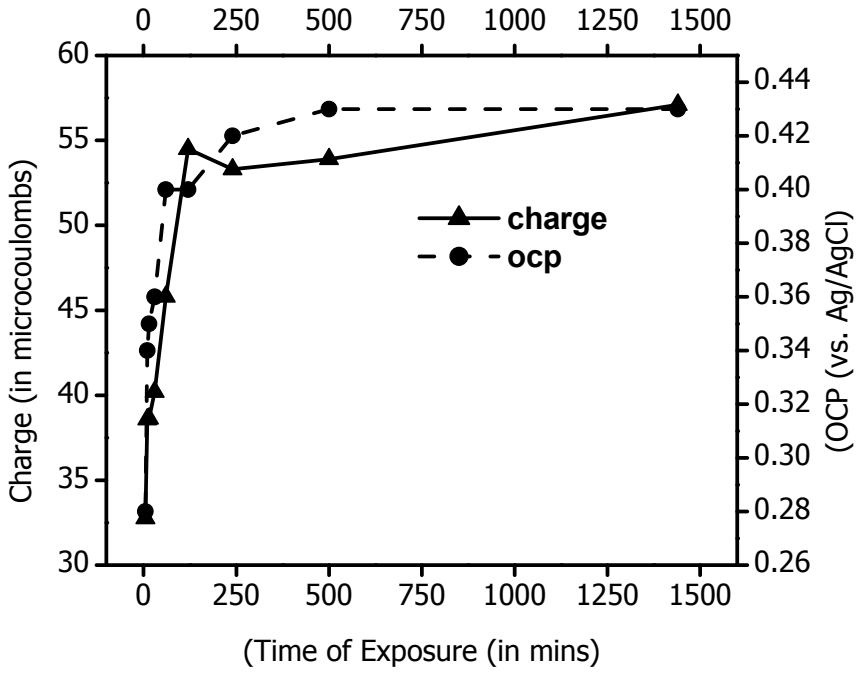

Figure 2.3 Pooled data of OCP and native oxide reduction charge vs. time of exposure of activated Ru in air.

The importance of this study lies in understanding the rapid formation of native oxide on Ru surface during its exposure to atmosphere and uniform coverage is obtained when exposed for 6 hours. Rapid formation of oxide layer is due to the higher oxygen affinity of Ru. At this moment, the oxidation state of Ru native oxide is unknown and more work has to be done to understand the chemical nature of native oxide. X-ray photoelectron spectroscopy (XPS) can be a very useful tool to predict the oxidation state by comparing the shift in the binding energy for native oxide covered Ru with pure metallic Ru. Also, imaging techniques like scanning tunneling microscope (STM) and atomic force microscope (AFM) can reveal about the coverage of oxides on the

surface. In the forthcoming section, one can understand that the presence of thin layer of native oxide can drastically affect metal deposition.

2.3.3 Electrodeposition of Cu on Air Exposed Ru

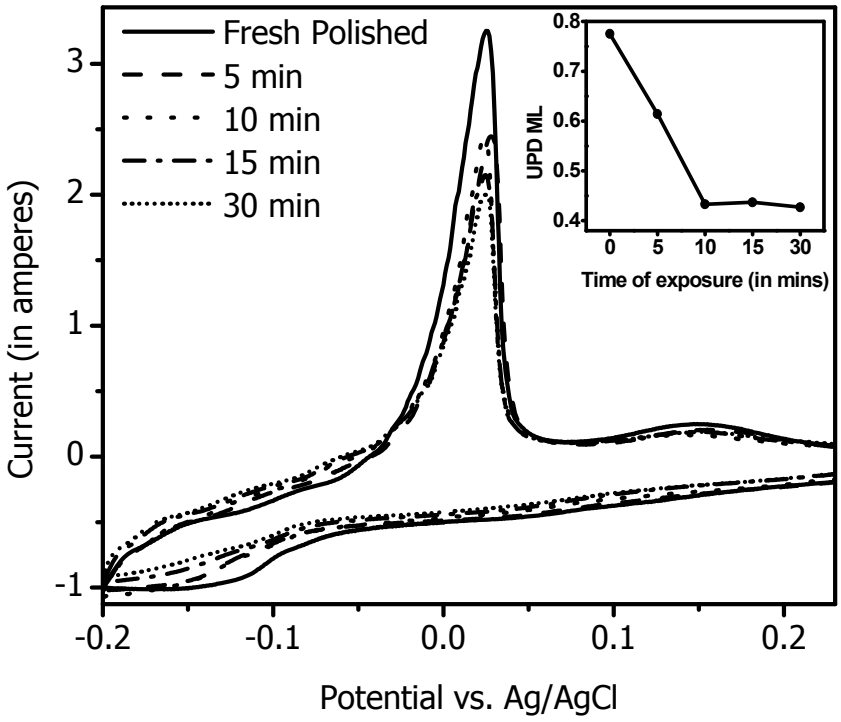

Figure 2.4 CV of Ru and its native oxides in N_2 purged 2 mM $CuSO_4$ + 0.1 M H_2SO_4. Scan rate is 20 mV/s. *Insert:* Cu UPD ML coverage on Ru and oxides formed at different time of exposure.

Cu electrochemical deposition (ECD) on Ru was done by immersing the Ru electrode in N_2 purged 2 mM $CuSO_4$ with 0.5 M H_2SO_4 as the supporting electrolyte. Native oxide was grown on Ru by exposing it in atmosphere at 5, 10, 15, and 30 minutes. CV's of Cu deposition in freshly polished Ru and its native oxide is shown in

the figure 2.4. Cu electrodeposition on Ru can be discussed under two classifications - underpotential deposition (UPD) and overpotential deposition (OPD). Underpotential deposition is a specific type of electrodeposition of a metal on a foreign metal at potentials positive to the Nernst potential of the metal deposition reaction.

In general, Nernst equation can be written as:

$$E = E^{o} - \frac{RT}{nF} \ln \frac{[Reduced]}{[Oxidized]}$$

$$E = E^{o} - \frac{0.0591}{n} \log \frac{[Reduced]}{[Oxidized]}$$

Where,

E – Nernstian potential

E^{o} – Standard electrode potential

R – Universal gas constant = 8.314 J K^{-1} mol^{-1}

T – Temperature in Kelvin

[Reduced] – Concentration of the reduced species

[Oxidized] – Concentration of the oxidized species

n – Number of electrons involved in the reaction

F – Faraday's constant = 96495 coulombs

For Cu electrodeposition, Nernst equation is given by,

$$E = 0.34 - \frac{0.0591}{2} \log \frac{[Cu^{2+}]}{[Cu]}$$

$$E = 0.34 - 0.02955$$

$$E = 0.2602 V_{SHE} \sim 0.06 V_{Ag/AgCl}$$

Cu electrodeposition on Ru happens at potential prior to 0.06 V vs. Ag/AgCl and is referred to as UPD followed by Cu overlayers. The oxidation peak of Cu OPD and UPD is centered on 0 V and 0.15 V respectively. In UPD only few monolayer's of the respective metal atoms are deposited onto a foreign metal substrate. The number of monolayer's can be determined from the charge of the UPD or its oxidation given by,

$$ML = \frac{QN_a}{nFA * 10^{15}}$$

Where,

ML – Number of monolayer's obtained

Q – Charge obtained from oxidation of Cu UPD in coulombs,

N_a – Avogadro number (6.0234×10^{23})

n – Number of electrons involved in the deposition of copper (n=2)

F – Faradaic constant, 69495 coulombs

A – Area of the working electrode, cm^2

For a freshly polished Ru surface, 0.78 ML of Cu UPD was obtained. However oxide present on the Ru surface greatly decreased the ML coverage of Cu UPD by 40 % (see insert in fig 2.4). Thus the presence of native oxide reduces the interfacial binding between Cu and Ru.

2.3.4 Activation of Ru by Hydrogen

A replacement to potentiodynamic activation of Ru involves the immersion of the electrode into H_2 purged 0.5 M H_2SO_4 solution. OCP decreases gradually from 0.45 V to

0.05 V and then rapidly reaching -0.29 V. The gradual decrease in the OCP is ascribed to the slow reduction of native oxide from the Ru surface by proton/hydrogen (H^+/H_2) interaction.

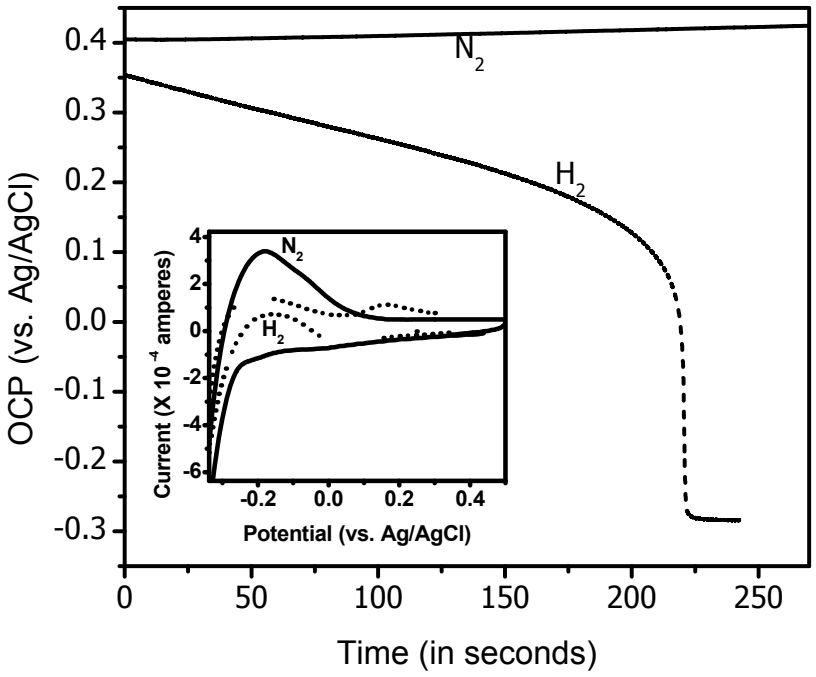

Figure 2.5 - OCP of freshly polished Ru in H_2 purged 0.5 M H_2SO_4 is pinned at -0.29 V due to H^+/H_2 interaction with the surface. *Insert:* CV indicates the absence of native oxide reduction in H_2 environment.

Also CV recorded in H_2 environment indicates complete absence of native oxide reduction wave indicating spontaneous activation of Ru by the removal of oxide layer from its surface.

2.3.5 Electrochemical Oxide Formation

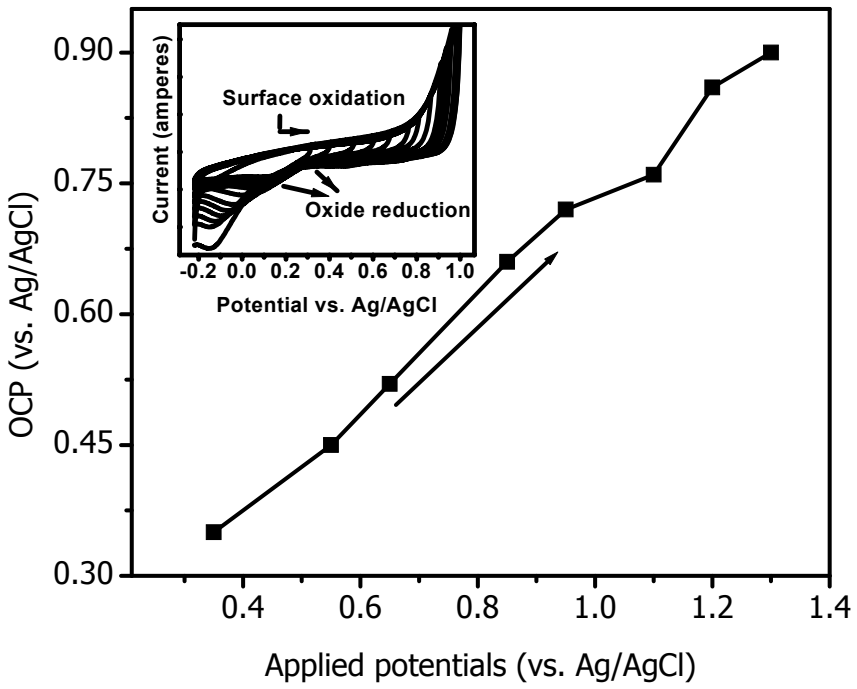

Figure 2.6 - OCP of RuO_xH_y formed at different anodic potentials in N_2 purged 0.5 M H_2SO_4. *Insert:* Progressive scanning CV of Ru showing the higher affinity for oxygen with the onset of oxidation at low positive potentials.

Electrochemical oxides are formed on Ru (RuO_xH_y) by holding the electrode in 0.5 M H_2SO_4 at positive potentials from 0.55 to 1.3 V for 30 seconds and OCP was measured as shown in figure 2.6. Figure 2.7 shows the optical images of RuO_xH_y. Oxide formed at 1.3 V showed clear grain boundaries on its surface. On electrochemical oxidation, two different oxides are formed on Ru surfaces. Oxides formed at potentials less than 1.1 V are reversible and can be reduced on activation. However oxide formed greater than 1.2 V are irreversible which can be reduced at more negative potentials.

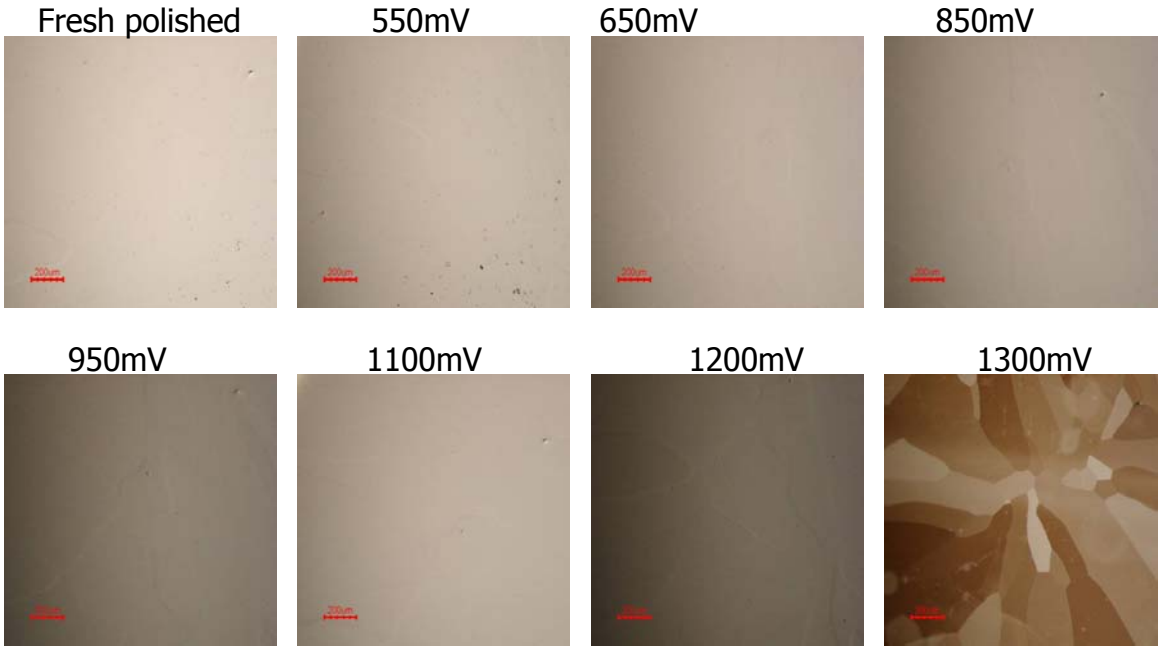

Figure 2.7 - Optical images of RuO_xH_y on freshly polished ruthenium surface.

Especially oxide formed at 1.3 V which is stable in acidic conditions, needs higher mechanical force on polishing step. Thus irreversible oxides are practically robust in nature.

2.3.6 Cu ECD on RuO_xH_y

It is interesting to investigate the Cu UPD on Ru as a function of the oxide forming electrochemical potential. RuO_xH_y were formed as described in the above section and Cu electrodeposition was done by immersing the oxide covered Ru electrode in 2 mM $CuSO_4$ + 0.5 M H_2SO_4. Figures 2.8 and 2.9 are the CV's obtained from the oxidation of Cu OPD and UPD.

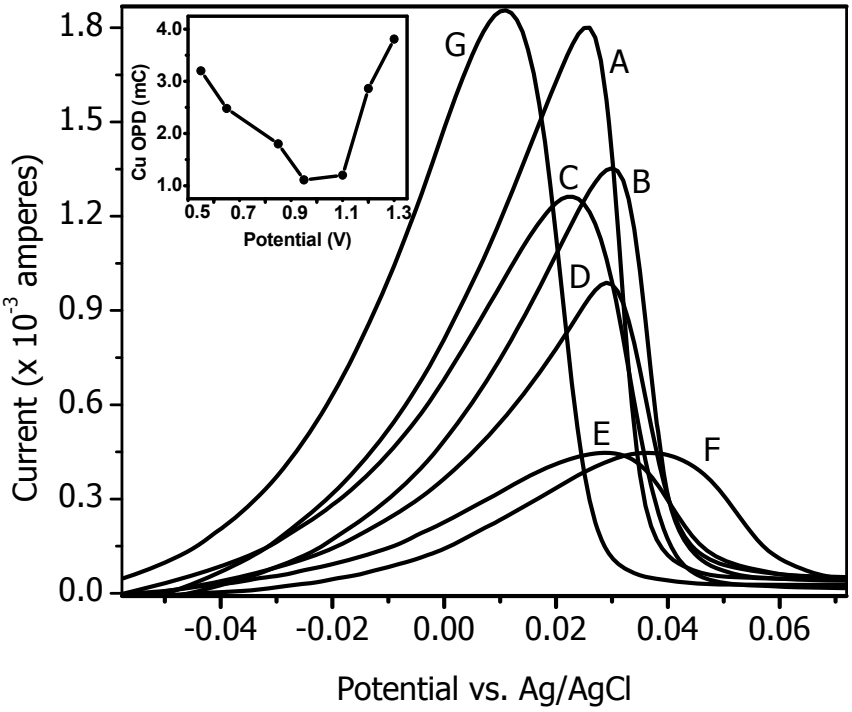

Figure 2.8 - Anodic stripping by the oxidation of RuO_xH_y in 2 mM $CuSO_4$ + 0.5 M H_2SO_4 at a scan rate of 20 mV/s. Oxide formed at A – 0.55 V; B – 0.65 V; C – 0.85 V; D – 0.95 V; E – 1.1 V; F – 1.2 V; G – 1.3 V.

Charge calculations for Cu OPD and ML coverage for Cu UPD indicate that the reversible oxide (< 1.1 V) hinders Cu deposition whereas irreversible oxide (> 1.1) favors Cu deposition. "V" profile for Cu UPD (see insert in figure 2.9) indicates that 1.1 V wherein Cu UPD is completely absent acts as a transition between reversible and irreversible oxides of Ru.

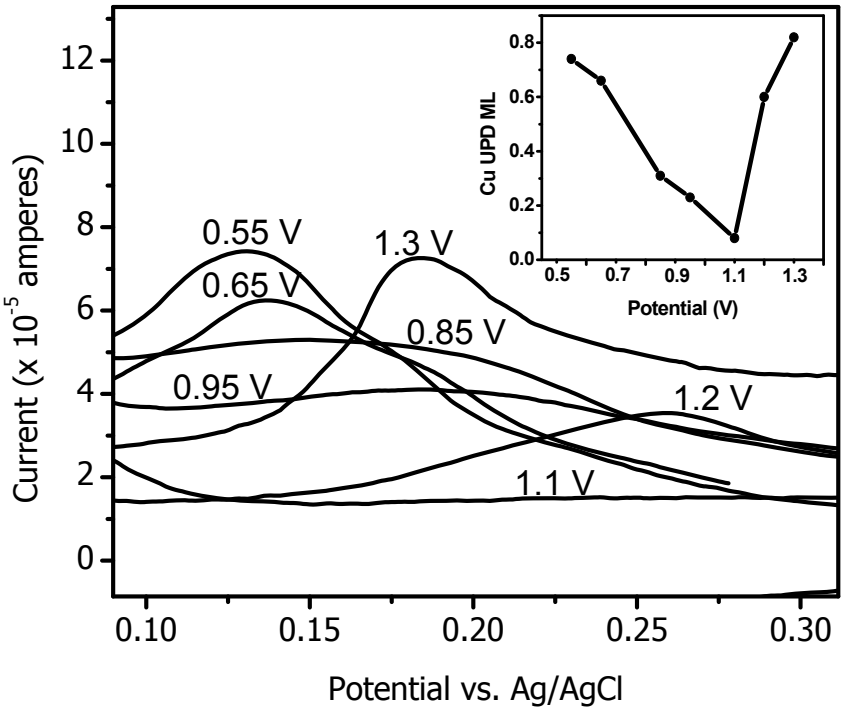

Figure 2.9 - Anodic stripping of Cu UPD on RuO_xH_y. *Insert:* V-profile in Cu UPD ML coverage showing no Cu UPD at $RuO_xH_{y,1.1\ V}$ as the transition value.

2.3.7 UPD Shift

UPD of a metal on another foreign metal substrate depends on the difference in work function between the two metals. Kolb et al.[28] found that

$$\Delta U_p = 0.5\Delta\Phi$$

Where ΔU_p – underpotential shift in volts and

$\Delta\Phi$ – Work function difference between the two metals in eV.

UPD shift (ΔU_p) is calculated by the difference in the anodic peak potentials of Cu OPD and UPD ($\Delta U_p = E_{bulk} - E_{upd}$). The consequence of the above equation is that, for

UPD to occur, the work function of the substrate should be larger than the work function of the UPD metal:[29]

$$\Phi_{subs} > \Phi_{upd}$$

The atomic number of Ru is 44 which has an electronic configuration of [Kr] $4d^7$ $5s^1$ and falls under the category of Pt group metals. Besides Ru and Pt, the other Pt group metals are rhodium (Rh), palladium (Pd), osmium (Os), iridium (Ir). Since the 4d orbitals are partially filled, Ru can accept electrons from oxygen. It has been previously shown that the oxidation tendency of Pt group metals follows:[19]

Ruthenium > Rhodium > Iridium > Palladium > Platinum

Work function of a metal can be defined as the minimum energy needed to remove an electron to a point immediately out of the solid. Upon insertion of oxide to the metal, the work function increases. Hartmann reported the difference in the work function for Ru and its oxides.[30] For metallic ruthenium, work function is 4.6~0.1 eV and 4.9-5.0 eV for completely oxidized Ru at +4 oxidation state. Bottcher and Niehus have shown an increase in 1.3 eV to the work function of clean Ru(0001) which is ca. 5.3-5.4 eV.[31] Also during deposition, the work function can change. Christmann reported the work function change for Ru from 4.5 eV to 4.9 eV during Cu deposition.[32]

Figure 2.10 show the collective diagram of UPD shift and energy for the Cu ML deposition on Ru calculated from the first cyclic voltammogram.

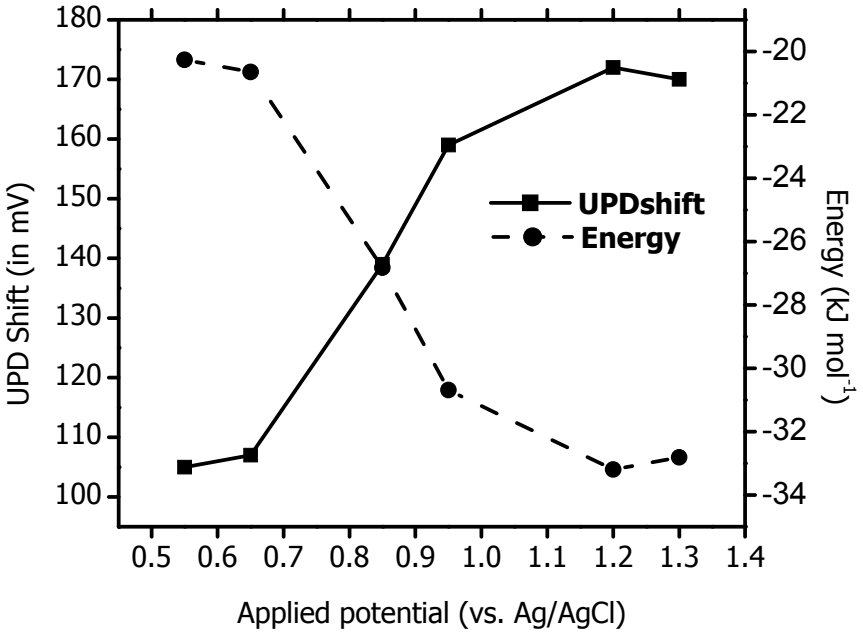

Figure 2.10 - UPD shift and energy calculated from the stripping peaks separation between Cu OPD and UPD.

With positive increase in the oxide forming potentials, UPD shift also increases indicating a stronger interfacial binding between Cu and oxide covered Ru surface. Nguyen Van Huong reported the similar observation in positive shift in the Cu UPD.[33] Quiroz suggested that the electron density of adjacent metallic Ru sites has been modified by the adsorbed oxygen in turn affecting Cu UPD.[34] High UPD shift for the oxide formed on Ru at +1.3 V indicates the stronger interfacial binding than Cu and metallic Ru by 12 kJ mol^{-1}.

2.4 Conclusion

Oxide formation on Ru when exposed in atmosphere has been studied in detail. Its effect on Cu UPD was shown by the decrease in ML coverage. Other than air exposed oxide formation on Ru, growth of two different electrochemical oxides namely the reversible and irreversible oxides on Ru have been shown by varying the anodic potentials. From the decrease in Cu UPD ML coverage, reversible oxides behave similarly to native oxide. Oxide formed at 1.1 acts as the transition potential. More work in understanding the oxidation state of Ru has to be done. Probably Ru formed at 1.1 V holding potential might be in +3 state which can be confirmed by X-ray photoelectron spectroscopy (XPS) or X-ray absorption near edge structure (XANES) studies. However irreversible oxide formed at 1.3 V on Ru at +4 oxidation state form a more conductive platform for Cu electrodeposition. Increase in Cu UPD ML indicates the structural change on the Ru surface by oxidation which can be used to improve the Ru barrier performance by inserting RuO_xH_y as a diffusion plug between Cu and Ru.

2.4 References

1. Moore's law, http://www.intel.com/technology/mooreslaw/ (retrieved 06/27/07)
2. Wasson, S. Intel's Pentium 4 Prescott processor Plus Northwood's last ride, http://techreport.com/reviews/2004q1/p4-prescott/index.x?pg=1 (retrieved 06/27/07)

3. Microprocessor Quick Reference Guide, http://focus.ti.com/docs/pr/pressrelease.jhtml?prelId=sc05262 (retrieved 06/27/07)
4. Intel First to Demonstrate Working 45 nm Chips, http://www.intel.com/pressroom/archive/releases/20060125comp.htm (retrieved 06/27/06)
5. Texas Instruments 45-Nm Chip Manufacturing Process Doubles Output Per Wafer, http://focus.ti.com/docs/pr/pressrelease.jhtml?prelId=sc06117 (retrieved 06/27/06)
6. Singer, Peter *Semiconductor International*, **1996**, 88-90, 92, 94, 96.
7. Ho, Paul S.; Lee, Ki-Don; Yoon, Sean; Lu, Xia; Ogawa, Ennis T.; *Materials Science in Semiconductor Processing,* 7, **2004**, 157-163.
8. Chyan, O.; Arunagiri, T. N.; and Ponnusamy, T. *J. Electrochem. Soc.,* 150, **2003**, C347-C350.
9. Josell, D.; Wheeler, D.; Witt, C.; and Moffat, T. P.; *Electrochemical and Solid-State Letters*, 6, **2003**, C143-145.
10. Josell, D.; Bonevich, J. E.; Moffat, T. P.; Aaltonen, T.; Ritala, M.; and Lekela, M.; *Electrochemical and Solid-State Letters,* 9, **2006**, C48-C50.
11. Josell, D.; Witt, C.; and Moffat, T. P. *Electrochemical and Solid-State Letters*, 9, **2006**, C41-C43.
12. Goswami, Ishita; and Laxman, Ravi *Semiconductor International*, May **2004.**

13. Kim, K. S; Lee, Y. S.; Lee W. S.; Hwang G. W.; Hwang, C. S.; Lee, J. W.; Jeong J. *J. Electrochem. Soc.,* 154, **2007**, D95-D101.

14. Kwon, Se-Hun; Kwon, Oh-Kyum; Min, Jae-Sik; and Kang, Sang-Won *J. Electrochem. Soc.,* 153, **2006**, G578-G581.

15. Massalski, Thaddeus B. *Binary alloy phase diagrams,* Materials park, Ohio : ASM International, c**1990**.

16. Zhang, Y.; Huang, L.; Arunagiri, T. N.; Ojeda, O.; Flores, S.; Chyan, O.; and Wallace R. M. *Electrochem. Solid-State Lett.,* 7, **2004**, C107-C110.

17. Arunagiri, T. N.; Zhang, Y.; Chyan, O.; El-Bouanani, M; Kim, M. J.; Chen, K. H.; Wu, T. C., and Chen, L. C. *App. Phys. Letters,* 86, **2005**, 083104.

18. Singer, Peter *Semiconductor International,* April **2007**, 28.

19. Yeung, Ho; Chan, H.; Zou, S.; and Weaver, M. J.; *J. Phys. Chem. B*, 103, **1999**, 11141-11151.

20. Liu, J.; Lei, J.; Magtoto, N.; Rudenja, S.; Garza, M.; Kelber, J. A.; *J. Electrochem. Soc.,* 152, **2005**, G115-G121.

21. Moffat, T. P.; Walker, M.; Chen, P. J.; Bonevich, J. E; Egelhoff, W. F.; Richter, L.; Witt, C.; Aaltonen, T.; Ritala, M.; Leskela, M.; and Josell, D.; *J. Electrochem. Soc.,* 153, **2006**, C37-C50.

22. Hadzi-Jordanov, S.; Angerstein-Kozlowska, H.; Yukoyic, M.; and Conway, B.E *J. Electrochem. Soc.,* 125, **1978**, 1471-1480.

23. Krusin-Elbaum, L.; and Wittmer, M. *J. Electrochem. Soc.,* 135, **1988**, 2610.

24. Conway, B.E *Electrochemical Supercapacitors,* Kluwer-Plenum, New York, **1999**.

25. Lin, W.F.; Jin, J. M.; Christensen, P. A.; and Scott, K. *Electrochim. Acta*, 48, **2003**, 3815.

26. (a) Kolawa,E.; So, F. C. T.; Pan, E. T.; and Nicloet, M. A.; *Appl. Phys. Lett.,* 50, 1987, 854 and (b) Maeder, T.; Muralt, P.; Sagalowicz, L.; and Setter, M. *J. Electrochem. Soc.,* 146, 1999, 3393.

27. Zhang, Y.; Ojeda, O.; Venkataraman, S.; Chyan, O. *ACS Meeting-in- Miniature*, University of Texas at Arlington, Arlington, TX (April **2005**)

28. Kolb, D. M.; Przasnyski, M.; and Gerischer, H. *J. Electroanal. Chem. Interfacial Electrochem.,* 54, **1974**, 25

29. Bockris, John O'M. and Khan, Shahed U. M. *Surface electrochemistry: A molecular level approach,* Plenum press, pp. 379

30. Hartmann, A. J.; Neilson, M.; Lamb, R. N.; Watanabe, K.; *Appl. Phys. A,* 70, **2000**, 239-242.

31. Böttcher, Artur; and Niehus, Horst *Physical Review B,* 60, **1999**, 14 396-404

32. Christmann, K.; Ertl, G.; and Shimizu, H.; *J. Catal.,* 61, **1980**, 397.

33. Van Huong, N. C.; and Gonzalez-Tejera, M. J. *J. Electroanal. Chem.,* 244, **1988**, 249.

34. Quiroz, M. A.; and Meas, Y. *J. Electroanal. Chem. Interfacial Electrochem.,* 157, **1983**, 165.

CHAPTER 3 – BIMETALLIC CORROSION OF Cu/Ru: EFFECT OF TRIHYDROXYL SUBSTITUTED BENZENES

3.1 Introduction

Corrosion can be defined as the loss of the essential properties in a material when exposed to its surroundings. Well known example is the corrosion of iron (Fe) by oxidation on exposure to air. The corrosion product is called the rust (usually Fe (III) oxide) and the process is called rusting. Corrosion eventually leads to the gross failure of the material and damage will be significant in economy. Even though the material loss is quite common during corrosion, some corrosion products can stop further corrosion. For example, patination takes place on metal surfaces like copper and brass when exposed to atmosphere and presence of patina layer on the metal surfaces significantly stops further corrosion.[1,2] Another well known example is the passivation of metal surfaces by the formation of an oxide layer preventing further corrosion.[3,4]

Bimetallic corrosion or galvanic corrosion can be defined as the corrosion associated from an electrical coupling of two different metals in an electrolyte containing active ions or species. Bimetallic corrosion results in the preferential attack of the more active metal; however the corrosion of the less active or more noble metal is inhibited. Nobility of any metal can be found in galvanic series.[5] The more active metal is referred as "anodic" and more noble metal is referred as "cathodic." The electrochemical process of bimetallic corrosion is due to the flow of positive current from the anode to the cathode through the electrolyte. Bimetallic corrosion (or galvanic

corrosion) is a common issue during chemical mechanical planarization (CMP) and post-chemical mechanical planarization (post-CMP) processes.[6,7] Copper (Cu) and underneath tantalum (Ta) on exposure to the slurry used in CMP and post CMP experience galvanic corrosion due to the difference in nobility in two different metals.[8,9] In Cu-Ta bimetallic system, Cu is cathodic and Ta is anodic one will expect Cu not to corrode. However in the electrochemical process of bimetallic corrosion, some of the copper oxidizes to give copper ions which reduce back to copper by gaining the electrons released during Ta oxidation. However the reduced back copper can deposit on Ta leading to the failure of the interconnect lines. With the current trend of miniaturization leading to find an alternative to Ta/TaN diffusion barrier, understanding CMP and post CMP of Cu with underneath novel barrier layer is necessary. In this study, ruthenium (Ru) is used as the novel diffusion barrier layer. For the Ru CMP, data's available in the literature are scarce[10] and more investigation is called for. Bimetallic corrosion of Cu/Ru is evaluated and compared with Cu/Ta, Cu/TaN and Cu/Si bimetallic systems. Electrolytes used for this investigation are antioxidants which are widely used in the post CMP process.[11,12]

Antioxidants undergo autoxidation by scavenging oxygen in the solution and hence antioxidants play a major role in post CMP by minimizing the oxygen attack on Cu surface. Different polyphenols with mono, bi or tri hydroxyl substituted benzenes are used as antioxidants.[11,12] The first step in the oxidation is the abstraction of hydrogen from hydroxyl group forming semiquinone radical species and further oxidation results in the formation of stable oxidized species in quinonic form.[13,14] The rate of dissociation

or the abstraction of hydrogen can be enhanced by increasing pH of the solution.[15] In some polyphenols, oxidation in more alkaline conditions leads to the formation of oligomers which have higher tendency for scavenging oxygen and hydroxyl radicals present in the solution.[16,17] Presence of transition metal ions like Al^{3+}, Fe^{3+}, Cu^{2+} can catalyze the oxidation of polyphenols.[18-21] Not all polyphenols can act as good antioxidants. It depends on various factors like bond dissociation energy (BDE), internal hydrogen bonding (IHB) between OH groups, position of OH groups, presence of electron withdrawing or releasing groups.[22-26] Besides the antioxidant activity, polyphenols can also act as chelating agent for different transition metal ions.[27-31]

This chapter investigates the influence of trihydroxyl substituted benzenes on the corrosion of Cu in contact with different substrates like Ru, Ta, TaN and Si. Gallic acid (3,4,5-trihydroxybenzoic acid), commonly used as a polyphenol antioxidant in post CMP, is selected as the model compound in this corrosion study.[10,11] Our data indicate that Cu receives no protection but instead actively being corroded in gallic acid under alkaline conditions (7 <pH < 11) similar to that of the post CMP clean. Other trihydroxyl substituted benzenes like pyrogallol, methyl gallate, phloroglucinic acid, pyrogallol 4-carboxylic acid, and ellagic acid were also studied. Our experimental results suggest that solution chemistry of polyphenol antioxidants and the bimetallic contacts with underlying substrates plays a determining role on the Cu corrosion observed.

3.2 Structures of Different Compounds used

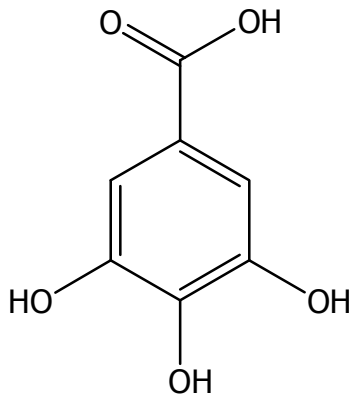

Gallic acid
(Model Compound)

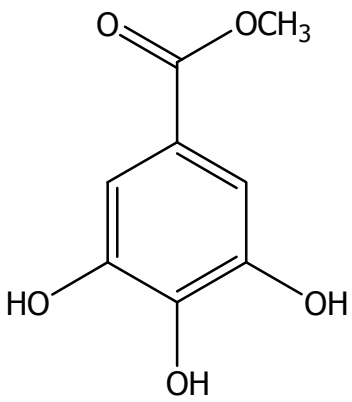

Methyl gallate

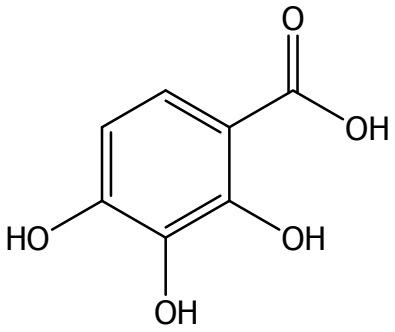

Pyrogallol-4-carboxylic acid

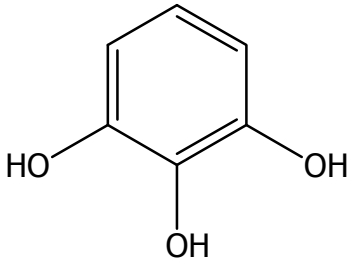

Pyrogallol

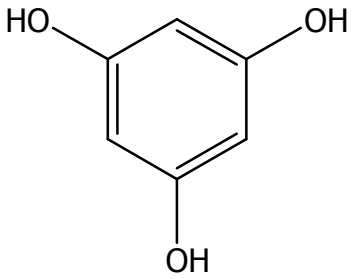

Phloroglucinol

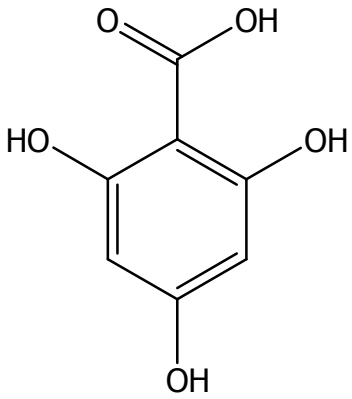

Phloroglucinic acid

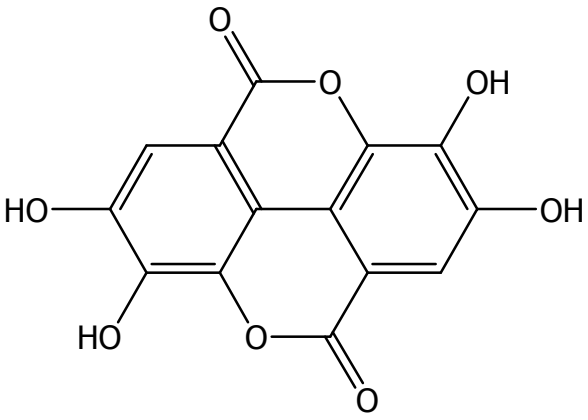

Ellagic acid

3.3 Experimental Setup

Ruthenium thin film (30 nm) was deposited on Si wafers using an in house standard magnetron RF sputtering system. Unpatterened tantalum and tantalum nitride wafers (50 nm Ea.) were obtained from Texas Instruments (TI). Cu was deposited using a vacuum evaporator (Jeol® Inc., www.jeol.com,). Current of 18 amperes was applied to the tungsten filament (Ernest F. Fulam, Inc. www.fullam.com, Latham, NY) to heat the copper target for the metal evaporation. Gallic acid (98% Fluka Chemicals), pyrogallol (99% Acros Organics), methyl gallate (99 % Acros organics), phloroglucinic acid (95 % Acros Organics), phloroglucinol (99+%, Acros Organics), pyrogallol 4-carboxylic acid (99% Alfa Aesar), ellagic acid hydrate (97%, Acros Organics) and potassium hydroxide pellets (EM Science) were used as received. Buffer solutions of different pH values are prepared by mixing varying volumes of 0.2 M KOH with 0.04 M acetic acid (EM Science, 99.7 %), 0.04 M boric acid (Sigma, 99%), and phosphoric acid (Fisher Scientific, 85%). Solutions of different dilutions are prepared by Millipore DI water (Millipore specs). pH of the test solution was adjusted by adding drops of 0.2 M KOH and pH was monitored using Orion pH meter. Prior to pH monitoring, the pH electrode were calibrated using pH 4, 7 and 10 buffers. Electrochemical analyses were done using CHI 760B potentiostat (CH instruments, Austin, TX, www.chinstruments.com). A glassy carbon electrode was used as working electrode in cyclic voltammetry (CV) measurement for the investigation of redox behavior of different polyphenols used. Cu, Ru and Ta electrodes of diameter of 6 mm each were used as working electrodes for Tafel plots. Working electrodes were prepared as

described in chapter 1 (Sec 1.3.1.6). Ag/AgCl and Pt foil were used as reference and counter electrodes respectively. All electrochemical potential measurements in this paper are referred against Ag/AgCl. Different ambients like N_2 and O_2 are used to carry out electrochemical measurements. To maintain constant gas environment, electrolyte was prepurged with N_2 or O_2 for 15 minutes and during the course of experiment, the corresponding gas blanket was maintained around the cell. UV-Vis spectra's for different polyphenols were obtained using Multi-Spec 1501 Shimadzu equipment (Shimadzu Scientific Instruments, Columbia, MD, www.shimadzu.com). Disposable semi-micro plastic cuvettes (Fisher Scientific, www.fishersci.com) were used to hold the solution to obtain spectrum. Nikon digital microscope eclipse ME 600 (www.nikonusa.com) was used to record high resolution optical images. For direct current measurements, Keithley 2400 source meter (Keithley Instruments, Inc., Cleveland, OH, www.keithley.com) was used. To characterize chelation between copper and gallic acid, electronic spectra were obtained by mixing $CuSO_4.5H_20$ (99.99%, J. T. Baker) in gallic acid containing solution. FTIR-ATR spectra were obtained using Bruker Equinox 55 (Bruker Optics, Billerica, MA, www.brukeroptics.com).

3.3.1 Development of Micropattern

Copper micropatterns were developed to investigate the bimetallic corrosion of Cu on different substrates. Copper microdots were obtained on Ru, Ta, TaN and Si wafers using a micropatterned mask (figure 3.1). Roughly 70 nm Cu dots of 120 microns in diameter were obtained for 3 minutes deposition (or evaporation) time.

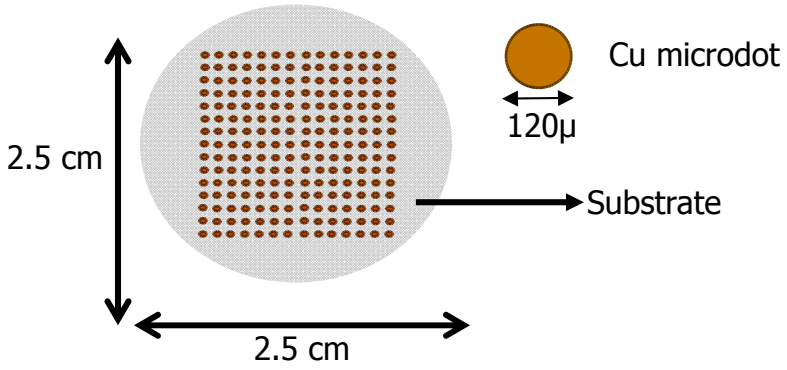

Figure 3.1 - Micropattern mask used for Copper deposition.

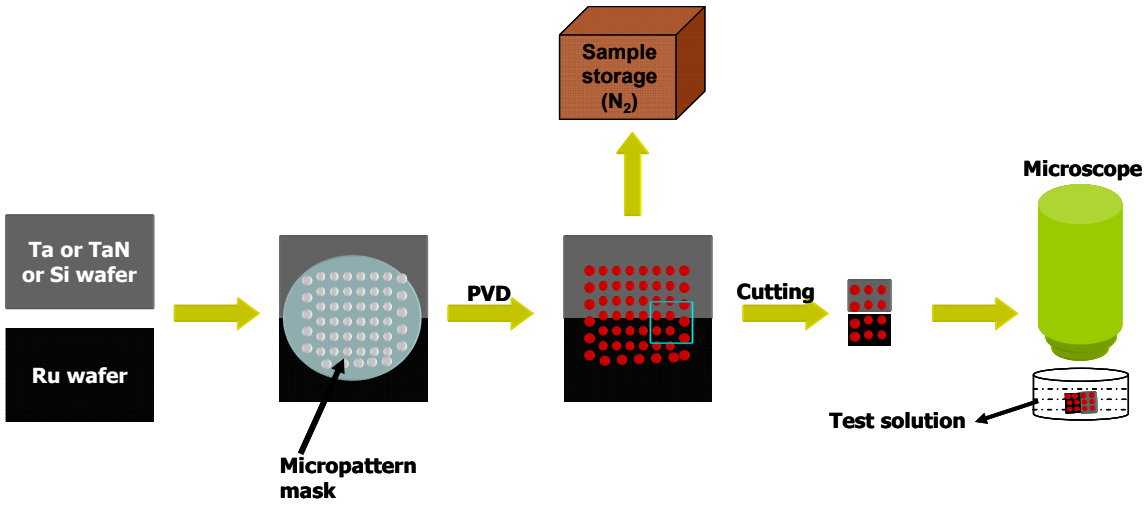

Figure 3.2 - Fabrication of bimetallic wafers for *insitu* micropattern testing.

Pre-cut Ru and Ta wafers were used as substrates and copper was deposited on these substrates using the micropattern mask. For *insitu* micropattern testing, small wafers are feasible and hence cut accordingly. The rest of the uncut wafers are stored in a controlled environment for future use. Then micropatterns were immersed in the chemicals to be investigated and images were recorded.

Corrosion time was calculated by the total time taken by the Cu dots to disappear from the substrate on immersion to the test solution.

$$T_{corrosion} = T_{disappearance} - T_{immersion}$$

Where, $T_{corrosion}$ – Total time for corrosion; $T_{disappearance}$ – Time at which Cu dot disappear; $T_{immersion}$ – Initial time when Cu pattern on a substrate was immersed in the test solution.

And corrosion rate is determined by,

$$R_{corrosion} = \frac{Cu_{\mu,thickness}}{T_{corrosion}}$$

Where, $R_{corrosion}$ – Rate of corrosion in nm/min; $Cu_{\mu,thickness}$ – Thickness of one Cu microdot, nm; $T_{corrosion}$ – Total time of corrosion of Cu dot, minutes

3.3.2 Advantages of the Micropattern

The following advantages of the micropattern make it reliable for this study:

1. Rapid corrosion screening; can be used at wide pH ranges
2. Simple establishment of bimetallic contacts between Cu and other metal substrates
3. Easy testing of different chemicals and faster estimation of corrosion rate of Cu
4. Good ambient control
5. Cost effective by using small samples for analyses especially while using a Ru substrate; Data for Cost of Ru: In 1999, cost was $ 1286 per Kg, currently cost is $ 5465.5 per Kg (Source – www.lipmann.co.uk)

6. Live monitoring of any changes on the Cu surface and easy recording of the changes using an optical microscope with a CCD camera.
7. Consistency among the results and repetitive experiments are easy to perform

Even though this technique has several advantages, there is always a room for error due to the surface inhomogeneity during deposition. The time of flight (TOF) can cause Cu deposition to be non-uniform depending on the position of the substrate. Due to this problem, one can observe few Cu dots on some places not corroded compared to the other dots which have corroded already.

3.4 Results and Discussions

3.4.1 Micropattern Testing in Fresh Gallic Acid

In-situ copper micropattern testing was carried out in different pH solutions of freshly prepared gallic acid from 5 to 12. Figure 3.3 shows the optical images of Cu/Ru and Cu/Ta micropatterns in 5 mM gallic acid solution at different pH conditions. At pH 5, Cu on Ru gets passivated while Cu still remained in metallic color on Ta. At pH 7, Cu corrodes on Ru and passivates on Ta. At pH 9, Cu on Ru and Ta substrates corrodes however with significant difference in corrosion rate. The estimated corrosion rate of Cu on Ru and Ta was ca. 3.2 nm/min and 1.7 nm/min respectively. Color change indicates the oxidation and black ring formation was always observed surrounding Cu microdots on Ru. Similar trend was observed at pH 10 and 11. However at pH 12, the scenario was completely changed. No corrosion of Cu on Ru and Ta was seen for 2 hours.

pH 5

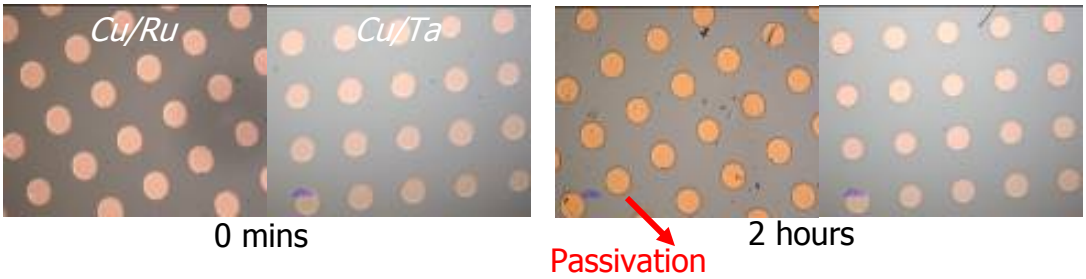

Figure 3.3 (a) Cu micropatterns on Ru and Ta in 5 mM gallic acid at pH 5.

pH 7

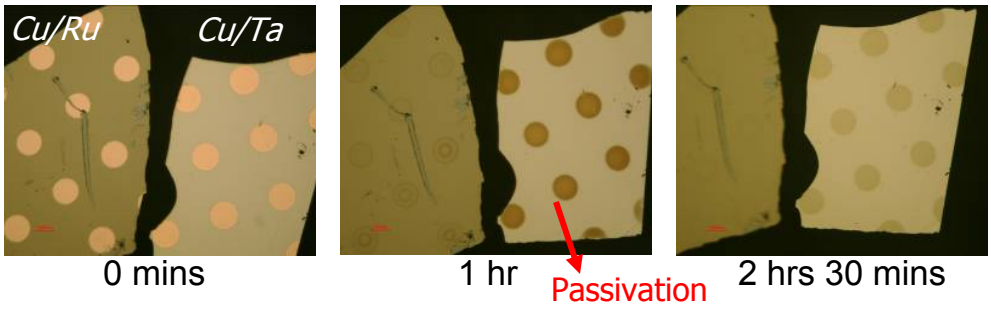

Figure 3.3 (b) Cu micropatterns on Ru and Ta in 5 mM gallic acid at pH 7.

pH 8

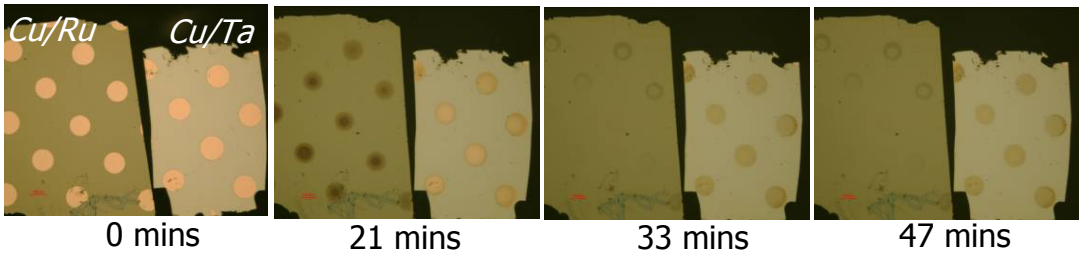

Figure 3.3 (c) Cu micropatterns on Ru and Ta in 5 mM gallic acid at pH 8.

pH 9

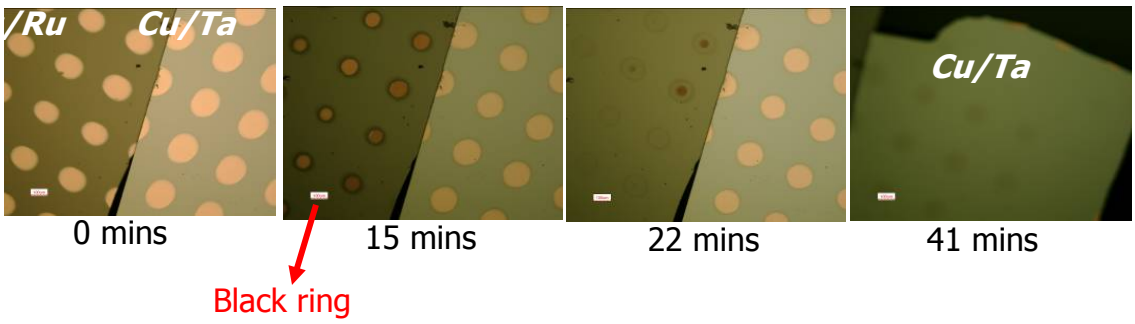

Figure 3.3 (d) Cu micropatterns on Ru and Ta in 5 mM gallic acid at pH 9.

pH 10

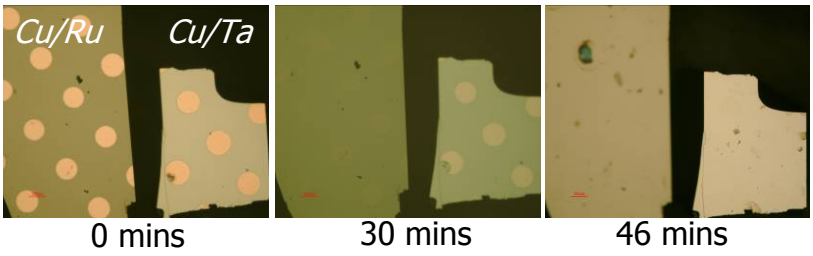

Figure 3.3 (e) Cu micropatterns on Ru and Ta in 5 mM gallic acid at pH 10.

pH 11

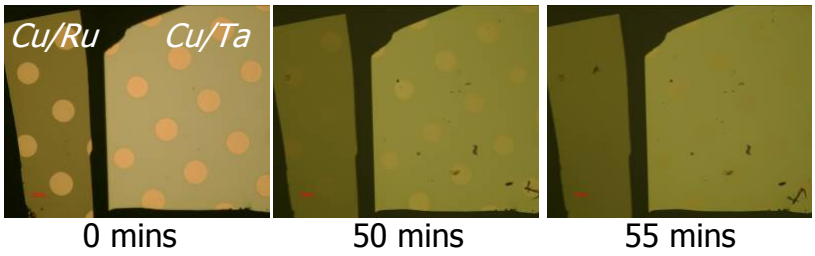

Figure 3.3 (f) Cu micropatterns on Ru and Ta in 5 mM gallic acid at pH 11.

pH 12

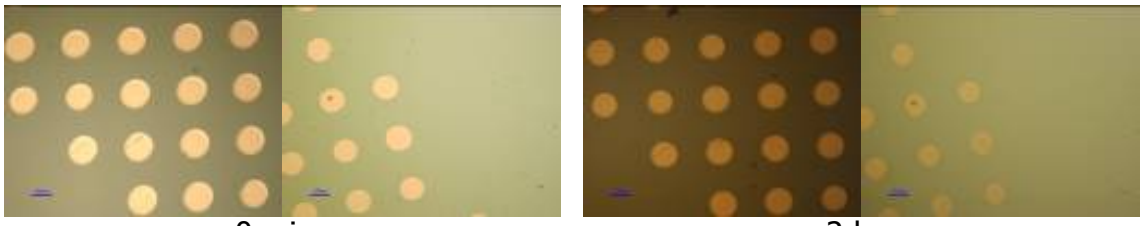

0 mins 2 hrs

Figure 3.3 (g) Cu micropatterns on Ru (left) and Ta (right) in 5 mM gallic acid at pH 12.

Corrosion of Cu was observed at 7 < pH < 11 with enhanced corrosion of Cu on Ru substrates compared to Ta. This pH range is highly important because post CMP is done in this pH conditions wherein gallic acid offers no corrosion protection instead accelerates the corrosion of Cu microdots. Figure 3.4 is the graphical representation showing the maximum corrosion activity at pH 9 and hence used in this study.

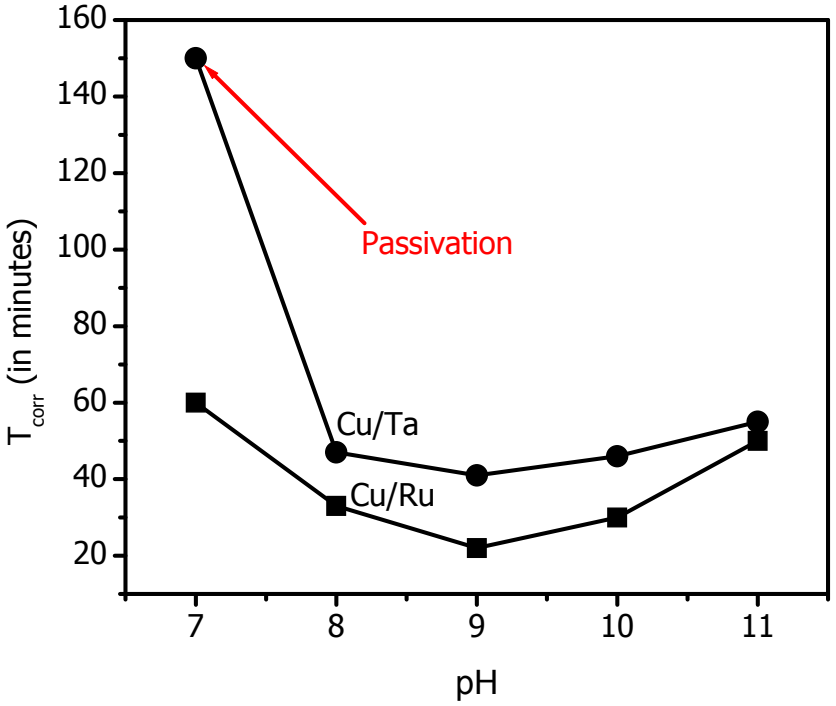

Figure 3.4 - Time of corrosion of Cu on Ru and Ta substrates in freshly prepared 5 mM gallic acid at different alkaline pH conditions.

Similar micropattern testing was carried out in nitrogen environment to minimize the oxygen content in the solution and optical images recorded are shown in figure 3.5.

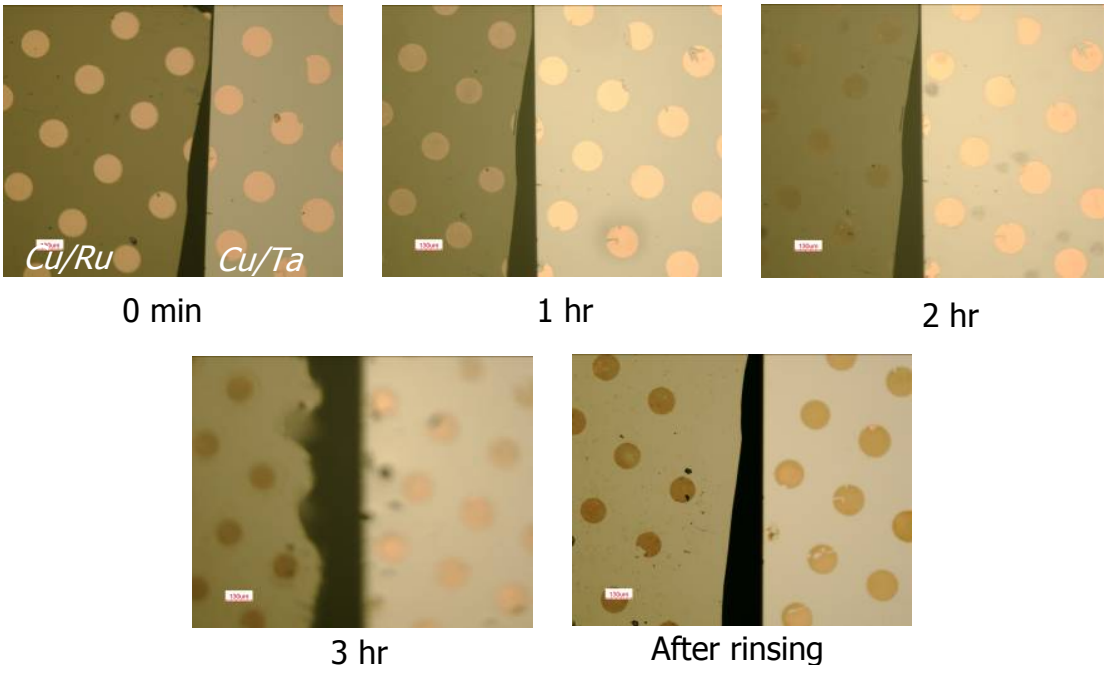

Figure 3.5 - Insitu micropattern testing of Cu on Ru and Ta substrates in N_2 purged 5 mM gallic acid at pH 9. No corrosion was observed instead passivation of the surface can be seen.

Absence of corrosion in presence of N_2 indicates that oxygen plays a main role in the corrosion of Cu. Purging N_2 into the solution decreases the available amount of oxygen which prevents (i) oxidation of Cu and (ii) autoxidation of gallic acid. Further discussion on the effect of N_2 in minimizing ORR in understanding the substrate effect can be found in later sections. Micropattern testing was also done for air exposed gallic acid. 5 mM gallic acid solutions freshly prepared at pH 9 and 12 were intentionally exposed in lab ambient for 24 hours to complete oxidation process. Solution pH was found to drop from 9 to 7.5 and 12 to 10.5 respectively. In aged pH 9 gallic acid, Cu microdots on Ru and Ta were completely corroded at time period of 4 mins 30 seconds and 6 minutes respectively. However no corrosion was observed even in aged pH 12.

3.4.2 Factors Affecting Cu Corrosion

Primary results obtained by micropattern testing indicate the dual corrosion behavior of Cu in alkaline conditions. Various factors are involved in the corrosion of Cu which is described as below:

a) Oxidation of Cu:

Potential-pH diagram (Pourbaix diagram) of Cu-H_2O system indicates the easier oxidation in alkaline conditions which might lead to corrosion of Cu.[32,33] However micropattern testing of Cu in DI H_2O in alkaline pH conditions didn't show any corrosion. In general, gallic acid is an effective scavenger for oxygen and hydroxyl radicals thereby minimizing its availability to oxidize copper. Instead, active Cu corrosion was observed in alkaline gallic acid solution. Thus the corrosion of Cu is not attributed to the oxidation alone; instead the main contribution is due to the chemical interaction (chelation) of the oxidized Cu copper ions with the oxidized gallic acid species.

Active corrosion of Cu metal requires not only thermodynamically favorable conditions conducive to oxidation of Cu but also proper channels that can rapidly remove oxidized Cu species from its surface. In general, surface oxidation of Cu could form stable oxides or hydroxides in alkaline conditions forming a passivated layer on the surface.

b) Bimetallic Corrosion:

Enhanced corrosion of Cu on Ru compared to Ta can be attributed to the nobility nature of different metals. Cu is more noble to Ta and Ru is more noble to Cu. In

common, Cu receives no protection due to its anodic nature in Cu-Ru bimetallic systems and hence corrosion of Cu is enhanced. In Cu-Ta bimetallic systems, Cu receives cathodic protection; however corrosion seen in micropattern testing will be shown in the later section is due to the effect of local anodic reaction.

c) Oxidation of Gallic Acid:

Autoxidation behavior of gallic acid needs more understanding in this system. Corrosion observed at $7 < pH < 11$ and absence of corrosion at $pH \geq 12$ indicates the nature of two different products at different pH conditions. If gallic acid undergoes complete autoxidation forming its quinone, one may argue the absence of corrosion due to the stable oxide formation on Cu surface. Another route for this inhibition tendency can be explained as suggested in the literature that gallic acid can form its oligomer at very high alkaline conditions.[34] Oligomers usually are better scavengers than their parent molecule thereby protecting from Cu corrosion.

Thus with preliminary results from micropattern testing and knowledge gained from the literature, systematic investigations are necessary in understanding the Cu corrosion behavior in gallic acid. Autoxidative behavior of gallic acid at different pH conditions leads to the formation of different products which can be characterized by UV Vis and IR spectroscopic techniques. Besides it, UV Vis spectroscopy can also give insightful information on the chelation of different gallic acid species which are nascent to interact with the copper ions. Investigation of the corrosion potential (E_{corr}) values from tafel plots combined with the direction of current flow from microampere measurements will be helpful in perceptive of bimetallic effect.

3.4.3 UV Vis Spectroscopy

Gallic acid autoxidation at different pH conditions forming different oxidized species was characterized by UV Vis spectroscopy and shown in figure 3.6. Gallic acid shows no oxidation till neutral pH conditions. In alkaline conditions, rapid oxidation takes place by the appearance of quinone peaks ca. 380-450 nm.[35] Literature has been reported on the absorption of phenoxyl radicals ca. 430 nm.[36] Figure 3.7 shows the rate of autoxidation of gallic acid on exposure to atmosphere. Even after prolonged exposure in atmosphere, gallic acid does not oxidize as seen at pH 5. In neutral pH conditions, gallic acid undergo slow

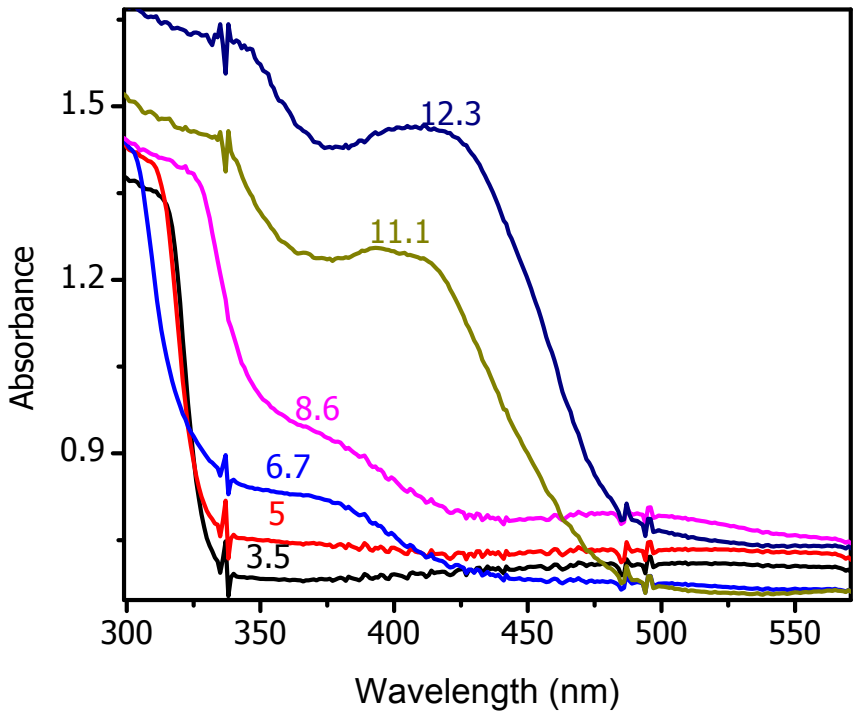

Figure 3.6 - UV Vis spectra of freshly prepared 5 mM gallic acid at different pH conditions. Rapid autoxidation takes place in alkaline conditions.

rate of autoxidation. In alkaline conditions at pH 9 and 12, the rate of oxidation is rapid seen by pronounced increase in absorbance and wavelength which is attributed to the change in the number of chromophores with change in the molecular moieties which are pi electron functions and heteroatoms due to quinone formation. The electronic spectra at different pH conditions shows the difference in oxidation behavior of gallic acid which also reflected in the solution color.

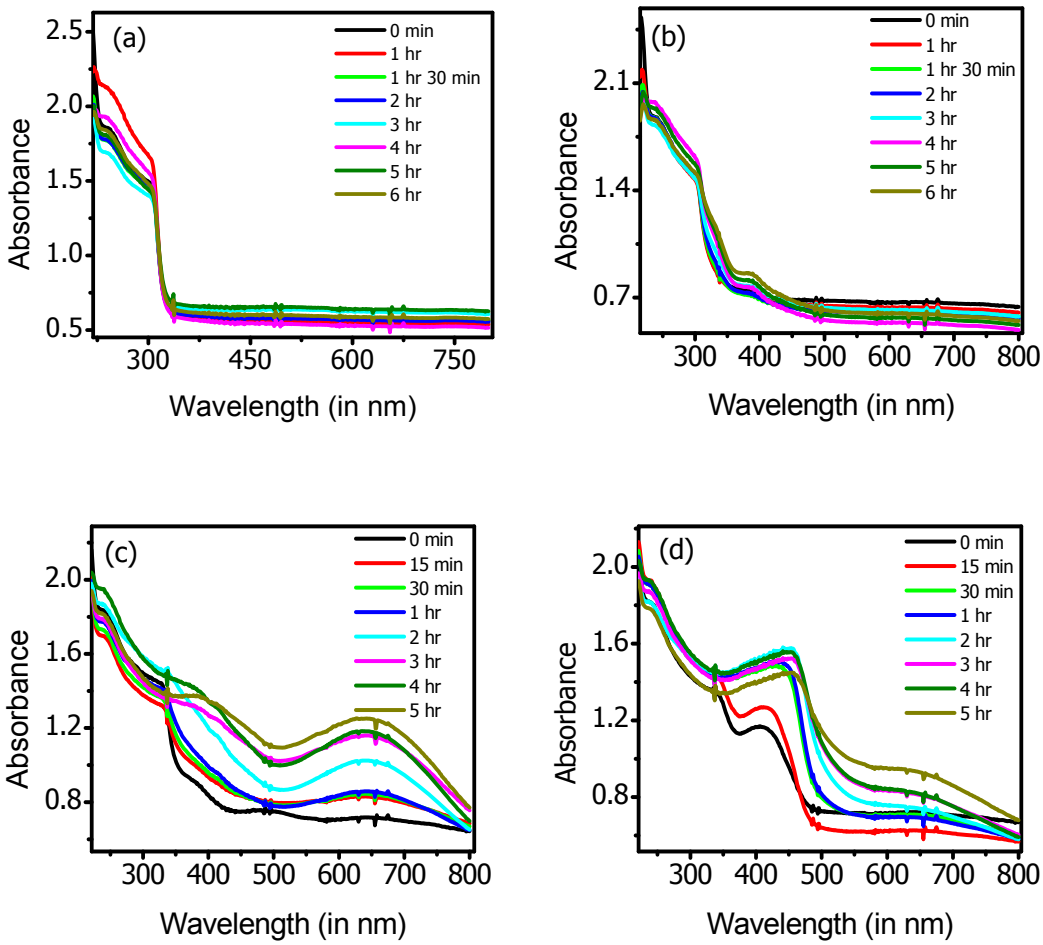

Figures 3.7 - Time dependent UV Vis spectra of freshly prepared 5 mM gallic acid at (a) pH 5; (b) pH 7; (c) pH 9; and (d) pH 12 exposed to atmosphere at different time intervals.

In acidic conditions, gallic acid remains colorless. From pH 7-11, solution was green in color and at pH 12, the solution acquires a combination color of deep orange and brown. As suggested by Singleton gallic acid can form dimer, ellagic acid at high alkaline conditions. UV Vis (Fig 3.8) shows the similarity for 1 day exposed gallic acid prepared at pH 12 and ellagic acid at pH 12.

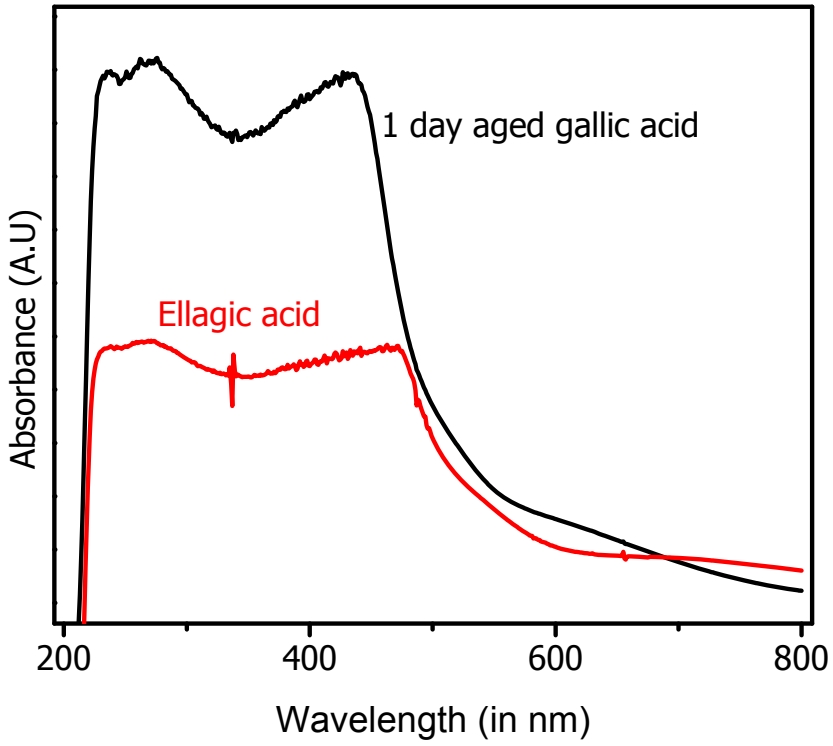

Figure 3.8 - Comparison of UV Vis of 5 mM solutions of aged-gallic acid and ellagic acid at pH 12.

Besides the difference in UV Vis spectra at pH 9 and 12, visible color difference was also observed. Freshly prepared gallic acid solution was colorless and green color was exhibited from pH 7 to 11. However at pH 12, the solution turned deep orange-brown color.

3.4.4 FTIR-ATR Spectroscopy

Fourier transform infra red (FTIR) spectroscopy with attenuated total reflectance (ATR) technique was used to investigate the difference in the

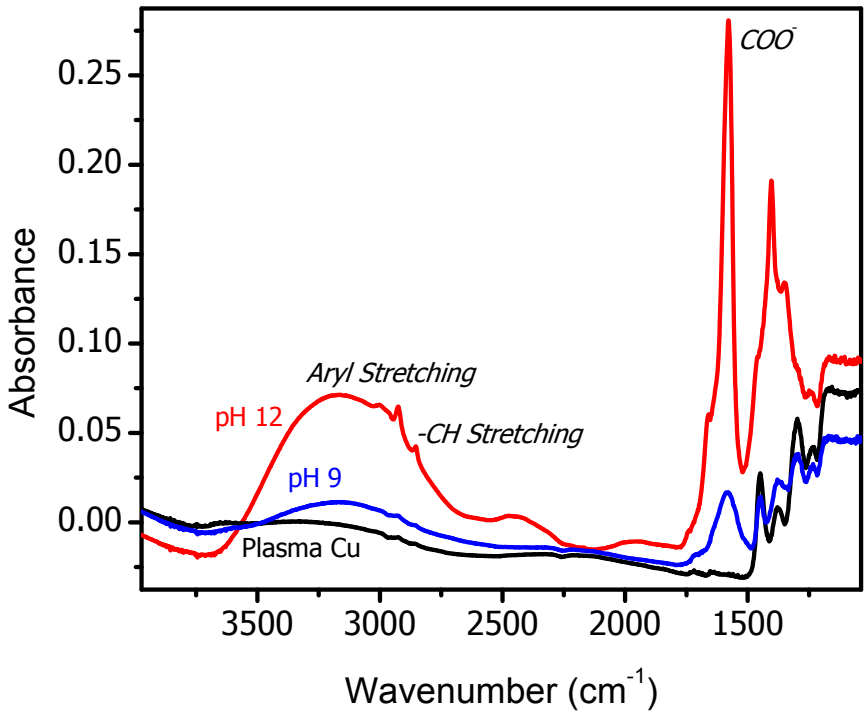

Figure 3.9 - IR signatures of physically adsorbed species of freshly prepared gallic acid at pH 9 and 12 with plasma Cu as background.

chemical structure of the organic species formed by the air oxidation of gallic acid at pH 9 and 12. Plasma cleaned Cu thin film of 2 nm in thickness on Si crystal was used as the internal reflection element (IRE). Comparing physically adsorbed species of pH 12 with pH 9 as shown in figure 3.9, C=O in COO^- stretching at 1500-1700 cm^{-1} and aromatic C-H stretching at ca. 3100 cm^{-1} were enhanced due to the formation of conjugated species (dimer) by the autoxidation of gallic acid.

3.4.5 Cyclic Voltammetry

For this potentiodynamic experiment, glassy carbon was used as the working electrode. Freshly prepared 5 mM gallic acid solution with buffer was used as the electrolyte. Pt foil was used as the counter electrode and all potentials were referred against Ag/AgCl reference electrode. Cyclic voltammogram's (CV's) were recorded at a scan rate of 50 mV/s.

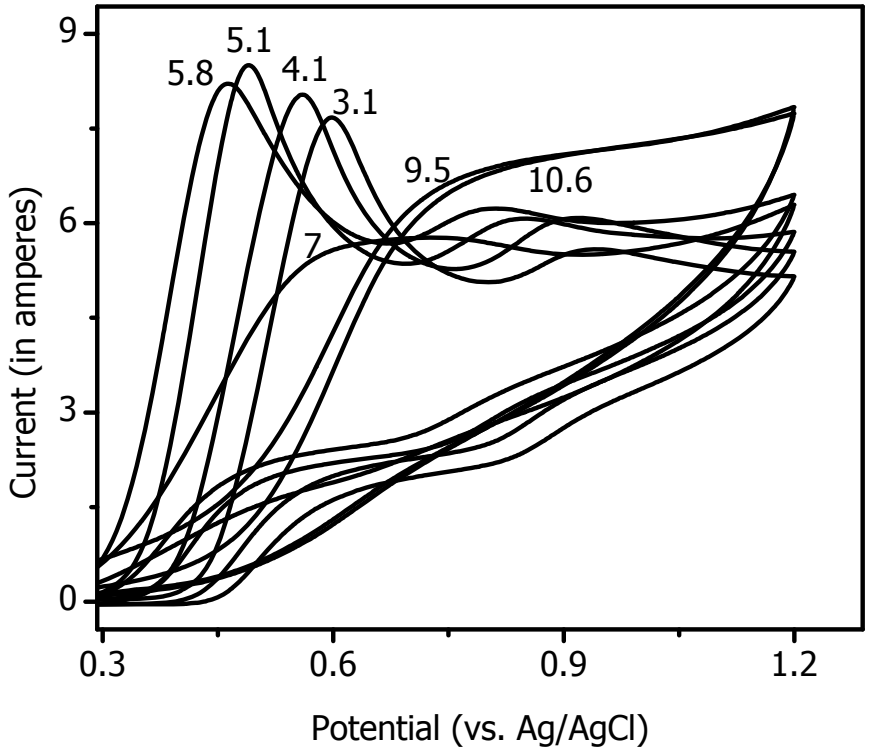

Figure 3.10 - Cyclic voltammogram's of freshly prepared 5 mM gallic acid in different pH buffer solutions. CV indicates the irreversible behavior of oxidation.

Till pH 5.8, CV exhibited quasi reversible behavior with potentials shifting more negative indicating the nucleophilic nature of the species formed by the oxidation of gallic acid.[14,37] In neutral and alkaline conditions, the CV behavior indicated irreversible

behavior with potentials shifted towards positive reflecting the electrophilic nature of the quinone species formed. Thus from pH 7 to 11, gallic acid leads to quinone formation via generation of phenoxyl radicals and semiquinone species.

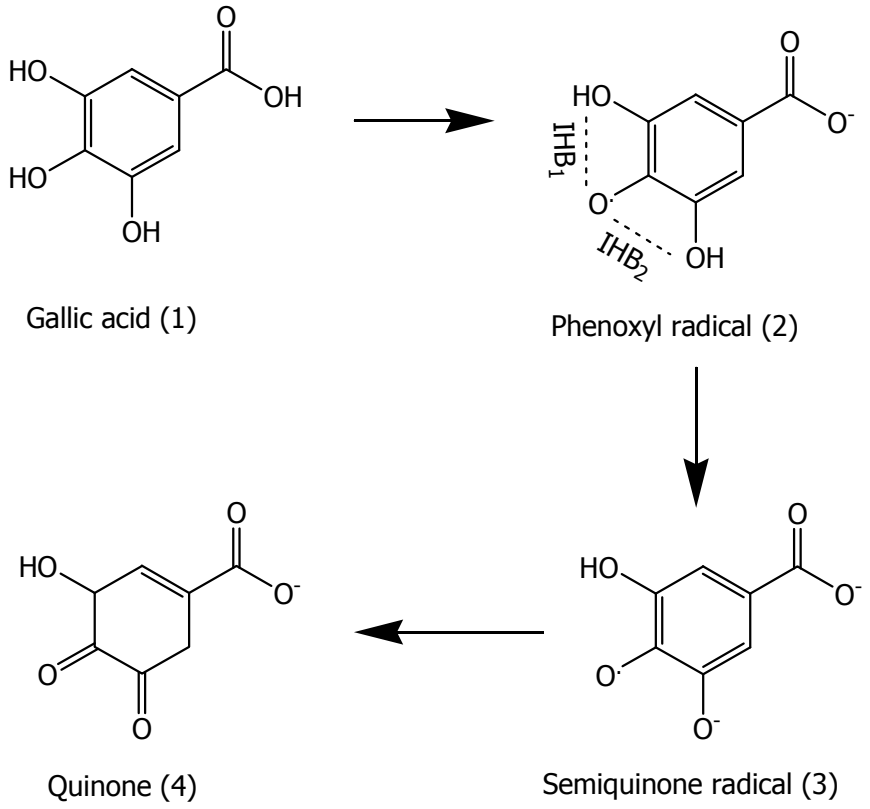

Mechanism 3.1 Oxidation of gallic acid to quinone via semiquinone formation.

Quinone is electrophilic in nature with all its electrons filled are not reactive and its chemical reaction with surrounding metal ions is less favorable. However Cu corrosion in air exposed gallic acid solution indicates its interaction with a highly reactive species generated by the autoxidation mechanism. Semiquinone species are highly nucleophilic in nature with their opened shell configuration and highly reactive

which are likely to take part in chemical reactions. Interaction of semiquinone with Cu ions is highly possible due to its resonance stabilization.[14]

3.4.6 Tafel Plots – Effect of Ambients

Corrosion potential (E_{corr}) values obtained from tafel plots are important in learning the thermodynamic nature between two different metals connected in an electrical circuit immersed in an electrolyte solution containing active species or ions. In this study, Cu is noble to Ta and Ru is noble to Cu. However the shift in E_{corr} values in presence of gallic acid species at different pH conditions enables us to understand the corrosion trend.

Lab ambient

In lab ambient conditions (figure 3.11), E_{corr} of al the three metals show a decreasing trend with increasing pH due to the scavenging effect of oxygen by gallic acid thereby decreasing oxygen availability to the metal surfaces. Ru always stays noble to Cu and Cu is noble to Ta. In Cu-Ta system, bimetallic corrosion is absent and micropattern testing showing the corrosion of Ta can be attributed to the interaction of copper ions generated by the local anodic reaction with the oxidized gallic acid species. Due to the potential difference between Ru and Cu, there exists always a bimetallic effect leading to the corrosion of Cu which explains the enhancement of corrosion of Cu.

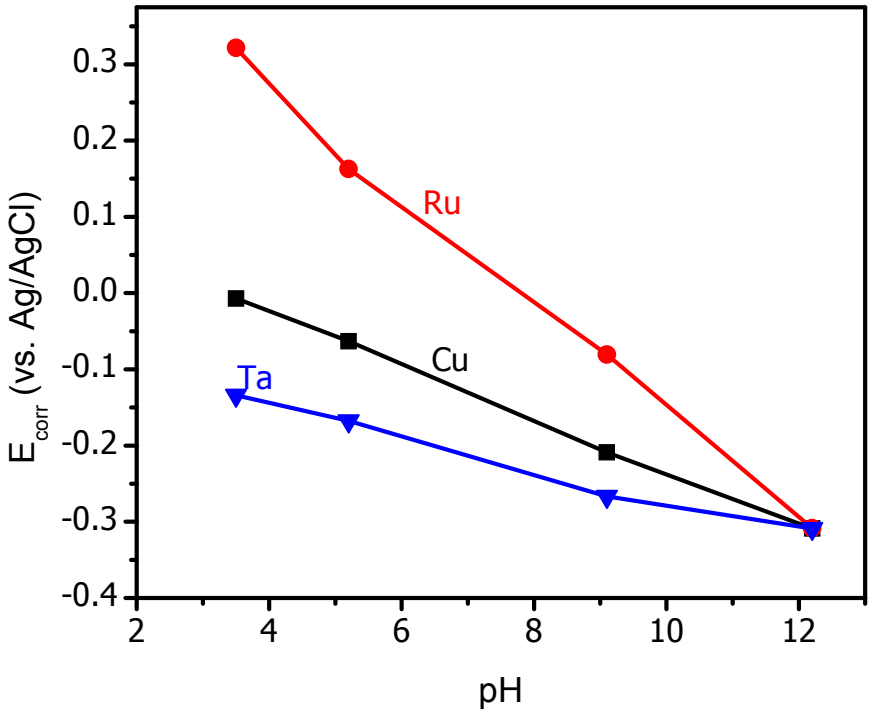

Figure 3.11- E_{corr} obtained from tafel plot measurements for Ru, Cu and Ta electrodes immersed in freshly prepared 5 mM gallic acid plotted against different pH values in lab ambient conditions.

Oxygen

Figure 3.12 show the E_{corr} vs. pH in oxygen environment. Oxygen was purged into freshly prepared gallic acid at pH 9 for 15 minutes. Purging O_2 into the gallic acid solution greatly enhances the autoxidation which can be observed by the change in the solution color. Freshly prepared gallic acid in alkaline conditions acquires green color. While purging O_2, the color change was rapid and the solution color turned dark green. E_{corr} values indicate the nobility nature of Cu, Ru and Ta (not shown) are maintained in O_2 environment. However at pH 3 and 5, E_{corr} for Cu and Ru does not show any

significant change due to the maximum oxygen scavenging ability of gallic acid at this pH conditions.

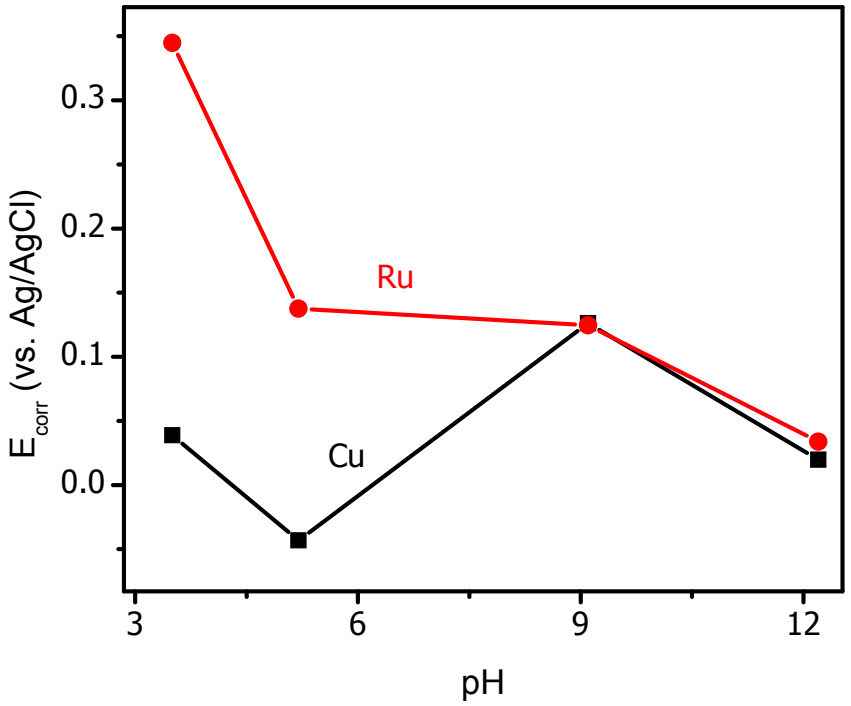

Figure 3.12 - E_{corr} for Cu and Ru in 5 mM gallic acid at different pH conditions in O_2 environment. E_{corr} for Cu is significantly high at pH 9.

However at pH 9 in presence of oxygen, Ru show an increase of 300 mV indicating the oxidation of the surface due to the decreased scavenging ability of gallic acid by autoxidation. At pH 12, again E_{corr} follows as a decreasing trend compared at pH 9 due to the dimer formation which has higher oxygen scavenging ability. However the E_{corr} is still higher compared to the lab ambient conditions.

Air

Similar argument is valid for air purged conditions in the pH range of 3 to 11. Besides the decreasing trend of E_{corr} of Cu and Ru at pH ≥ 12, potentials also switch over (swapping) therefore the nobility of the metals has changed which explains why no bimetallic corrosion was absent at pH 12. Air purging experiments are similar to the *insitu* micropatterns testing period.

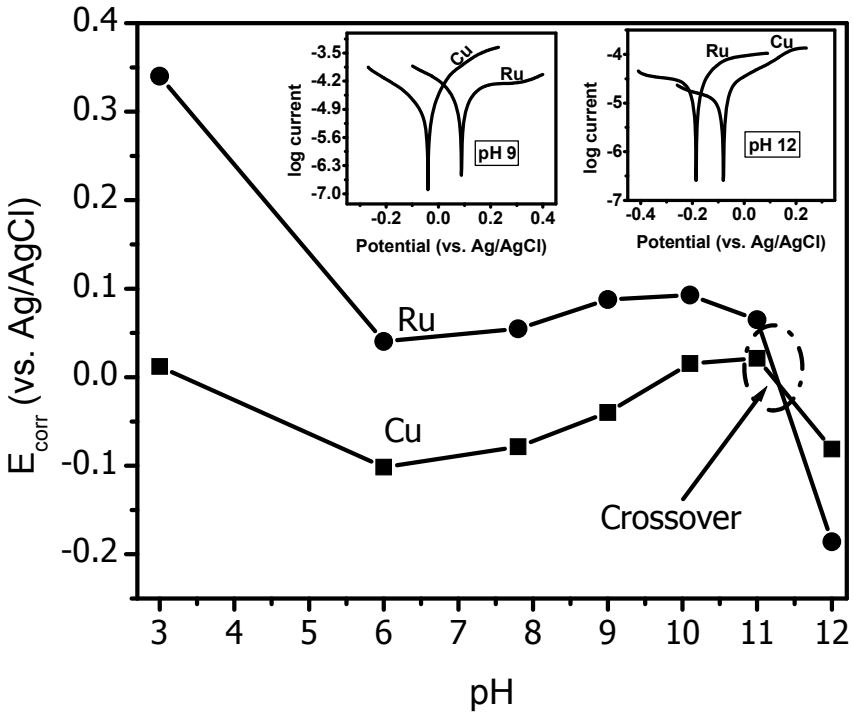

Figure 3.13 - E_{corr} vs. pH for Cu and Ru in air purged 5 mM gallic acid solution. Compressed air consisting of 21% of O_2 with 78% of N_2 changes the nobility of Cu at pH 12.

The drop of E_{corr} for Ru is more significant than for Cu. Drop in the corrosion potential (and also OCP) indicates the reductive state of Ru. One can think about the removal of any oxide (air exposed) layer from Ru surface. But this statement is in

contrast once the nobility of Ru is assumed. As anode at pH 12, Ru should undergo oxidation and the OCP or E_{corr} should increase. Therefore the drop in the E_{corr} of Ru and Cu is confined to the higher scavenging ability of dimer formed by the autoxidation of gallic acid at pH 12. Thus the nature of Ru at pH 12 is still under scrutiny.

Nitrogen

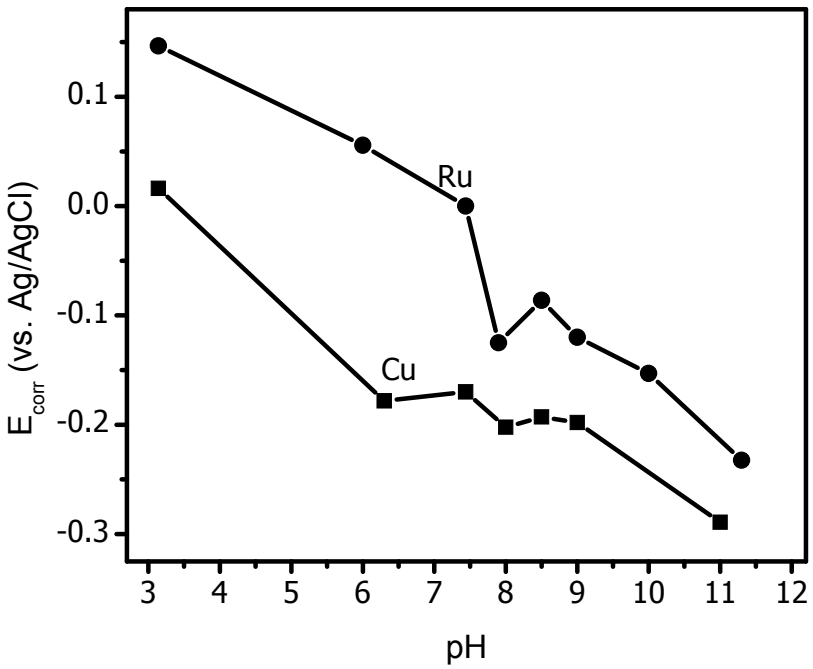

Figure 3.14 - E_{corr} vs. pH for Cu and Ru in N_2 purged 5 mM gallic acid solution. Irrespective of pH values, E_{corr} always show a decreasing trend.

Purging nitrogen minimizes oxygen content in the solution thereby decreasing the autoxidation tendency of gallic acid. Due to this combinational effect, E_{corr} for Cu and Ru show only decreasing trend irrespective of any pH conditions.

3.4.7 Microampere Measurements

Experimental Setup

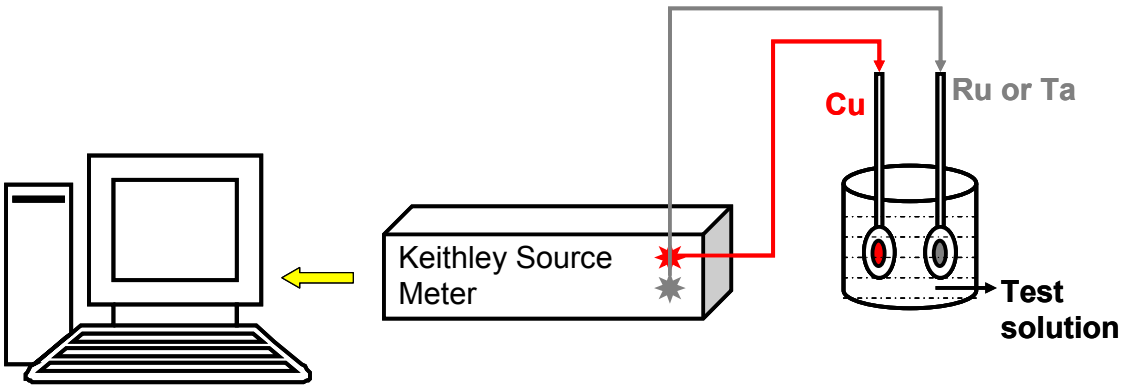

Figure 3.15 - Outlay of the experimental design used for direct current measurements in a bimetallic system.

Direction of current flow is useful in determining the corrosion tendency in a bimetallic system. Figure 3.15 show the experimental setup for the direct current measurements. Keithley source meter capable of reading micro and nano currents was used. In the front arm, the two terminals present in the meter were used for connections. Cu terminal was always fixed and the other terminal was varied with Ru or Ta depending on the bimetallic system studied. Then each bimetallic system was immersed in the test solution, gallic acid in this case. Readings were recorded in computer and graphs were plotted with current in y-axis and time in x-axis.

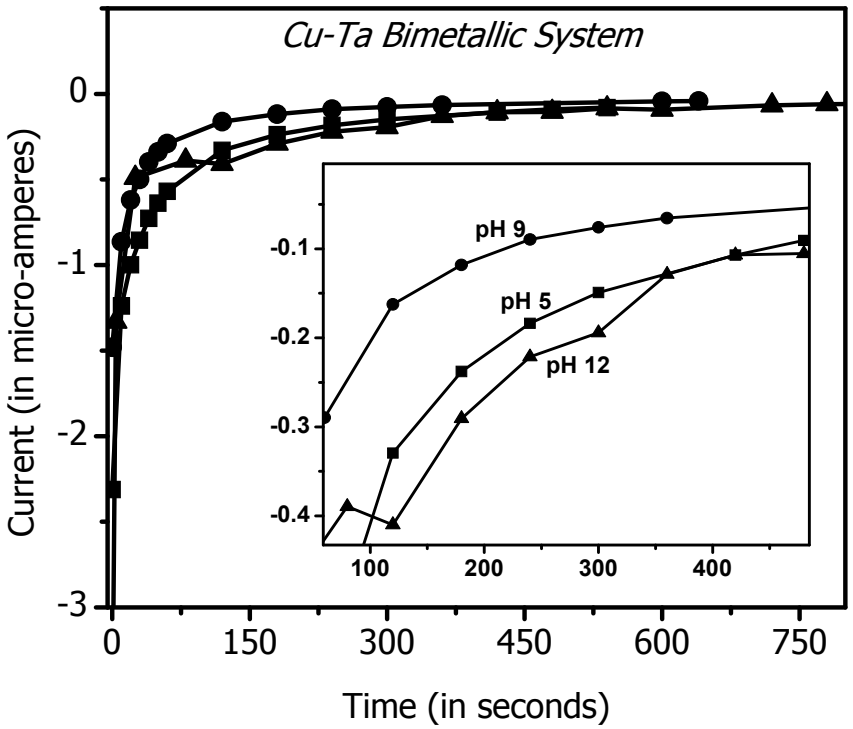

Figure 3.16 - Microampere measurements of Cu-Ta bimetallic system showing negative direction of current flow due to the oxidation of Ta with maximum current at pH 9.

Figure 3.16 show the negative flow of current in Cu-Ta bimetallic system and thus the flow of current is from Ta to Cu due to the formation of tantalum oxide (Ta_2O_5). One might expect Cu to receive complete protection by cathodic protection. However this is in conflict and the corrosion of Cu on Ta is solely attributed to the local anodic reaction of copper wherein the copper ions interact with the oxidized gallic acid species. Figure 3.17 show the current flow in Cu-Ru bimetallic system.

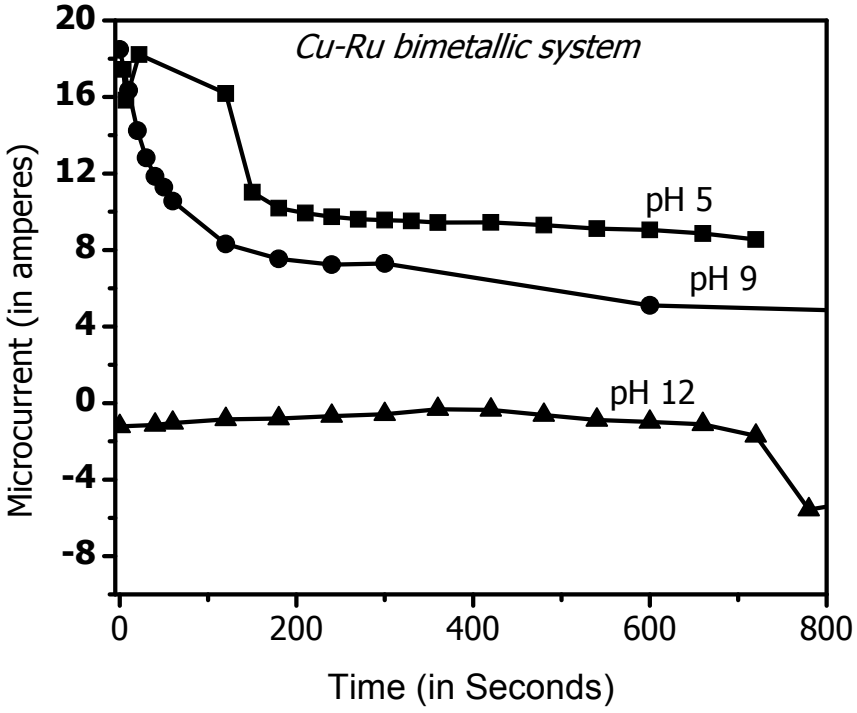

Figure 3.17 - Microampere measurements of Cu-Ru bimetallic system showing positive direction of current flow due to the oxidation of Cu. Negative direction of current flow is seen at pH 12.

Positive current flow at pH 5 and 9 indicates the flow of electrons from Cu to Ru due to the oxidation of copper. Higher current indicates the enhancement of bimetallic corrosion in Cu/Ru micropattern testing. Positive current flow is common in Cu-Ru bimetallic system as reported before in ammonium citrate test solution. At pH 12, the direction of current flow has changed to negative indicating the absence of oxidation of Cu. The results further corroborates with the swapping potentials as seen in the tafel plot measurements at pH 12.

Thus gallic acid on oxidation at pH 12 leads to the generation of a dimer as suggested by Singleton[34] which has a higher oxygen scavenging ability than its parent molecule. Formation of the dimer is as follows:

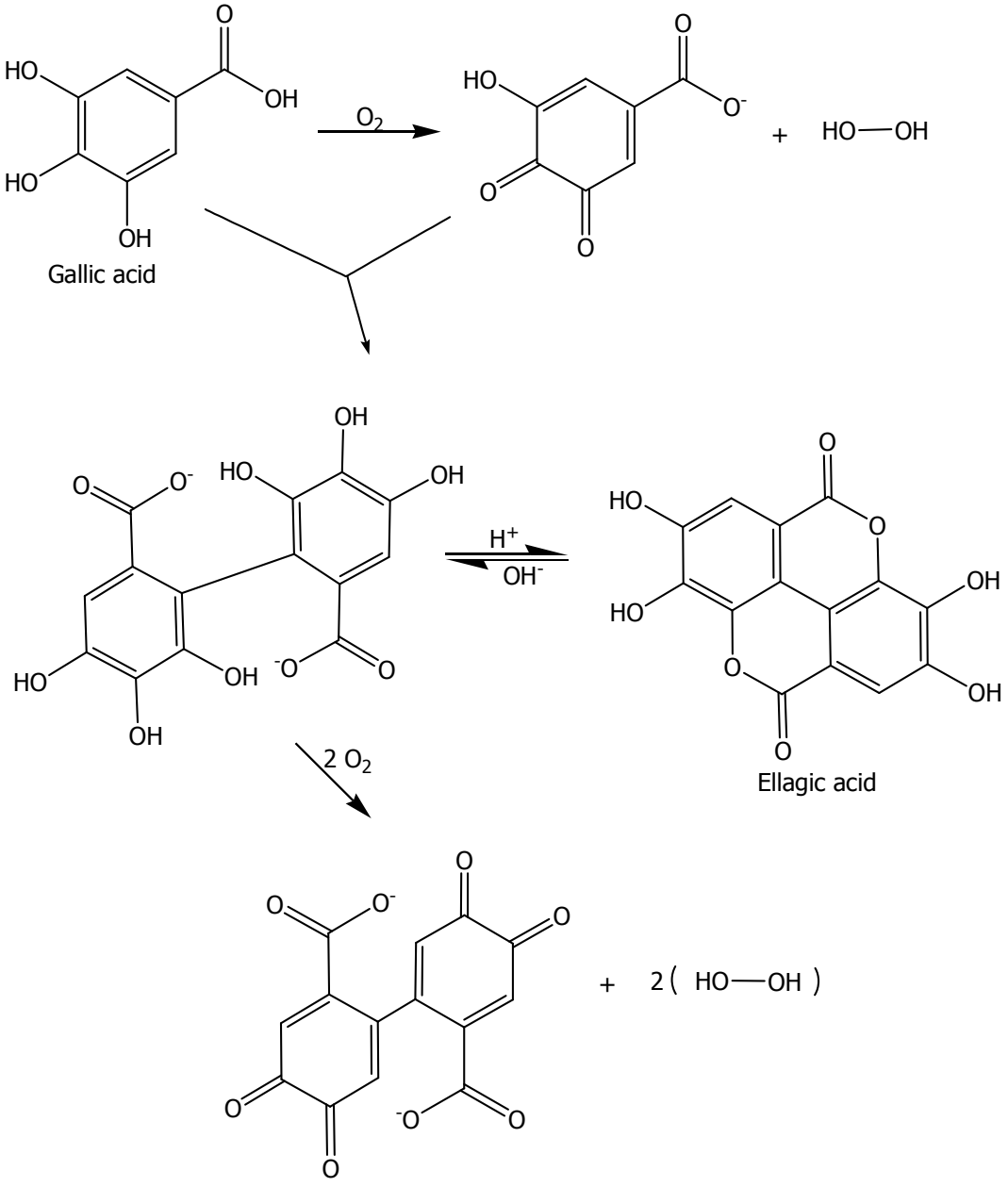

Mechanism 3.2 Oxidation of gallic acid to form dimer at pH 12. [Reprinted with permission from Tulyathan, V.; Boulton, R. B.; and Singleton, V. L. "Oxygen uptake by gallic acid as a model for similar reactions in wines," *J. Agric. Food Chem.,* 37 (4), **1989**, 844-849. Copyright 2007 American Chemical Society.]

Freshly prepared 5 mM gallic acid at pH 9 was intentionally exposed in atmosphere for ageing. pH drop from 9 to 7.5 indicates autoxidation of gallic acid. Direction of current flow of Cu in Cu-Ta system has changed to positive from its conventional negative flow of current. In both the bimetallic systems, the saturation current is higher for aged gallic acid indicative of faster corrosion of Cu within a time period of 6 minutes. Thus the micro-/nano- ampere measurements are useful in determining the corrosion rate of a metal in any bimetallic system.

3.4.8 Effect of Substrate

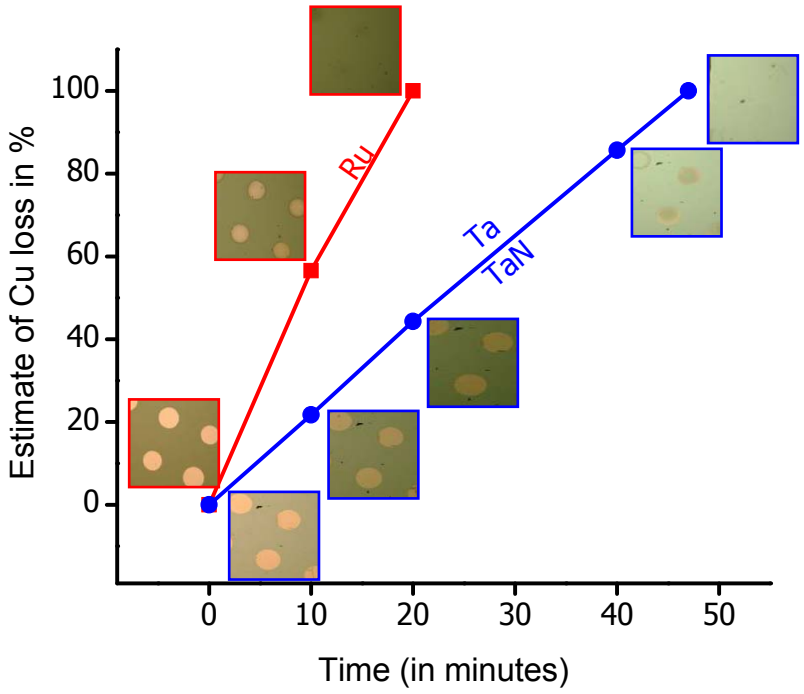

Figure 3.18 Graph showing the estimate of Cu loss indicating faster rate of corrosion on Ru substrate than Ta and TaN.

pH 5:

For corrosion to occur, copper ions chelating with oxidized products of gallic acid species is the important reaction. Thus faster corrosion of Cu directly links to faster

chelation due to the easier generation of Cu^{2+} ions. In typical bimetallic system, anodic reaction is usually the generation of metal ions while oxygen reduction reaction (ORR) to form water or hydroxyl ions takes place on cathodic site depending on the pH conditions.

ORR's given by,

$$O_2 + 4H^+ + 4e^- \rightarrow 2H_2O(\text{acidic})$$
$$O_2 + 2H_2O + 4e^- \rightarrow 4OH^-(\text{near}-\text{neutral}/\text{neutral}/\text{basic})$$

Hydrogen evolution reaction (HER) is not considered in this systems since HER is favorable only in low pH conditions. Besides ORR, reduction of water can also happen in near neutral or basic conditions given by:

$$2H_2O + 2e^- \rightarrow H_2 + OH^-$$

In Cu-Ru bimetallic system, Ru acts as cathode. Ru belonging to the Pt group metals have higher tendency for ORR. ORR on cathodic Ru site leads to the generation of OH^- ions thereby increasing its interfacial pH which will enhance the oxidation of Cu. In acidic conditions at pH 5, gallic acid autoxidation is absent. Thus O_2 is not scavenged and available for Cu to form oxide on its surface leading to passivation. Passivation of Cu on Ru substrate inhibits further corrosion which is confirmed by the change in the color of Cu microdots on Ru as shown in figure 1.

Oxidation of Cu at pH 5 is given by the formation of its low oxidation state copper (I) oxide.

$$2Cu + 2H_2O \rightarrow Cu_2O + 2H^+ + 2e^-$$

In Cu-Ta bimetallic system, Cu is cathodically protected by Ta anode which forms thick Ta_2O_5 on its surface by,

$$2Ta + 5H_2O \rightarrow Ta_2O_5 + 10H^+ + 10e^-$$

Cathodic protection of Cu indicates the absence of oxidation on its surface and hence remained in metallic color on Ta substrate.

7 < pH < 11:

Cu oxidation is enhanced by the pH as indicated in the Cu-H_2O pourbaix diagram. In alkaline conditions, irrespective of bimetallic systems, anodic reaction of Cu is possible. In Cu-Ru, Cu totally behaves as anode while in Cu-Ta local anodic sites are present on Cu. Further, enhancement of Cu oxidation will be present in Cu-Ru bimetallic system. Hence oxidation of Cu leads to the generation of Cu ions given by,

$$2Cu + 2H_2O \rightarrow Cu_2O + 2H^+ + 2e^-$$
$$Cu_2O + 2H^+ \rightarrow 2Cu^{2+} + H_2O + 2e^-$$

Or in simple,

$$Cu \rightarrow Cu^{2+} + 2e^-$$

Equation 3.10 will be the rate determining step in the corrosion of Cu. Faster the generation of cupric ions faster the corrosion of Cu.

pH 12:

From previous results we have seen swapping potentials with decreased E_{corr} for Cu and change in the direction of current flow at pH 12. Dimer formed is a better scavenger of hydroxyl and oxygen radicals thereby preventing the oxidation of Cu.

3.4.9 Chelate Effect

Polyphenols have been widely studied as chelating agents for Cu^{2+} and other transition metal ions.[27-31] Gerega et al.[29] have shown that for 3,4 dihydroxybenzoic acids that both adjacent hydroxyl sites and acidic group chelates with copper ion. However the chelation of acidic group is weaker compared to the adjacent hydroxyl sites (phenolate). Tamas Kiss et al.[27] reported that in low pH range the ligands in dihydroxybenzoic acids coordinate through the carboxylate group. However above pH 5, the major species are chelated complexes in which the metal ions bind through the carboxylate and adjacent phenolate groups. Electronic spectra are useful in the investigation of chelation of metal ions with ligands by characterizing the charge-transfer band. Based on the shift in absorbance as shown in the UV Vis spectra, complexation of Cu^{2+} can be observed with gallic acid at 503 nm. 1:1 stoichiometric ratio between Cu^{2+} and gallic acid was found by method of continuous variation (refer insert in the figure) with log K_f value of 3.61. Based on the acid dissociation values of gallic acid in presence of copper at pH 5, acidic group tends to dissociate forming carboxylate ion. Thus chelation is due to the bridging of copper ion with carboxylate ion forming a weaker monodentate complex.

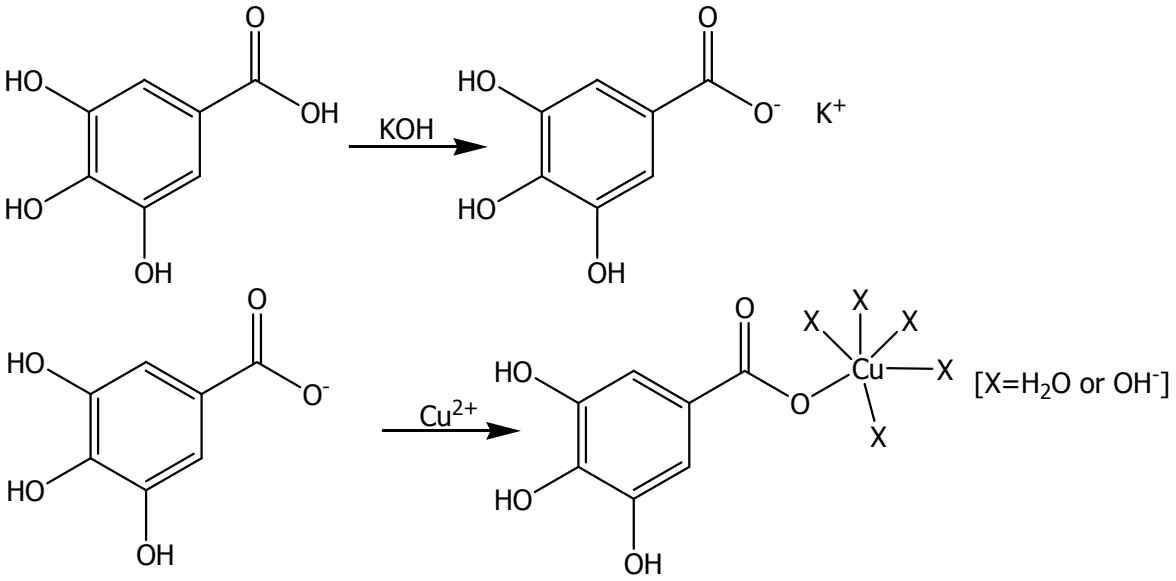

Mechanism 3.3 Chelation of gallic acid with Cu^{2+} at pH 5.

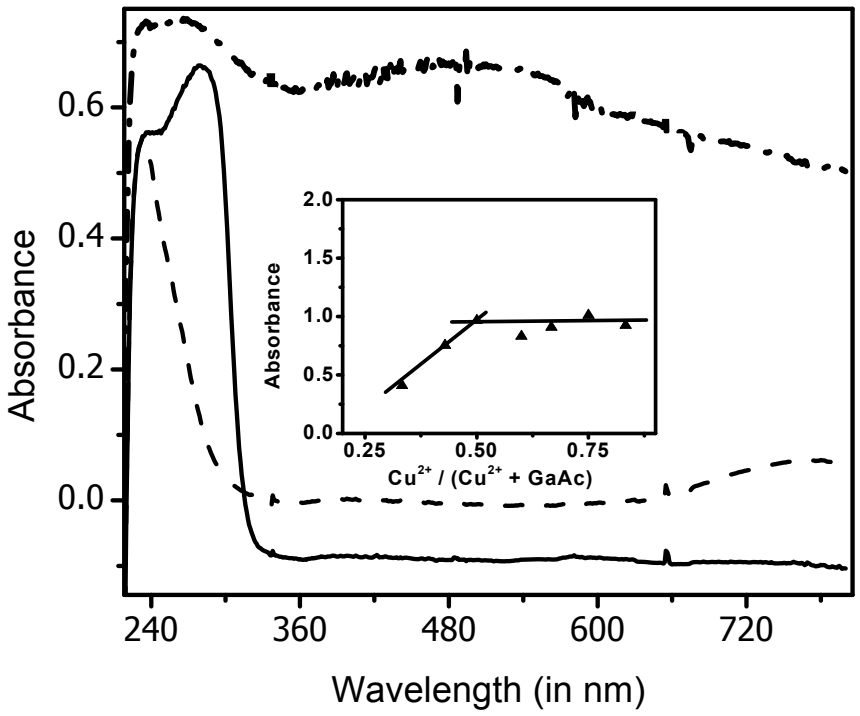

Figure 3.19 - UV Vis spectra of complexation between 10 mM Cu^{2+} and 1 mM gallic acid observed at 503 nm. *Insert:* Method of continuous variation calculation gives a stoichiometric ratio of 1:1 between metal ions and ligand species.

Determination of stoichiometric ratio and formation constant between Cu^{2+} and gallic acid is rather difficult at pH 9. In alkaline conditions, precipitation of metal ions due to the formation of hydroxide takes place which interferes during the investigation of electronic spectra. Based on the dissociation values of gallic acid, adjacent hydroxyl sites dissociate to form phenolate groups which have stronger ability to form stable complexes with copper ions. In the presence of Cu^{2+} ions, it has been reported that acid dissociation values of gallic acid decreases[38] and hence there is a higher chance for bidentate or tridentate complexes formation in alkaline conditions as shown below. In experimental conditions, precipitation starts occurring when the metal concentration exceeds 1:3 ratio (Cu^{2+}: GaAc). For chelation to occur, phenolate ions (semiquinone species) should interact with copper ions. Thus this chelate effect is the key reason behind the corrosion of copper irrespective of substrates. More investigation has to be done to understand the minimal effect of substrate in corrosion of Cu in gallic acid. This can be done by insitu micropattern testing of Cu on Carbon substrates. Another way is by immersing a thin film of Cu in gallic acid solution. Any corrosion is by the dissolution of Cu and the dissoluted Cu present in the solution can be analyzed using atomic absorption spectroscopy. From the rate of dissolution one can establish the corrosion rate of Cu alone with no influence of substrate.

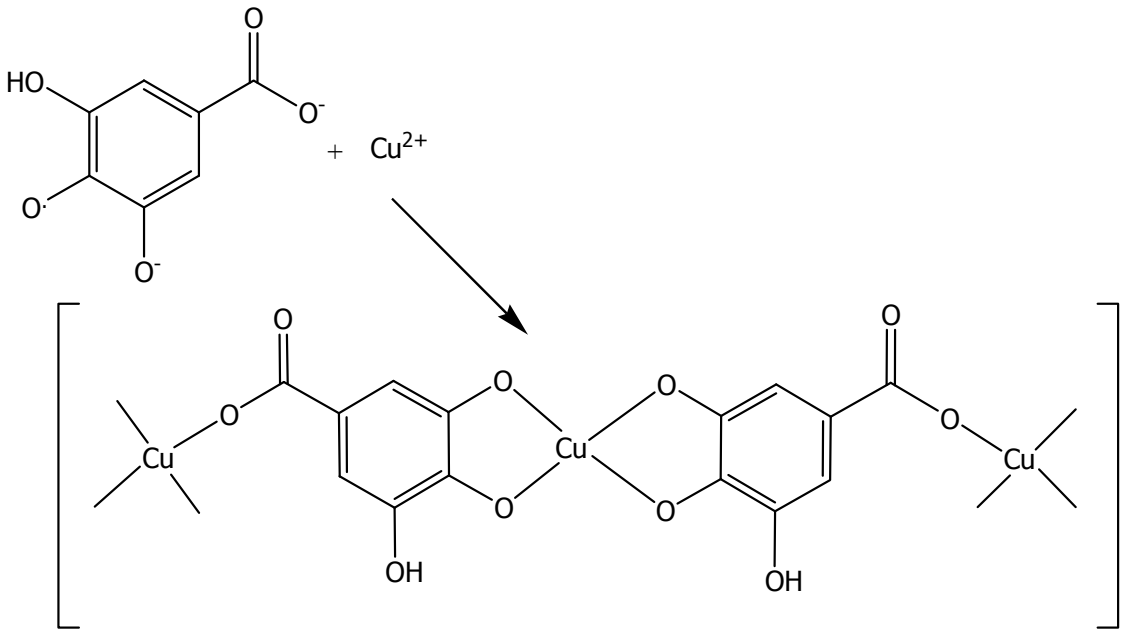

Mechanism 3.4 Chelation of gallic acid with Cu^{2+} at pH 8 to 11.

In case of aged gallic acid, the faster corrosion rate is attributed to the generation of higher amount of semiquinone species generated by autoxidation of gallic acid which has pronounced stability in alkaline conditions.[39]

3.4.10 Testing of Other Polyphenols

Other trihydroxyl substituted benzenes were used to validate the above proposed mechanism. New insights in understanding the structure of different antioxidants to perform as a chelating agent will be discussed in this section.

Modifying the structure of gallic acid (GaAc) chosen as model compound in this study will enable us to understand the differences in chelation tendency of different trihydroxyl substituted benzenes with copper ions. Polyphenols to act as an antioxidant depends on the abstraction of first hydrogen atom from the hydroxyl sites. The

abstraction of the first hydrogen atom depends on the bond dissociation energy. For all these studies, Cu micropatterns on Ru substrate were chosen to study the bimetallic corrosion at pH 9.

Pyrogallol (PyGa)

Pyrogallol is similar to gallic acid with the absence of acidic group. Pyrogallol is a better antioxidant than gallic acid due to its easier oxidation tendency. The route of pyrogallol oxidation should be similar to gallic acid via semiquinone radical formation leading to quinone as the final product. Abstraction of hydrogen from the para hydroxyl site leads to the formation of phenoxyl radical which gets stabilized by the internal hydrogen bonding from the adjacent hydroxyl sites. Insitu micropattern testing of Cu on Ru in pyrogallol didn't show any corrosion indicating the absence of chelation. The inhibition or the absence of copper corrosion can be explained in three different ways:

1. The presence of acidic group destabilizing the internal hydrogen bondings like in gallic acid[22,23] is completely absent in pyrogallol and hence chance of formation of semiquinone radicals to chelate with copper ions might be less.

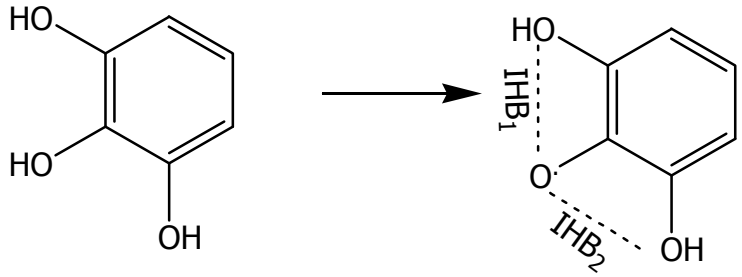

2. Pyrogallol with its better antioxidant tendency tends to scavenge oxygen effectively than gallic acid thereby protecting copper from getting oxidized.

3. As reported in the literature, cleavage of pyrogallol in alkaline conditions can take place forming oxalic and formic acids.[40]

Oxalic acid has two bridging carboxylate group has better chelation tendency with copper ions in acidic conditions rather than in alkaline conditions due to the formation of passive film on Cu which is difficult to remove even by polishing step.[41,42]

Assumption 1 might not be valid due to its higher oxidation tendency and if stabilization of IHB's is dominant, further autoxidation will be minimized and does not act as a good antioxidant. Assumption 2 and 3 are valid but needs more investigation. Assumption 2 can be valid if E_{corr} of Cu in pyrogallol is less than the value reported in gallic acid.

UV Vis spectroscopy will be a valuable technique to investigate the complexation between Cu^{2+} ions and pyrogallol species. Electron spray combined with mass spectrometry will also provide insightful information on the stoichiometric ratio if any complexation is favorable between copper and pyrogallol species.

No corrosion of Cu micropatterns on Ru and Ta were observed for aged pyrogallol prepared at pH 9 which had a significant drop to pH = 6.5. Also, Cu micropatterns on Ru were tested insitu in freshly prepared pyrogallol at pH 5 and 7 and no corrosion was observed.

Phloroglucinol (PhGl) And Phloroglucinic Acid (PhGlAc)

Phloroglucinol and phloroglucinic acid belongs to trihydroxybenzene family. However instead of being in adjacent position compared to pyrogallol, all the –OH groups are placed separately. Based on their higher bond dissociation energy values,

both of the above compounds have lower oxidation tendency.[22] Also any formation of oxidized products will not chelate with copper ions due to the absence of ortho dihydroxyl groups (or) adjacent hydroxyl groups.

Methyl Gallate (MeGa)

Methyl gallate is an ester of gallic acid and the pathway for Cu corrosion is similar to the proposed mechanism. Increasing the alkyl chain decreases the destabilization of internal hydrogen bondings between the phenolate and hydroxyl sites. This decreases the rate of formation of semiquinone species responsible for chelation which is reflected by the decreased corrosion rate of Cu.

Pyrogallol 4 – Carboxylic Acid (PyGa 4-COOH)

Pyrogallol 4-carboxylic acid (2,3,4 – trihydroxybenzoic acid) has similar structure to gallic acid with shift in the position of the acidic group. Intramolecular hydrogen bonding between the carboxylate ion and nearby –OH group competes with the intermolecular hydrogen bondings between ortho and meta hydroxyl groups as shown in the figure. Thus the effect of acidic group in breaking the internal hydrogen bondings has been minimized and chelation tendency is greatly reduced. However aged 2,3,4 THBA show faster rate of Cu corrosion.

Ellagic Acid (ElGa)

Finally ellagic acid was tested and no corrosion was observed. This can be attributed to the large size of the molecule to form bidentate or tridentate complexes with copper ions. Figure 3.20 shows the corrosion rate of Cu on Ru in 5 mM trihydroxyl substituted benzenes at pH 9.

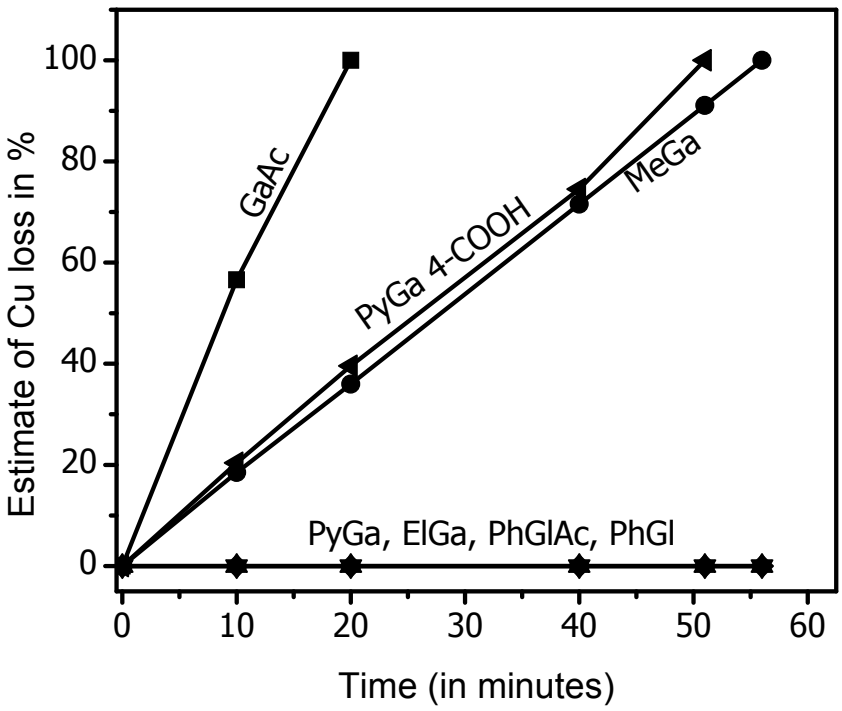

Figure 3.20 - Estimate of Cu loss (in %) on Ru substrate in different polyphenols.

Experiments similar to section 1.5.6 were carried out for all the above polyphenols to find the chelating ability with copper ions. Copper ions mixed with the corrosive compounds namely methyl gallate and pyrogallol 4-carboxylic acid do not precipitate forming hydroxides till the stoichiometric ratio is 3:1 and when mixed with the non-corrosive compounds namely pyrogallol, phloroglucinol, phloroglucinic acid and

ellagic acid do not precipitate till the ratio is 2:1. Thus the non-corrosive trihydroxyl substituted benzenes form weaker complexes with the copper ions.

3.5 Conclusion

Gallic acid was used as the model compound in the corrosion of Cu on Ru and Ta at different pH conditions. It was shown that the corrosion of Cu at pH 9 is attributed to the interaction of copper ions generated by the oxidation of metallic copper with the oxidized products of gallic acid and overall scheme of corrosion mechanism has been proposed. In high alkaline conditions at pH > 12, dimerization of gallic acid results in the formation of ellagic acid which is a better scavenger of oxygen than its parent molecule. Thus gallic acid can act both as an accelerator and inhibitor of Cu corrosion depending on the pH conditions.

Other trihydroxyl substituted benzenes and polyphenols like pyrogallol, methyl gallate, phloroglucinic acid, phloroglucinol, pyrogallol 4-carboxylic acid, and ellagic acid were tested to confirm the proposed mechanism described in section 1.4 and held valid for all chemicals. The importance of the whole paper lies in understanding the structure of different antioxidants. For a better oxygen scavenger and metal chelator, adjacent hydroxyl groups are necessary. Any functional group which has low tendency for weakening the IHB's can be chosen to optimize the metal chelation tendency as seen in methyl gallate. In this study, the enhanced corrosion of Cu on Ru in freshly prepared polyphenol is attributed to ORR and bimetallic potential difference alone cannot be accountable. Of course thermodynamic driving force plays the role in bimetallic corrosion, however the rate of corrosion depends on the interaction of copper and its

ions with oxygen and oxidized products of gallic acid. Ageing of polyphenol increases the corrosion rate with minimizing bimetallic effect. With the preliminary investigation, proposed mechanism is also held valid for dihydroxyl substituted benzenes.

3.6 References

1. Watanabe, M.; Toyoda, E.; Handa,T.; Ichino, T.; Kuwaki, N.; Higashi, Y.; Tanaka, T. *Corrosion Science* 49, **2007**, 766-780.
2. Fitzgerald, K. P.; Nairn, J.; Skennerton, G.; Atrens, A. *Corrosion science* 48, **2006**, 2480-2509.
3. Doyle, F. M.; Wang, L. *Proceedings VMIC 2003 (Twentieth Int. VLSI Multilevel Interconnection Conf.) Marina Del Rev. CA.* September **2003**, 267-276.
4. Wang, L.; Doyle, F. M. *Mat. Res. Soc. Symp. Proc.* 767, **2003**, F6.5.1-6.5.10
5. Vanýsek, P. *CRC Handbook of chemistry and physics*, 77th edition, **1996**, 8-20 – 8-24.
6. Ernur, D.; Terzieva, V.; Schuhmacher, J.; Sutcliffe, V.; Whelan, C. M.; and Maex, K. *Journal of the Electrochemical Society,* 152, **2005**, B512-B518.
7. Tai, K.; Ohtorri, H.; Takahashi, S.; Komai, N.; Horikoshi, H.; Sato, S.; Ohoka, Y.; Segawa, Y.; Ishihara, M.; Yasuda, Z.; Nogami, T. *IEEE*, **2002**, 194-196.
8. Tamilmani, S.; Huang, W.; Raghavan, S. *Journal of the Electrochemical Society* 153, **2006**, F53-F59.
9. Assiongbon, K. A.; Emery, S. B.; Gorantla, V. R. K.; Babu, S. V.; Roy, D. *Corrosion Science* 48, **2006**, 372-388.

10. Lee, W. J.; Park, H. S.; Lee, S. I.; Sohn, H. C.; *Journal of Applied Electrochemistry* 34, **2004**, 119-125.
11. Chandrakant, T. D.; Banerjee, Gautam *Eur. Pat. Appl.* (**2005**) EP 1577934 20050315.
12. Naghshineh, Shahriar; Barnes, Jeff; Oldak, Ewa B *US. Pat. Appl. Publ.* 20010004633 (**2001**).
13. Mochizuki, Manabu; Yamazaki, Shin-ichi; Kano, Kenji; Ikeda, Tokuji *, Biochim. Biophys. Acta,* **2002**, 35-44.
14. Gunckel, S.; Santander, P.; Cordano, G.; Ferreira, J.; Munoz, S.; Nunez-Vergara, L. J.; Squella, J. A.; *Chemico-Biological Interactions,* 114, **1998**, 45-59.
15. Friedman, Mendel and Jürgens, Hella S. *J. Agric. Food Chem*. 48, **2000**, 2101-2110.
16. Hotta, Hiroki; Sakamoto, Harumi; Nagano, Satomi; Osakai, Toshiyuki; Tsujino, Yoshio *Biochim. Biophys. Acta* 1526, **2001**, 159-167.
17. Hotta, Hiroki; Nagamo, Satomi; Ueda, Masashi; Tsujino, Yoshio; Koyama, Junko Koyama; Osakai, Toshiyuki *Biochimi. Biophys. Acta* 1572, **2002**, 123-132.
18. McBride, M. B.; and Sikora, F. J.; *Journal of Inorganic Biochemistry,* 39, **1990**, 247-262.
19. Benitez, F. J.; Real, F. J.; Acero J. L.; Leal, A. I.; Garcia, C.; *, Journal of Hazardous Materials* B126, **2005**, 31-39.
20. Rouchon-Quillet, V.; Remazeilles, C.; Bernard, J.; Wattiaux, A.; Fournes, L. *Appl. Phys. A* 79, **2004**, 389-392.

21. Oess, A; Cheshire, M. V.; McPhail, D. B.; and Vedy J. C.; *Effect of mineral-organic microorganism interactions on soil and freshwater environments*, Kluwer Academic / Plenum publishers, New York, **1999**, 151-158.
22. Thavasi, V.; Leong, L. P.; Phillip, R.; Bettens, A.; *J. Phys. Chem. A* 110, **2006**, 4918-4923.
23. Ji, H. F.; Zhang, H. Y.; *New J. Chem.,* 29, **2005**, 535-537
24. Giacomelli, C.; Miranda, F. S.; Gonçlaves, N. S.; Spinelli, A.; *Redox Report*, 9, **2004**, 263-269.
25. Mandado, M.; Graňa, A. M.; Mosquera, R. A.; *Chemical Physics Letters* 400, **2004**, 169-174.
26. Lucarini, M.; Mugnaini, V.; and Pedulli, G. F.; *J. Org. Chem.* 67, **2002**, 928-931.
27. Kiss, T.; Kozlowski, H.; Micera, G.; and Erre, L. S.; *Polyhedron* 8, **1999**, 647-651.
28. Cariati, F.; Deiana, S.; Erre, L.; Micera, G.; and Piu, P. *Inorganica Chimica Acta*, 64, **1982**, L213-L215.
29. Gerega, K.; Kozlowski, H.; Kiss, T.; Micera, G.; Erre, L. S.; and Cariati, F. *, Inorganica Chimica Acta* 138, **1987**, 31-34.
30. Oess, A.; Cheshire, M. V.; Spack, L.; and Vedy, J. C. *Analusis* 27, **1999**, 424-427.
31. McDonald, M.; Mila, I.; and Scalbert, A. *J. Agric. Food Chem.* 44, **1996**, 599-606.
32. Beverskog, B.; and Puigdomenech, I. *J. Electrochem. Soc.,* 144, **1997**, 3476-3483.

33. Aksu, S. *Mater. Res. Soc. Symp. Proc*. 867, W1.6.1-1.6.6.

34. Tulyathan, V.; Boulton, R. B.; and Singleton, V. L. *J. Agric. Food Chem.,* 37, **1989**, 844-849.

35. (a) Schuchmann, M. N.; Bothe, E.; Sonntag, J. Von.; Sonnatag, C. Von. *J. Chem. Soc., Perkins Trans. 2,* **1998**, 791-796; (b) Fink, W. D.; Stong, J. D.; *Spectrochimica Acta* 38A, **1982**, 1295-1298.

36. Dwibedy, P.; Dey, G. R.; Naik, D. B.; Kishore, K.; and Moorthy, P. N *Phys. Chem. Chem. Phys.,* 1, **1999**, 1915-1918.

37. Zare, H. R.; Golabi, S. M. *J. Solid State Electrochem.* 4, **2000**, 87-94.

38. Oess, A.; Cheshire, M. V.; McPhail D. B.; Stoll, S.; Alaili, M. E.; Vedy, J. C. *The Science of the Total Environment,* 228, **1999**, 49-58.

39. Giacomelli, C.; Ckless, K.; Galato, D.; Miranda, F. S.; and Spinelli, A.; *J. Braz. Chem. Soc.,* 13, **2002**, 332-338.

40. El-Shayeb H. A.; El Wahab F. M. A.; El Abedin S. Z. *British Corrosion Journal* 342, **1999**, 145-150.

41. Pernel, C.; Farkas, J.; Louis, D.; *J. Vac. Sci. Technol. B* 24, **2006**, 2467-2471.

42. Gorantla, V. R. K.; Babel, A.; Padija, S.; Babu, S. V. *Electrochemical and Solid State Letters,* 8, **2005**, G131-G134.

CHAPTER 4 – SUMMARY

In the following sections, conclusions that were drawn from the results discussed in chapters 2 and 3 are presented below.

4.1 Conclusions from Chapter 2

Ru has higher oxygen affinity and forms oxides on its surface easily. Air exposed oxide or native oxide formed on Ru affects the interfacial binding between Cu and Ru shown by the decrease in monolayer coverage of Cu atoms. Hence activation of Ru is necessary to reduce the native oxide prior to Cu deposition. Formation of two different electrochemical oxides has been demonstrated. Reversible oxides formed at potentials < 1.1 $V_{Ag/AgCl}$ behaves similarly to native oxide by inhibiting the under potential deposition of Cu on Ru. 1.1 $V_{Ag/AgCl}$ acts as a transition potential and oxides formed > 1.1 $V_{Ag/AgCl}$ are irreversible and conductive thereby enhancing the interfacial binding strength between Cu and Ru. Conductive Ru oxides can be used as diffusion plug between Cu and Ru.

4.2 Conclusions from Chapter 3

The antioxidant and chelation tendency of different trihydroxyl substituted benzenes (polyphenols) used as antioxidants with Cu deposited on different substrates like Ru, Ta, TaN and Si in post chemical mechanical planarization conditions were studied. Gallic acid was chosen as the model compound in this study. Oxidation of Cu linked with its interaction to oxidized gallic acid species leads

to the chelation of Cu which eventually leads to the corrosion of Cu. Ortho dihydroxyl groups are necessary for chelation. Corrosion of Cu in gallic acid depends on pH conditions. Chelation of gallic acid is quite weak in acidic conditions and hence no corrosion was observed. When the pH is increased, the oxidation activity of gallic acid is enhanced generating more semiquinone species. Our data indicate that Cu receives no protection but instead actively being corroded in gallic acid under alkaline conditions ($7 < pH < 11$) similar to that of the post CMP clean. At pH ≥ 12, gallic acid oxidizes itself to form dimer species which effectively scavenges more amounts of oxygen and hydroxyl radicals thereby preventing the corrosion of Cu. Mechanism of chelation/corrosion is proposed for Cu in gallic acid. Other trihydroxy substituted benzenes have been tested and mechanism was held valid.

Bimetallic corrosion of Cu on Ru and Ta in gallic acid and other chemicals were compared. Ru with its noble nature enhances the corrosion of Cu due to the generation of OH- ions by oxygen reduction reaction (ORR). ORR eventually increases the oxidation of Cu to form its ions at faster rate and corrosion is linked to the rate kinetics between Cu ions and semiquinone species of gallic acid.

REFERENCE LIST

Moore's law, http://www.intel.com/technology/mooreslaw/ (retrieved 06/27/07)

Wasson, S. Intel's Pentium 4 Prescott processor Plus Northwood's last ride, http://techreport.com/reviews/2004q1/p4-prescott/index.x?pg=1 (retrieved 06/27/07)

Microprocessor Quick Reference Guide, http://focus.ti.com/docs/pr/pressrelease.jhtml?prelId=sc05262 (retrieved 06/27/07)

Intel First to Demonstrate Working 45 nm Chips, http://www.intel.com/pressroom/archive/releases/20060125comp.htm (retrieved 06/27/06)

Texas Instruments 45-Nm Chip Manufacturing Process Doubles Output Per Wafer, http://focus.ti.com/docs/pr/pressrelease.jhtml?prelId=sc06117 (retrieved 06/27/06)

Aksu, S. *Mater. Res. Soc. Symp. Proc*. 867, W1.6.1-1.6.6.

Assiongbon, K. A.; Emery, S. B.; Gorantla, V. R. K.; Babu, S. V.; Roy, D. *Corrosion Science* 48, **2006**, 372-388.

Arunagiri, T. N.; Zhang, Y.; Chyan, O.; El-Bouanani, M; Kim, M. J.; Chen, K. H.; Wu, T. C., and Chen, L. C. *App. Phys. Letters,* 86, **2005**, 083104.

Benitez, F. J.; Real, F. J.; Acero J. L.; Leal, A. I.; Garcia, C.; *, Journal of Hazardous Materials* B126, **2005**, 31-39

Beverskog, B.; and Puigdomenech, I. *J. Electrochem. Soc.,* 144, **1997**, 3476-3483.

Bockris, John O'M; and Khan, Shahed U. M. *Surface electrochemistry: A molecular level approach,* Plenum press, **1993**.

Böttcher, Artur; and Niehus, Horst *Physical Review B,* 60, **1999**, 14 396-404.

Christmann, K.; Ertl, G.; and Shimizu, H.; *J. Catal.,* 61, **1987**, 397.

Chan, R.; Arunagiri, T. N.; Zhang, Y.; Chyan, O.; Wallace, R. M.; Kim, M. J.; Hurd, T. Q.; *Electrochemical and Solid-State Letters,* 7, **2004**, G154-157.

Chandrakant, Tambol; Banerjee, Gautam: *Alkaline post chemical mechanical planarization cleaning compositions*. Eur. Pat. Appl. (**2005**), EP 1577934.

Cariati, F.; Deiana, S.; Erre, L.; Micera, G.; and Piu, P. *Inorganica Chimica Acta*, 64, **1982**, L213-L215.

Chyan, O.; Arunagiri, T. N.; and Ponnusamy, T. *J. Electrochem. Soc.,* 150, **2003**, C347-C350.

Conway, B.E *Electrochemical Supercapacitors,* Kluwer-Plenum, New York (**1999**).

Doyle, F. M.; Wang, L. *Proceedings VMIC 2003 (Twentieth Int. VLSI Multilevel Interconnection Conf.) Marina Del Rev. CA.* September **2003**, 267-276

Dwibedy, P.; Dey, G. R.; Naik, D. B.; Kishore, K.; and Moorthy, P. N *Phys. Chem. Chem. Phys.,* 1, **1999**, 1915-1918.

Edelstein, D.; Heidenreich, J.; Goldblatt, R.; Cote, W.; Uzoh, C.; Lustig, N.; Roper, P.; Mcdevitt, T.; Motsiff, W.; Simon, A.; Dukovic, J.; Wachnik, R.; Rathore, H.; Schulz, R.; Su, L.; Luce, S.; Slattery, *J. IBM Semiconductor Research and Development Center*, Hopewell Junction, NY, USA. Technical Digest - International Electron Devices Meeting, **1997**, 773-776.

El-Shayeb H. A.; El Wahab F. M. A.; El Abedin S. Z. *British Corrosion Journal* 34, **1999**, 145-150.

Ernur, D.; Terzieva, V.; Schuhmacher, J.; Sutcliffe, V.; Whelan, C. M.; and Maex, K. *Journal of the Electrochemical Society,* 152, **2005**, B512-B518.

Fink, W. D.; Stong, J. D.; *Spectrochimica Acta* 38A, **1982**, 1295-1298.

Fitzgerald, K. P.; Nairn, J.; Skennerton, G.; Atrens, A. *Corrosion science* 48, **2006**, 2480-2509.

Friedman, Mendel and Jürgens, Hella S. *J. Agric. Food Chem*. 48, **2000**, 2101-2110.

Giacomelli, C.; Ckless, K.; Galato, D.; Miranda, F. S.; and Spinelli, A.; *J. Braz. Chem. Soc.,* 13, **2002**, 332-338.

Giacomelli, C.; Miranda, F. S.; Gonçlaves, N. S.; Spinelli, A.; *Redox Report*, 9, **2004**, 263-269.

Gerega, K.; Kozlowski, H.; Kiss, T.; Micera, G.; Erre, L. S.; and Cariati, F. *, Inorganica Chimica Acta* 138, **1987**, 31-34.

Gorantla, V. R. K.; Babel, A.; Padija, S.; Babu, S. V. *Electrochemical and Solid State Letters,* 8, **2005**, G131-G134.

Goswami, Ishita; and Laxman, Ravi *Semiconductor International*, May **2004**.

Gross, M. E; Lingk, C; Brown, W. L.; Drese, R; *Solid State Technology,* **1999**, 47-52

Gunckel, S.; Santander, P.; Cordano, G.; Ferreira, J.; Munoz, S.; Nunez-Vergara, L. J.; Squella, J. A.; *Chemico-Biological Interactions* 114, **1998**, 45-59.

Hadzi-Jordanov, S.; Angerstein-Kozlowska, H.; Yukoyic, M.; and Conway, B.E *J. Electrochem. Soc.,* 125, **1978**, 1471-1480.

Hartmann, A. J.; Neilson, M.; Lamb, R. N.; Watanabe, K.; *Appl. Phys. A,* 70, **2000**, 239-242.

Ho, Paul S.; Lee, Ki-Don; Yoon, Sean; Lu, Xia; Ogawa, Ennis T.; *Materials Science in Semiconductor Processing,* 7, **2004**, 157-163.

Holloway, Karen and Fryer, Peter M. *Appl. Phys. Lett.*, 57, **1990**.

Hotta, Hiroki; Sakamoto, Harumi; Nagano, Satomi; Osakai, Toshiyuki; Tsujino, Yoshio *Biochim. Biophys. Acta* 1526, **2001**, 159-167.

Hotta, Hiroki; Nagamo, Satomi; Ueda, Masashi; Tsujino, Yoshio; Koyama, Junko Koyama; Osakai, Toshiyuki *Biochimi. Biophys. Acta* 1572, **2002**, 123-132.

Hu, C.K; Harper, J. M. E, *Materials Chemistry and Physics*, 52, **1998**, 5-16.

Hu, C. K.; Luther, B.; Kaufman, F. B.; Hummel, J.; Uzoh, C.; Pearson, D. J. *Thin Solid Films,* 262, **1995**, 84-92.

Ji, H. F.; Zhang, H. Y.; *New J. Chem.,* 29, **2005**, 535-537.

Josell, D.; Bonevich, J. E.; Moffat, T. P.; Aaltonen, T.; Ritala, M.; and Lekela, M.; *Electrochemical and Solid-State Letters,* 9, **2006**, C48-C50.

Josell, D.; Wheeler, D.; Witt, C.; and Moffat, T. P.; *Electrochemical and Solid-State Letters*, 6, **2003**, C143-145.

Josell, D.; Witt, C.; and Moffat, T. P. *Electrochemical and Solid-State Letters*, 9, **2006**, C41-C43.

Kim, K. S; Lee, Y. S.; Lee W. S.; Hwang G. W.; Hwang, C. S.; Lee, J. W.; Jeong J. *J. Electrochem. Soc.,* 154, **2007**, D95-D101.

Kiss, T.; Kozlowski, H.; Micera, G.; and Erre, L. S.; *Polyhedron* 8, 1999, 647-651.

Kolawa,E.; So, F. C. T.; Pan, E. T.; and Nicloet, M. A.; *Appl. Phys. Lett.,* 50, **1987**, 854.

Kolb, D. M.; Przasnyski, M.; and Gerischer, H. *J. Electroanal. Chem. Interfacial Electrochem.,* 54, **1974**, 25.

Krusin-Elbaum, L.; and Wittmer, M. *J. Electrochem. Soc.,* 135, **1988**, 2610.

Kwon, Se-Hun; Kwon, Oh-Kyum; Min, Jae-Sik; and Kang, Sang-Won *J. Electrochem. Soc.,* 153, **2006**, G578-G581.

Lakshminarayanan, S.; Steigerwald, J.; Price, D. T.; Bourgeois, M.; Chow T. P.; Gutmann, R. J.; Murarka, S. P. *IEEE Electron Device Letters*, 15, **1994**, 307-309.

Lee, W. J.; Park, H. S.; Lee, S. I.; Sohn, H. C.; *Journal of Applied Electrochemistry* 34, **2004**, 119-125.

Lin, W.F.; Jin, J. M.; Christensen, P. A.; and Scott, K. *Electrochim. Acta*, 48, **2003**, 3815.

Liu, J.; Lei, J.; Magtoto, N.; Rudenja, S.; Garza, M.; Kelber, J. A.; *J. Electrochem. Soc.,* 152, **2005**, G115-G121.

Lucarini, M.; Mugnaini, V.; and Pedulli, G. F.; *J. Org. Chem.*, 67, **2002**, 928-931.

Maeder, T.; Muralt, P.; Sagalowicz, L.; and Setter, M. *J. Electrochem. Soc.,* 146, **1999**, 3393.

Mandado, M.; Graňa, A. M.; Mosquera, R. A.; *Chemical Physics Letters* 400, **2004**, 169-174.

Massalski, Thaddeus B. *Binary alloy phase diagrams,* Materials park, Ohio : ASM International, c**1990**

McBrayer, J. D.; Swanson, R. M., Sigmon, T. W. *J. Electrochem. Soc.*, 133, **1986**, 1242-1246.

McBride, M. B.; and Sikora, F. J.; *Journal of Inorganic Biochemistry,* 39, **1990**, 247-262.

McDonald, M.; Mila, I.; and Scalbert, A. *J. Agric. Food Chem.* 44, **1966**, 599-606.

Mochizuki, Manabu; Yamazaki, Shin-ichi; Kano, Kenji; Ikeda, Tokuji *, Biochim. Biophys. Acta* **2002**, 35-44.

Moffat, T. P.; Walker, M.; Chen, P. J.; Bonevich, J. E.; Egelhoff, W. F.; Richter, L.; Witt, C.; Aaltonen, T.; Ritala, M.; Leskela, M.; and Josell, D. *J. Electrochem. Soc.*, 153, **2006**, C37-C50.

Naghshineh, Shahriar; Barnes, Jeff; Oldak, Ewa B: *Postchemical mechanical planarization (CMP) cleaning composition*; (ESC, Inc, USA Advanced technology materials, Inc.) US. Pat. Appl. Publ. (**2001**).

Olowafe, J. O; Mogab, C. J.; Gregory, R. B.; Kottke M. *J. Appl. Phys.*, 72, **1992**, 4099-4103.

Ono, H., Nakano, T. and Ohta, T. *Appl. Phys. Lett.*, 64, **1994**,

Oess, A; Cheshire, M. V.; McPhail, D. B.; and Vedy J. C.; *Effect of mineral-organic microorganism interactions on soil and freshwater environments*, Kluwer Academic / Plenum publishers, New York, **1999**, 151-158.

Oess, A.; Cheshire, M. V.; Spack, L.; and Vedy, J. C. *Analusis* 27, **1999**, 424-427.

Oess, A.; Cheshire, M. V.; McPhail D. B.; Stoll, S.; Alaili, M. E.; Vedy, J. C. *The Science of the Total Environment* 228, **1999**, 49-58.

Paunovic, Milan; Schlesinger, Mordechay *Fundamentals of electrochemical deposition,* Electrochemical Society Series, John Wiley & Sons, **1998**.

Pernel, C.; Farkas, J.; Louis, D.; *J. Vac. Sci. Technol. B* 24, **2006**, 2467-2471.

Quiroz, M. A.; and Meas, Y. *J. Electroanal. Chem. Interfacial Electrochem.,* 157, **1983**, 165.

Rao, C. N. R. *Ultra-violet and Visible spectroscopy: Chemical applications,* Plenum press, **1967**.

Rouchon-Quillet, V.; Remazeilles, C.; Bernard, J.; Wattiaux, A.; Fournes, L. *Appl. Phys. A* 79, **2004**, 389-392.

Schuchmann, M. N.; Bothe, E.; Sonntag, J. Von.; Sonnatag, C. Von. *J. Chem. Soc., Perkins Trans. 2,* **1998**, 791-796.

Setton, M.; Van der Spiegel, J.; Rothman, B. *Appl. Phys. Lett.,* 57, **1990**, 357-359.

Sharma, B. K. , *Instrumental methods of chemical analysis,* GOEL Publishing house,

Singer, Peter *Semiconductor International* 19, **1996**, 88-90, 92, 94, 96.

Singer,Peter *Semiconductor International*, 20, **1997**, 79-80 and 82.

Singer, Peter *Semiconductor International*, May **2004**.

Singer, Peter *Semiconductor International,* April **2007**, pp. 28.

Skoog; West; Holler; *Fundamentals of analytical chemistry,* Eighth edition, Saunders College Publishing

Steigerwald, Joseph M.; Murarka, Shyam P.; Gutmann, Ronald J. *Chemical Mechanical Planarization of Microelectronic Materials,* John Wiley & Sons, **1997**.

Tai, K.; Ohtorri, H.; Takahashi, S.; Komai, N.; Horikoshi, H.; Sato, S.; Ohoka, Y.; Segawa, Y.; Ishihara, M.; Yasuda, Z.; Nogami, T. *IEEE* **2002**, 194-196.

Tamilmani, S.; Huang, W.; Raghavan, S. *Journal of The Electrochemical Societry* 153, 2006, F53-F59.

Thavasi, V.; Leong, L. P.; Phillip, R.; Bettens, A.; *J. Phys. Chem. A* 110, **2006**, 4918-4923.

Tulyathan, V.; Boulton, R. B.; and Singleton, V. L. *J. Agric. Food Chem.,* 37, **1989**, 844-849.

Van Huong, N. C.; and Gonzalez-Tejera, M. J. *J. Electroanal. Chem.,* 249, **1988**, 244.

Vanýsek, P. *CRC Handbook of chemistry and physics*, 77th edition, **1996**, pp. 8-20 – 8-24

Wang, L.; Doyle, F. M. *Mat. Res. Soc. Symp. Proc.* 767, **2003**, F6.5.1-6.5.10

Wang, M. T.; Lin, Y. C.; and Chen M. C. *J. Electrochem. Soc.,* 145, **1998**

Watanabe, M.; Toyoda, E.; Handa,T.; Ichino, T.; Kuwaki, N.; Higashi, Y.; Tanaka, T. *Corrosion Science* 49, **2007**, 766-780.

Yeung, Ho; Chan, H.; Zou, S.; and Weaver, M. J.; *J. Phys. Chem. B*, 103, **1999**, 11141-11151.

Zare, H. R.; Golabi, S. M. *J. Solid State Electrochem.* 4, **2000**, 87-94.

Zhang, Y.; Huang, L.; Arunagiri, T. N.; Ojeda, O.; Flores, S.; Chyan, O.; and Wallace R. M. *Electrochem. Solid-State Lett.,* 7, **2004**, C107-C110.

Zhang, Y.; Ojeda, O.; Venkataraman, S.; Chyan, O. *ACS Meeting-in- Miniature*, University of Texas at Arlington, Arlington, TX (April **2005**)